BIOSPHERE-ATMOSPHERE EXCHANGE OF AMMONIA FROM A FERTILIZED CORN CANOPY IN CENTRAL ILLINOIS

BY

ANDREW JOSEPH NELSON

DISSERTATION

Submitted in partial fulfillment of the requirements
for the degree of Doctor of Philosophy in Environmental Engineering in Civil Engineering
in the Graduate College of the
University of Illinois at Urbana-Champaign, 2018

Urbana, Illinois

Doctoral Committee:

Professor Mark J. Rood, Chair and Co-Director of Research
Dr. Sotiria Koloutsou-Vakakis, Co-Director of Research
Professor Tami Bond
Associate Professor Nicole Riemer
Dr. Christopher Lehmann, Illinois State Water Surve

ABSTRACT

Chemical fertilizer use is the primary source of anthropogenic atmospheric NH_3 in Illinois. Atmospheric NH_3 is a precursor to secondary particulate matter (PM) and it also contributes to eutrophication and soil acidification following wet or dry deposition. Uncertainty in NH_3 emissions due to sparse measurements limit the ability of air quality models to predict secondary PM in the atmosphere and depositional loads of nitrogen to ecosystems. To address this challenge, it is necessary to improve understanding of NH_3 emission through experimental measurements and development and evaluation of NH_3 emission models. This research seeks to provide new measured NH_3 fluxes through an experimental field campaign in central Illinois, to investigate dependence of NH_3 flux on environmental conditions and field management practices, and to evaluate closure of field measurements and modeled NH_3 fluxes.

Two experimental field systems to quantify NH_3 flux were deployed above a corn canopy in Central Illinois during the 2014 corn-growing season: a relaxed eddy accumulation (REA) system to quantify NH_3 flux in 4 h intervals and a flux-gradient (FG) system to quantify 0.5 h averaged NH_3 flux. A new method to better the quantify the effect of flux footprint on REA flux measurements was developed, resulting in a subset of 82 concurrent measurements. Mean NH_3 flux was 205 ± 300 ng m^{-2} s^{-1} with REA and 110 ± 256 ng m^{-2} s^{-1} using FG for all concurrent measurements. REA and FG measurements were in agreement at a 0.95 confidence level. The FG method resolved NH_3 emission peaks at 0.5 h averaging time that were otherwise un-observed with 4 h REA averaging. Two early-season emission periods were identified (DOY 130-132 and 140-143), where the timing and intensity of such emissions are attributed to a combination of the use of urease inhibitor and localized soil temperature and precipitation.

Though general NH_3 flux trends were similar between this study and those at non-Midwest sites, differences in short-term NH_3 emission (i.e., hours to days) were found.

REA measurements were also used to evaluate closure with DeNitrification DeComposition (DNDC) model predictions of NH_3 flux. A new method to address practical issues of evaluating closure was developed to account for flux footprints extending outside the measurement site and differences in measurement and model temporal resolution. Modeled fluxes replicated experimental trends satisfactorily using association statistics during the first 33 days after fertilizer application when measured fluxes were to the atmosphere (association statistic, $r_a^2 > 0.74$). DNDC did not replicate measured trends as well during later time periods when depositional fluxes were measured ($r_a^2 < 0.52$). Evaluation of closure between model predictions and measurements identified a potential under-prediction of NH_3 deposition within the DNDC model. These new measurements, and evaluation of closure with the DNDC model, are important to improving understanding of NH_3 flux across varied ecosystems and for future upscaling of local measurements to regional scales using modeled parameterizations.

ACKNOWLEDGEMENTS

No path to completion of a doctoral degree is the same, and the breadth of individuals who are in some way responsible for helping me to reach this milestone demonstrates the unique nature of mine. I am, above all, thankful to my spouse Kate who has been with me every step of the way as a constant balance; willing to talk about my research and my frustrations and support me through it all. I am indebted to her for this and am working to pay it back with my own support as she continues her doctoral path. Further, the support of my parents, Alice and Scott, and many other family members and friends has helped me greatly through this process.

I am grateful to my advisors, Prof. Mark J. Rood and Dr. Sotiria Koloutsou-Vakakis, who have been tremendous mentors and colleagues. Their willingness to take on a student with a full-time career and to work across long distances required a unique commitment to me as a student, and I appreciate it. My doctoral committee, Prof. Tami Bond, Prof. Nicole Riemer, and Dr. Christopher Lehmann have helped to improve my research, broaden my understanding, and have encouraged me to think about how my research fits in the larger community. This has been undeniably reflected in the content and context of this dissertation.

As this research is interdisciplinary by nature, the number of people directly involved in its success are too many to name. Feedback and support from the University of Illinois at Urbana Champaign (UIUC) Air Quality Engineering and Science Group and the Nitrogen Group helped improve many presentations and publications with critical, constructive feedback. I am thankful in particular for the friendship and collaboration of Ms. Srinidhi Balasubramanian. I would also like to thank my colleagues and co-authors at the National Oceanic and Atmospheric Administration, Dr. LaToya Myles, Mr. Mark Heuer, and Dr. Nebila Lichiheb, and the UIUC Environmental Plant & Physiology Group, specifically Prof. Carl Bernacchi and Dr. Eva Joo. Dr.

Christopher Lehmann, Ms. Brenda Riney, and the rest of the team at the National Atmospheric Deposition Program Central Analytical Laboratory were critical to execution of the relaxed eddy accumulation measurements, as well as Dr. Marcelo Vieira-Filho and Ms. Jie Lin, who suffered with me through extreme cold, heat, and everything in between to make the field campaign a success. Mr. Timothy Mies and Mr. Collin Reeser at the UIUC Energy Farm taught me more than I ever thought I wanted to know about corn, fertilizer, and farm management practices. I am also appreciative of the support I have received from the U.S. Army Engineer Research and Development Center (ERDC), both financially and academically. Specifically, the guidance, mentorship, and encouragement of Dr. Ilker Adiguzel, Dr. Martin Page, Dr. Mike Case, Mr. Don Hicks, and Ms. Vicki VanBlaricum have been critical to my success.

Finally, I would like to acknowledge the funding that I have benefitted from to make this research a reality. The Department of Defense Science, Mathematics, and Research for Transformation (DoD SMART) Scholarship is the reason I started my M.S. studies. I was further supported for my Ph.D. by the U.S. Army ERDC and the Air and Waste Management Association Milton Feldstein Memorial Scholarship, as well as travel support from the UIUC Department of Civil and Environmental Engineering. This material is based on work supported by the National Science Foundation, under Grant Nos. AGS 12-36814 and AGS 12-33458. Any opinions, findings, and conclusions or recommendations expressed in this material are those of the author and do not necessarily reflect the views of the National Science Foundation.

TABLE OF CONTENTS

LIST OF SYMBOLS

‘	fluctuation from mean
$\bar{}$	time averaging
↑	updraft
↓	downdraft
↔	deadband
ℓ	discrete vertical transport distance
β	REA coefficient
$\bar{\theta}$	mean potential temperature
$\overline{\rho_d}$	mean dry air density
σ_C	standard deviation of concentration
σ_w	standard deviation of vertical wind velocity
σ_{wR}	standard deviation of vertical wind speed at z_R
χ	mixing ratio of chemical constituent
ζ	atmospheric stability parameter
A	flux footprint similarity constant
Ci	empirical coefficient, *where* i = 1, …, n
C	concentration
C_{inst}	instantaneous concentration
$C_{NH_3-denuder}$	NH_3 concentration for each denuder
$C_{NH_3-ambient}$	ambient atmospheric NH_3 concentration
$C_{NH_3-incanopy}$	in-canopy NH_3 concentration
D	molecular diffusion
E_{diff}	difference between E_M and E_S
E_M	experimentally measured emission
E_N	emission from neighboring plot
E_S	emission from study plot
f_{p1}	fractional flux from plot 1
$\overline{F}$	mean vertical flux
F_{FG}	flux measured via flux-gradient
$F_{FG30min}$	30 min averaged flux using FG
$F_{FG240min}$	240 min averaged flux using FG
F_{inst}	instantaneous vertical flux
F_H	sensible heat flux
F_{NH3}	NH_3 flux
F_{REA}	flux measured via REA
$\mathbf{G}_{ij}$	image source matrix
g	acceleration due to gravity
h_c	canopy height

i	concentration layer index
$inst$	instantaneous measurement
k	von Karman constant (0.4)
K_H	eddy diffusivity for sensible heat
L	Monin-Obukhov Length
n	number
O_i	i^{th} observation
P	flux footprint similarity constant
Pi	i^{th} prediction
R	flux footprint radius
R_S	relative contribution from study plot
R_N	relative contribution from neighboring plot
r_a	association statistic
RMSE	root mean square error
S	source/sink
$s_{interest}$	scalar of interest
T	temperature
T_*	scaling temperature
$\overline{T^{\uparrow}}$	mean updraft temperature
$\overline{T^{\downarrow}}$	mean downdraft temperature
t	time
u_*	friction velocity
u	streamwise wind velocity
v	lateral wind velocity
$V_{extract}$	volume of water during denuder extraction
V_{REA}	volume of air sampled with REA
w	vertical wind velocity
w_{inst}	instantaneous vertical wind speed
x_f	fetch distance
x_{pea}	peak flux distance
z	height
z_m	measurement height
z_o	roughness length
z_u	characteristic flux footprint length
z_R	reference height

LIST OF ACRONYMS

ABL	atmospheric boundary layer
AEM	automated exchange mechanism
AMoN	Ammonia Monitoring Network
AN	ammonium nitrate
AS	ammonium sulfate
ATDD	Atmospheric Turbulence and Diffusion Division
BNF	biological nitrogen fixation
CAL	Central Analytical Laboratory
CGP	Central Great Plains
CRDS	cavity ring-down spectrometer
CV	coefficient of variation
DI	deionized
DNDC	DeNitrification DeComposition
DOY	day of year
EA	eddy accumulation
EBI	Energy Biosciences Institute
EC	eddy covariance
FG	flux-gradient
FIA	flow injection analysis
GDD	growing degree days
HDPE	high density polyethylene
ICN	Illinois Climate Network
ID	inner diameter
IMPROVE	Interagency Monitoring of Protected Visual Environments
ISWS	Illinois State Water Survey
LAI	leaf area index
MFC	mass flow controller
NADP	National Atmospheric Deposition Program
nBTPT	N-(n-butyl)-thiophosphoric triamide
N	nitrogen
NCA	National Climate Assessment
NEI	National Emission Inventory
NFUE	nitrogen fertilizer use efficiency
Nr	reactive nitrogen
NOAA	National Oceanic and Atmospheric Administration
PAR	photosynthetically active radiation
PM	particulate matter
$PM_{2.5}$	particulate matter with diameter $\leq 2.5\mu m$
PVC	polyvinyl chloride

PVDF	polyvinylidene fluoride
REA	relaxed eddy accumulation
RH	relative humidity
RMSE	root mean square error
SAB	Science Advisory Board
SMOKE	Sparse Matrix Operator Kernel Emissions
SOP	standard operating procedure
UAN	urea ammonium nitrate
UIUC	University of Illinois at Urbana Champaign
US	United States
USEPA	United States Environmental Protection Agency
WARM	Water and Atmospheric Resources Monitoring Program

CHAPTER 1: BACKGROUND AND RESEARCH MOTIVATION*

1.1 The Nitrogen Cycle

Nitrogen is present abundantly in nature as a fundamental component of proteins and the most abundant gaseous component of the Earth's atmosphere, representing 78.08% of the total gaseous atmospheric constituents (Jacob, 1999). Atmospheric nitrogen is present in its diatomic molecular form, N_2, which is held together via a strong triple bond making it chemically stable (Seinfeld and Pandis, 2006). Nitrogen is a key component of many biological processes and is readily transported and transformed through a process known as the Nitrogen Cycle. The Nitrogen Cycle is composed of several key natural and anthropogenic transformations including fixation, ammonification (mineralization), nitrification, and denitrification, discussed below.

1.1.1 Fixation

Before N_2 can become bioavailable and play an active role in environmental processes, it must undergo a process known as fixation (Madigan et al., 2009). Nitrogen fixation is the process by which N_2 is converted from a chemically stable molecule to a myriad of nitrogen-containing compounds that can be utilized by organisms and react in the environment. Fixation is

---

* Reproduced in part with permission from:

A.J. Nelson, S. Koloutsou-Vakakis, M.J. Rood, L. Myles, C. Lehmann, C. Bernacchi, S. Balasubramanian, E. Joo, M. Heuer, M. Vieira-Filho and J. Lin (2017) Season-long ammonia flux measurements above fertilized corn in central Illinois, USA, using relaxed eddy accumulation, *Agr. Forest Meteorol*., 239, 202–212

A.J. Nelson, N. Lichiheb, S. Koloutsou-Vakakis, M.J. Rood, M. Heuer, L. Myles, E. Joo, J. Miller, and C. Bernacchi (2018) Ammonia Flux Measurements above a Corn Canopy using Relaxed Eddy Accumulation and a Flux-Gradient System. *Submitted to Agr. Forest Meteorol.* 2/12/18 (AGFORMET-D-18-00154)

S. Balasubramanian, A.J. Nelson, S. Koloutsou-Vakakis, J. Lin, M.J. Rood, L. Myles, C. Bernacchi (2017) Evaluation of DeNitrification DeComposition model for estimating ammonia fluxes from chemical fertilizer application, *Agr. Forest Meteorol*. 237–238, 123-134.

mediated naturally by lightning and microbiological processes and occurs anthropogenically via combustion of fossil fuels and other industrial processes.

Lightning ionization of N_2 to generate NO is the primary natural process responsible for atmospheric fixation (Seinfeld and Pandis, 2006). Certain microorganisms are capable of fixing nitrogen through a process known as biological nitrogen fixation (BNF). BNF is catalyzed by the nitrogenase enzyme, and occurs in free living microbes that can fix nitrogen without a host and in symbiotic processes requiring a specific bacteria-host pairing (Madigan et al., 2009). Through BNF, atmospheric N_2 is converted to NH_3 by nitrogenase:

$$N_2 + 8H \rightarrow 2NH_3 + H_2 \qquad \text{Reaction 1.1}$$

Fixation also occurs through anthropogenic means such as the generation of NO_x by combustion and through many industrial and agricultural processes (USEPA SAB, 2011). Many ecosystems are naturally nitrogen limited, meaning that the rate of biological growth is limited by bioavailable nitrogen (Rattray and Sievering, 2001). Under such circumstances, the introduction of bioavailable nitrogen beyond what is available through natural processes can have negative effects on the ecosystem, such as development of algal blooms in aquatic environments (USEPA SAB, 2011).

The advent of the Haber-Bosch process in 1909, allowing fixation of N_2 from air via a multi-step catalyzed process, radically changed methods of food production by making N_2 bioavailable in industrial fertilizers (Galloway et al., 2003; Erisman et al., 2008). This process now accounts for an estimated 30% of total nitrogen fixation (Smith et al., 2004). Many crops that are grown for human and animal consumption are also capable of fixing nitrogen, a process known as cultivation-induced BNF, and separated from natural BNF because it is a result of human activities, not natural ecosystem development (USEPA SAB, 2011).

1.1.2 Ammonification

Ammonification (also known as mineralization) is the process by which organic nitrogen compounds, such as amino acids, nucleotides, and other proteins are converted to ammonium (Madigan et al., 2009). Many organisms are able to covert organic nitrogen in this way. Organic nitrogen sources for ammonification include dead plants, plant litter, animal waste, and carcasses. Aerobically converted organic nitrogen can be quickly utilized by plants and microbes but may also be readily released from alkaline soils as NH_3 (Madigan et al., 2009).

1.1.3 Nitrification

The oxidation of NH_3 and NH_4^+ to nitrate, known as nitrification, occurs commonly in neutral pH soils, and is catalyzed by bacterial groups ubiquitous in soils. Nitrification is a two-step oxidation process, where NH_3 and NH_4^+ are first oxidized to NO_2^- and then further oxidized to NO_3^- according to the following reactions:

$$NH_3 + O_2 \rightarrow NO_2^- + 3H^+ + 2e^- \qquad \text{Reaction 1.2}$$

$$2\ NH_4^+ + 3\ O_2 \rightarrow 2\ NO_2^- + 2\ H_2O + 4H^+ \qquad \text{Reaction 1.3}$$

$$2\ NO_2^- + O_2 \rightarrow 2NO_3^- \qquad \text{Reaction 1.4}$$

where Reactions 1.2 and 1.3 are catalyzed by *Nitrosomonas* and Reaction 1.4 is catalyzed by *Nitrobacter* (Madigan et al., 2009).

Nitrification is an aerobic process, and occurs most readily in porous soils. As nitrate is highly soluble in water, the nitrification process may lead to undesirable transport of nitrogen through runoff and leaching of nitrates (Vitousek et al., 1997). This is particularly detrimental in agriculture, as nitrification can lead to loss of nitrogen applied as fertilizers. Nitrogen based

fertilizers are often applied as NH_3 and urea and incorporate specific enzymatic inhibitors to prevent or slow nitrification (Madigan et al., 2009).

1.1.4 Denitrification

The reduction of nitrates to gaseous nitrogen compounds is known as denitrification. When nitrates are fully reduced to inert N_2, denitrification effectively completes the Nitrogen Cycle, although several intermediaries occur during the process (Seinfeld and Pandis, 2006).

$$NO_3^- \rightarrow NO_2^- \rightarrow NO + N_2O \rightarrow N_2 \qquad \text{Reaction 1.5}$$

Denitrification is an anaerobic process, commonly performed by *Bacillus*, *Paracoccus,* and *Pseudomonas* bacteria (Madigan et al., 2009). This process can lead to detrimental effects in agricultural systems. When soils are saturated or standing water is present in fields, anaerobic conditions may favor denitrification. This can result in loss of fixed nitrogen from soils and reduced agricultural productivity. Additionally, when not fully reduced, the intermediate production of N_2O and NO through denitrification can lead to global warming, atmospheric ozone depletion, and rainwater acidification (Madigan et al., 2009).

1.2 Reactive Nitrogen

The products of nitrogen fixation, both organic and inorganic, are known as reactive nitrogen (Nr) (Galloway et al. 2003). Natural biological fixation pathways were responsible for maintaining the balance between N_2 and Nr in the environment in the pre-human era (Gruber and Galloway, 2008). Nr did not significantly accumulate in the environment prior to anthropogenic production because the rate of fixation was approximately equal to the rate of denitrification (Ayers et al. 1994). Nr includes inorganic chemically reduced forms of nitrogen (NH_x) (e.g., NH_3 and NH_4^+), inorganic chemically oxidized forms of nitrogen (NO_x, HNO_3, N_2O, N_2O_5, HONO,

peroxy acetyl compounds, and NO_3^-), as well as organic compounds (e.g., urea, amino acids, and proteins).

1.2.1 Anthropogenic Production of Reactive Nitrogen

In 2005, total global anthropogenic production of Nr was 187 Tg Nr/yr – more than a ten-fold increase from Nr production in mid-19th century, and a 20% increase from the 156 Tg Nr/yr produced in 1995 (Galloway et al. 2008, Bouwman et al., 2002a). A primary driver for the increase in Nr production is the associated increase in the production of cereals and meat, rising by 20% and 26%, respectively, from 1995 – 2005 (Galloway et al. 2008; FAO 2014). Globally, Nr production rates vary across different regions, with Europe and North America having the highest per-capita rates. In 2002 the United States (US) produced 28.5 Tg Nr/yr, representing 15% of global Nr production (USEPA SAB 2011).

1.2.2 The Nitrogen Cascade

Galloway (1998) described the movement and consequences of Nr through different environmental systems as the nitrogen cascade. Galloway's nitrogen cascade provides a framework for understanding the environmental transport, ecosystem interaction, fate, and consequences of anthropogenic Nr. A modified depiction of the nitrogen cascade is presented in Figure 1.1 based on Galloway's original work (1998) and further adaptations of his original presentation (Galloway et al. 2003; USEPA SAB 2011). The nitrogen cascade accounts for emission of Nr and how it interacts with the environment.

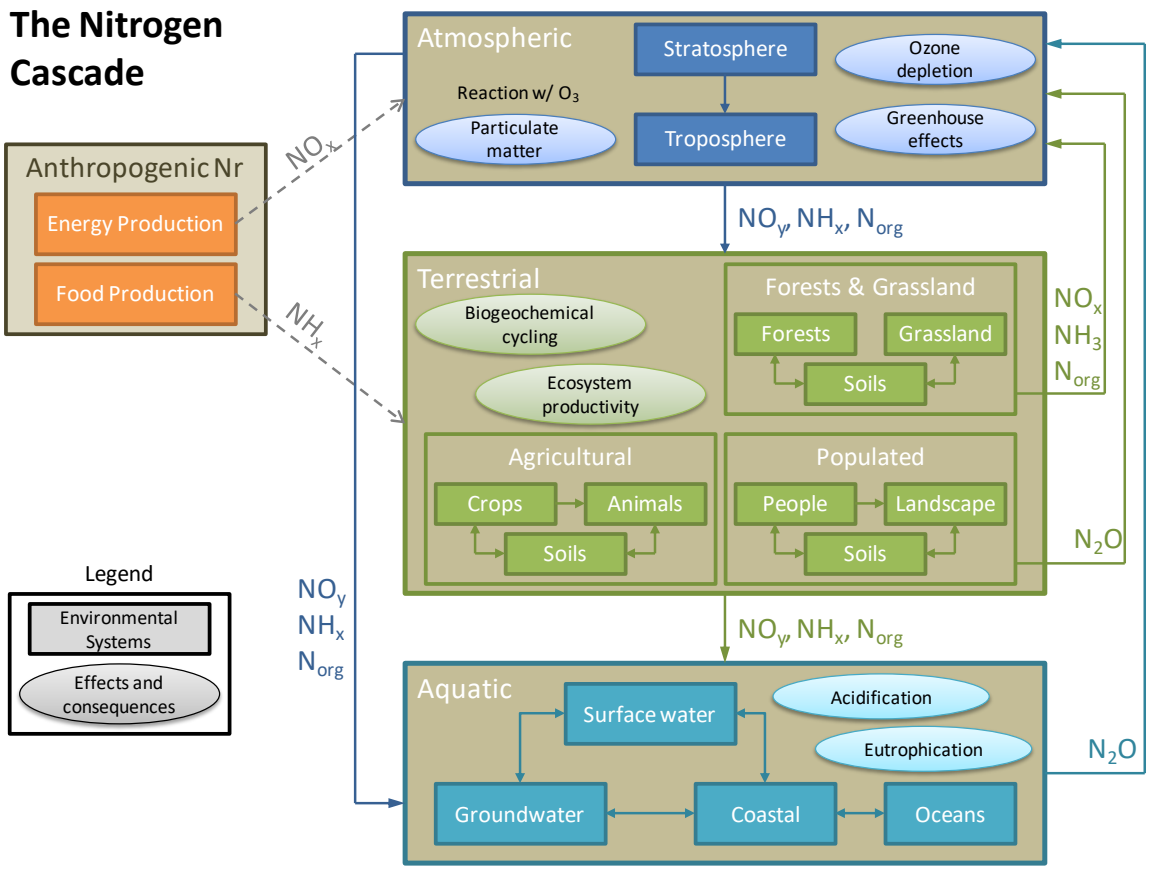

Figure 1.1: Depiction of the nitrogen cascade showing the interaction between different environmental systems with respect to anthropogenic Nr. Note: lines represent pathways between environmental systems and are not intended to link Nr species with specific effects, consequences, or reactions. (Figure developed from Galloway 1998, Galloway et al. 2003, and USEPA SAB 2011)

Galloway et al. (2003) grouped anthropogenic Nr emissions into two broad categories: energy production and food production. Energy production typically introduces Nr as NO_x and NH_x to the atmosphere via direct emission. NH_x and NO_x have short atmospheric lifetimes (< 10 days) and are readily able to accumulate and cycle within the troposphere (Galloway et al. 2003). N_2O has a much longer lifetime (~100 years) and contributes to climate change and stratospheric ozone depletion (Reis et al., 2009; Vitousek et al., 1997). Because the atmosphere is limited in its ability to act as a reservoir for Nr, atmospheric Nr is primarily lost to terrestrial and aquatic ecosystems via deposition of NO_y, NH_x, and organic N (Galloway 1998). Denitrification in the

atmosphere is limited, and primarily occurs through deposition and subsequent biological denitrification in the terrestrial and aquatic ecosystems (USEPA SAB 2011).

The food production category represents contributions from commercial crop cultivation and animal feeding operations, resulting in emission of Nr to the terrestrial ecosystem as NH_x (Galloway et al. 2003). The terrestrial ecosystem is further subdivided into agricultural, forest and grassland, and populated (urban) subsystems. Nr from food production is introduced to the agricultural subsystem and transferred to the populated system as food, where it is eventually re-deposited into soils and the aquatic ecosystem through landfills and sewage (USEPA SAB 2011). The terrestrial ecosystem acts as a sink for Nr via atmospheric deposition and denitrification. Nr that is cycled through the terrestrial ecosystem can be transferred to the aquatic ecosystem via leeching, runoff, and direct discharge (Galloway et al. 2003).

The aquatic ecosystem, encompassing surface freshwater, groundwater, coastal regions, and oceans is not subject to direct introduction of Nr by food or energy production. However, secondary effects such as atmospheric Nr deposition, leeching, and runoff from the terrestrial ecosystem lead to input of anthropogenic Nr to aquatic ecosystems. Nr can lead to acidification of freshwater and eutrophication of freshwater and coastal regions, resulting in biological imbalance within the ecosystem. (Galloway et al., 2003; USEPA SAB 2011).

The Haber-Bosch process is an important component of the food production category and is responsible for nearly 65% of total anthropogenic Nr released to the environment (Galloway et al. 2008). The Haber-Bosch process accounted for production of 121 Tg Nr/yr in 2005, of which 98 Tg Nr/yr was used in agricultural applications while the remainder was used for industrial applications (Galloway et al. 2008). While the utilization of the Haber-Bosch process to produce bioavailable nitrogen for agricultural purposes has reduced the stress on Nr-limited ecosystems

for food production, it is not without consequences and can lead to detrimental environmental effects (Galloway et al. 2008, USEPA SAB 2011).

1.3 Atmospheric Ammonia

While the use of nitrogen-based fertilizers for food production has improved the ability to cultivate crops in nitrogen-limited ecosystems, emission of NH_3 from fertilized cropland results in adverse environmental effects (USEPA, 2011; Erisman et al., 2013). Global anthropogenic NH_3 emissions nearly doubled from 1970 to 2005, increasing from 27.0 Tg NH_3-N to 48.4 Tg NH_3-N (Behera et al., 2013). Based on US Environmental Protection Agency (USEPA) National Emission Inventory (NEI) estimates, US totaled 3.7 Tg NH_3-N of anthropogenic NH_3 emissions in 2014 (USEPA, 2017). As a single nation, the US was the third highest contributor to global NH_3 emissions behind China (11.1 Tg NH_3-N) and India (5.5 Tg NH_3-N) in 2005 (Behera et al., 2013). NH_3 is released to the atmosphere by a number of processes including fertilizer application, residential and industrial fuel combustion, livestock waste, industrial processes, and waste disposal (Bouwman et al., 2002a; Krupa, 2003; Allen et al., 2011, USEPA 2004). The relative contribution of each emission source varies regionally throughout the US. Estimated source contributions of NH_3 in the US and Illinois from the 2014 NEI are presented in Figure 1.2.

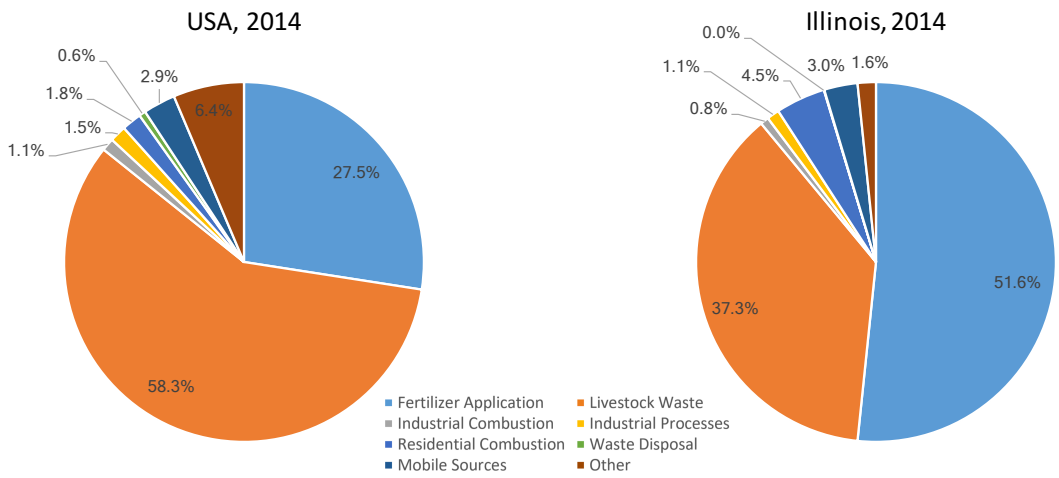

Figure 1.2: Source contribution of atmospheric NH_3 emissions in the United States (left) and in Illinois (right) in 2014 based on USEPA National Emission Inventory (USEPA 2017).

Natural emission sources of NH_3 include volcanic activity, the sea surface, undisturbed soils, and wild animals. However, such sources are the minority contributor to atmospheric NH_3, comprising only 20% of total global emissions (Behera et al., 2013). NH_3 emissions from agricultural sources are dominant over natural emissions and are the largest contributor to global NH_3 emissions (Allen et al., 2011; Bouwman et al., 2002b). In both the entire US and Illinois, fertilizer application and livestock waste – the two main agricultural emission sources – are together responsible for over 90% of total NH_3 emissions. However, the relative contributions from these two sources vary between the US average and Illinois. Fertilizer application accounts for 28% of anthropogenic NH_3 emissions in the US, and is regionally varied based on land use (USEPA, 2017). Illinois is one of the largest contributing states to US NH_3 emissions (in the top five) accounting for 3 - 6% of total US anthropogenic emissions (depending on emission inventory source; Goebes et al., 2003; USEPA, 2017), where fertilizer application accounts for 52% of anthropogenic NH_3 emissions in Illinois according to NEI estimates (USEPA, 2017). Fertilizer use for agricultural production of corn was the predominant contributor to NH_3 emissions from Central Illinois (95%), based on 2002 data (Balasubramanian et al., 2015). As

fertilizer application is the majority source of NH_3 emissions in Illinois, it is important to understand the emission of NH_3 from fertilized agricultural cropland within Illinois.

1.3.1 Mean Atmospheric Concentration

Mean atmospheric concentration of NH_3 may vary by several orders of magnitude depending on the measurement location. In remote areas, atmospheric NH_3 concentrations been reported as low as 0.035 μg m^{-3} at standard conditions (T = 21.1 °C, P = 101.353 kPa) (Alkezweeny et al., 1986; Lewin et al., 1986). Mean NH_3 concentrations near metropolitan areas in the US with mobile and stationary combustion and industrial sources have been reported from 1.11 – 1.64 μg m^{-3} (Allen et al., 2011; Myles et al., 2007; Edgerton et al., 2007). A two-year study in an agricultural area of Alberta, Canada observed atmospheric NH_3 concentration between 1.5 – 2.0 μg m^{-3} (Legge et al., 1990a), although measurements were reported as high as 11.9 μg m^{-3} (Legge et al., 1990b). Such fluctuations in agricultural areas are largely attributed to the application and subsequent volatilization of nitrogenous fertilizers (Legge et al., 1990b; Biermann et al., 1988). Atmospheric NH_3 concentrations depend highly on wind velocity and direction, particularly in agricultural areas where concentrations can change from > 10 μg m^{-3} to trace or undetectable levels with a shift in wind velocity and/or direction (Biermann et al., 1988; Bouwman et al., 2002b).

1.3.2 Environmental Fate

NH_3 is the most abundant alkaline trace atmospheric gas (Seinfeld and Pandis, 2006; Walker et al., 2006), with a lifetime of 1 to 5 days (Aneja et al., 2008). It reacts readily with sulfuric and nitric acid in the atmosphere to form ammonium containing PM:

$NH_{3(g)} + H_2SO_{4(l)} \rightarrow (NH_4)HSO_{4(l)}$ Reaction 1.6

$2NH_{3(g)} + H_2SO_{4(l)} \rightarrow (NH_4)_2SO_{4(s\ or\ l)}$ Reaction 1.7

$NH_{3(g)} + HNO_{3(g)} \rightarrow (NH_4)NO_{3(s\ or\ l)}$ Reaction 1.8

The short atmospheric lifetime of NH_3 leads to higher deposition near the source when compared with ammonium aerosols, while ammonium aerosols exhibit longer lifetimes (1 – 15 days) enabling deposition farther from the source location (Aneja et al. 2001). Gas-to-particle conversion is most effective in first 100 m height of the atmosphere (Lenhard and Gravenhorst, 1980), and the highest concentration of NH_3 is commonly observed close to the surface of the Earth (Ferm, 1998). NH_3 is rapidly converted to ammonium-salt particles that typically exist as fine particulate matter (PM) with diameter $\leq 2.5\mu m$ ($PM_{2.5}$). The rate of conversion varies diurnally, with faster conversion occurring during the daytime (Erisman et al., 1988). Fine PM can grow to larger diameter PM (> 2.5μm) (Aneja et al., 2008; Allen et al., 2011), contributing to local aerosol pollution as a significant driver of secondary aerosol formation (Wang et al., 2015).

The Interagency Monitoring of Protected Visual Environments (IMPROVE) program monitors chemical speciation and emission sources that contribute to visibility degradation across the US. Concentration of ammonium sulfate (AS, $(NH_4)_2SO_4$) and ammonium nitrate (AN, NH_4NH_3) are monitored in the IMPROVE program. Relative concentration of atmospheric AS and AN varies seasonally within the IMPROVE Central Great Plains (CGP) region, comprising parts of Illinois, Missouri, Kansas, Nebraska, South Dakota, Iowa, Minnesota, and Wisconsin (Hand et al., 2012). AS is the majority contributor to atmospheric PM during summer months, while AN is dominant in winter months in the CGP region. Dominance of AS in the summer months is attributed to favorable thermodynamic and meteorological conditions for sulfate formation, while AN is dominant in winter due to high relative humidity and cold temperatures favorable to formation of particulate AN (Hand et al., 2012; Kim et al., 2014).

NH_3 that is not rapidly converted to ammonium PM is deposited to plant or soil surfaces via dry or wet deposition processes (Allen et al., 2011; Bouwman et al., 2002b; Sutton et al., 1995). While runoff and leaching from agricultural fields are major contributors to Nr imbalance in the aquatic ecosystem, there is evidence that up to one-third of such occurs by atmospheric deposition of NH_3 and NH_4^+ PM (Baumgardner et al., 2002; Castro et al., 2003; Aneja, 2008). In areas near coastal rivers and estuaries, this is of particular concern. In Paerl's 1997 study, it was estimated that Nr introduced into North Carolina coastal waters by atmospheric deposition may contribute as much as 60% of total nitrogen loading.

Recent measurements from the National Atmospheric Deposition Program (NADP) National Trends Network indicate inorganic wet N deposition is now dominated by reduced N (i.e., NH_3 and NH_4^+; where oxidized N refers to HNO_3 and NO_3^-) across the US (Li et al., 2016). Further, Li et al. estimate reduced N is dominant in total N deposition (wet plus dry) across most parts of the US. The Upper Midwest domain (containing central and northern Illinois) exhibited 79% of total inorganic N deposition as dry deposition, with peak deposition occurring in spring and summer months (March through August), dominated by dry NH_3 deposition. This region also exhibited the highest fractional and total reduced N contributions to total inorganic N deposition compared to the rest of the US, attributed to the prevalence of nitrogen-based fertilizer use in the region (Li et al., 2016).

The variety of crops cultivated and differences in farming practices lead to an inhomogeneous distribution of NH_3 emissions from agricultural ecosystems. Further, agricultural systems exhibit bi-directional exchange of NH_3, meaning that NH_3 exchange occurs in both directions between the biosphere and atmosphere (Sutton et al., 2011; Duyzer, 1994; Bouwman et al., 2002b). In addition to the mechanisms described previously, NH_3 can be removed within a

plant canopy by absorption through leaf stomata (Wu et al., 2009) and to water on leaf surfaces (Nemitz et al., 2000a). While efforts have been made to model the bi-directional flux of NH_3, quantitative measurements in agricultural ecosystems to provide model inputs and evaluate closure are not widely available due to the high reactivity of NH_3 in the atmosphere and the variability associated with the bi-directional flux process (Phillips et al., 2004; Sutton et al., 2001; Bouwman et al., 2002b).

Urea ammonium nitrate (UAN) solution is commonly used as a synthetic nitrogen fertilizer in Illinois (UI, 2009). After application of UAN to bare soil, the urease enzyme (present in soils) catalyzes the hydrolysis of urea to NH_4^+ and, depending on weather conditions and soil properties such as temperature, moisture, and pH, part of the applied nitrogen volatizes as NH_3 to the atmosphere (Fenn and Hossner, 1985). However, the use of N-(n-butyl)-thiophosphoric triamide (nBTPT) urease inhibitors can reduce NH_3 emission in agricultural ecosystems. Urease inhibitors interact with the urease enzyme, temporarily reducing the activity of the enzyme, thereby limiting NH_3 emission (Watson et al., 1994). Chadwick et al. (2005) reported reductions of NH_3 emission from UAN ranging from 15 – 71% (44% average, n = 10) when nBTPT urease inhibitor was used on grasslands and cereal crops.

1.3.3 Consequences of Excess Atmospheric Ammonia

Because of its short atmospheric lifetime, many effects of NH_3 emissions are secondary (Pinder et al., 2011). The formation of $PM_{2.5}$ by reaction with acid gases is a relatively rapid result of NH_3 emissions when compared with the transformational process of the Nitrogen Cycle resulting in secondary effects following nitrification/denitrification. Secondary PM containing aerosol is of regulatory interest due to adverse health effects (USEPA, 2011) and contribution to visibility degradation (Green et al., 2012). Deposition of NH_3 or its secondary products can have

detrimental effects to plants depending on ecosystem characteristics and nutrient availability (Mattsson et al., 2008) and can alter the structure and diversity of plant communities (Krupa, 2003). Dry and wet deposition of NH_3 can promote soil acidification and exacerbate water quality and eutrophication problems in aquatic ecosystems (Erisman et al., 2013). Further, volatilization of NH_3 from fertilized agricultural fields to the atmosphere is a lost economic input (Conant et al., 2013). The USEPA SAB (2011) identified the following six major impacts of NO_x and NH_3 emissions:

1. Decreased visibility
2. Elevated ozone concentrations resulting in elevated greenhouse potential
3. Human health impacts due to elevated ozone and PM concentrations
4. Direct and indirect radiative forcing as a result of ammonium PM
5. Decreased productivity of agricultural, forest, and natural ecosystems due to elevated ozone deposition
6. Acidification, fertilization, and eutrophication caused by deposition of Nr

1.3.4 Extent of Ammonia Concentration and Flux Measurements in the United States

The NADP Ammonia Monitoring Network (AMoN) is a network of field measurement sites designed to quantify long-term trends in ambient NH_3 concentrations and deposition of reduced nitrogen species (NADP, 2017a). Data from AMoN are intended for use in evaluating closure with atmospheric models, estimating total nitrogen inputs to ecosystems, assessing changes in atmospheric chemistry due to SO_2 and NO_x reductions, and assessing compliance with $PM_{2.5}$ standards. The geographic extent of AMoN field sites in the US is depicted in Figure 1.3. Also included in Figure 1.3 are all known measurement sites of NH_3 flux in the US, corresponding to six unique studies.

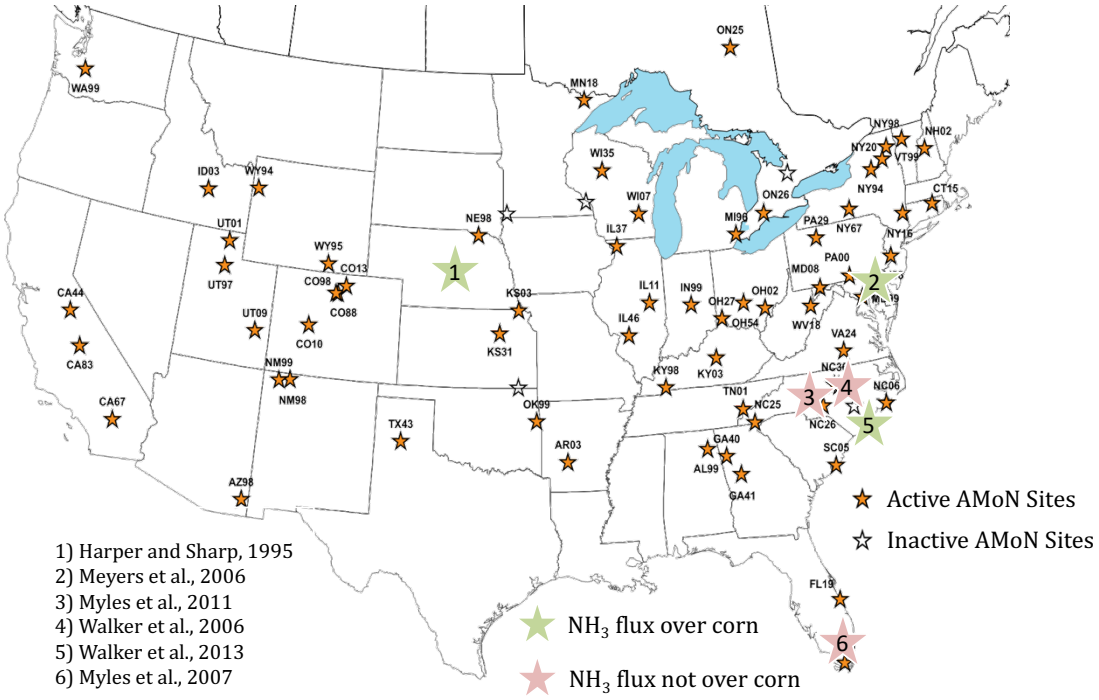

Figure 1.3: Map of United States measurement sites for ambient NH_3 concentration (small stars) from the National Atmospheric Deposition Program (NADP) Ammonia Monitoring Network (AMoN) and all reported measurements of NH_3 flux in the United States (large stars).*

Measurements of NH_3 flux over agricultural canopies in the US are limited in geographic location and crop type. Studies include measurements over grassland (Myles et al., 2007; Myles et al., 2011), soybean (Walker et al., 2006), and corn (Harper and Sharpe, 1995; Meyers et al., 2006; Walker et al., 2013). Despite the high fertilization rates and predominance of corn cultivation in the Midwest, only one study of NH_3 flux over corn in this region exists (Harper and Sharpe, 1995). Harper and Sharpe reported measurements of NH_3 flux in Nebraska using 24 h to 48 h integrated samples. Though Nebraska and Illinois are located in the region defined as Midwest for census purposes, they belong to different climate regions, as defined in the National Climate Assessment (NCA) (USDOC-NOAA, 2013). Further, there are no reported

* Figure reproduced in part from: http://nadp.sws.uiuc.edu/amon/AMoNFactSheet.pdf

measurements over a corn canopy using exclusively UAN fertilizer – a common management practice in Illinois. Other studies of NH_3 flux from corn canopies in the US have been reported for a site in North Carolina (Walker et al., 2013; He et al., 2013) and Maryland (Meyers et al., 2006). Walker et al. (2013) studied NH_3 fluxes during a 64-day period immediately after field fertilization, observing peak emissions and high variability in the first 31 days (339.2 ± 601.7 ng m^{-2} s^{-1}) followed by a lower, less variable emission profile (61.4 ± 10.2 ng m^{-2} s^{-1}).

In addition to terrestrial measurements, several satellite measurement systems exist to quantify tropospheric NH_3 concentration. Examples of such satellite-based observation systems include the Tropospheric Emissions Spectrometer (TES), the Atmospheric Infrared Sounder (AIRS), and the Infrared Atmospheric Sounding Interferometer (IASI), all of which are designed to quantify ambient NH_3 concentration using a column based absorption measurement (Warner et al., 2017). The AIRS system provides global NH_3 concentration, with a data record dating to 2003, enabling characterization of locations of elevated NH_3 concentrations (hotspots), as well as seasonal and spatial trends in concentration (Warner et al., 2017). Data from these satellite measurements were used by Warner et al. (2017) to identify increases of NH_3 over the US, driven primarily by control of SO_2 and NO_x, an unintended secondary consequence on regulation of these species as contributors to acid rain. Limiting factors in the usefulness of satellite measurements are spatial density of observations and the applicability of column-based measurements to identify surface concentration of NH_3. Even the relatively high spatial resolution of TES (5 x 8 km^2 on the surface) would typically represent multiple different land uses for a single grid cell (Zhu et al., 2015). Since NH_3 predominantly exists in the first 100 m of the atmosphere, a column-based measurement would still provide useful information to identify areas of elevated concentration at the surface (Kim et al., 2014).

1.3.5 Current and Future Needs

Successful SO_x and NO_x regulatory policies combined with increased use of nitrogen based fertilizers have led to an increased amount of NH_3/NH_4^+ in the environment, as evidenced by a shift of inorganic nitrogen deposition in the US from oxidized to reduced nitrogen (Li et al., 2016). However, further regulation of NO_x and SO_x may no longer be cost beneficial when compared with control of NH_3 emissions to reduce atmospheric particulate matter concentration (Pinder et al., 2007). Improved understanding of NH_3 emissions is important to more fully characterize the impact on the global Nitrogen Cycle and to develop targeted strategies for emission reduction and reduction in formation of secondary air pollutants (Flechard et al., 2013; Li et al., 2016).

It is difficult to determine the contribution of NH_3 to ecosystem degradation because of the uncertainty of total Nr deposition, caused by limited measurements of bi-directional NH_3 flux (Mathur and Dennis, 2003; Beusen et al., 2008). Studies have indicated that atmospheric NH_3 may have a meaningful role in the development of such pollution. Indeed, the 2011 USEPA Science Advisory Board (SAB) report on reactive nitrogen in the US states:

> *"…the EPA presumption that NH_3 is not a $PM_{2.5}$ precursor should be reversed and states should be encouraged to address NH_3 as a harmful $PM_{2.5}$ precursor."*

Further, the SAB also recommended that direct measurements from production scale agricultural fields should be collected to better understand nitrogen fertilizer use efficiency (NFUE). NFUE is a measure of how well nitrogen fertilizer is utilized by the crop to which it is applied. Higher NFUE values indicate more efficient utilization of nitrogen-based fertilizers, thereby reducing the release of Nr from fertilized agricultural fields. According to the SAB,

measurements are required to identify which regions and crop systems are the largest contributors to atmospheric NH_3 pollution. In turn, this will allow more focused development of policy to mitigate NH_3 emissions and improve the value of investments in research and development (USEPA SAB, 2011).

1.4 Turbulent Transport in the Atmosphere

1.4.1 Structure of the Atmosphere

The Earth's atmosphere is composed of five different layers, presented here in order from ground level up: troposphere, stratosphere, mesosphere, thermosphere, and exosphere. The boundaries of the individual layers are defined based on the atmospheric temperature gradient. The bottom-most layer, known as the troposphere, is characterized by a reduction in temperature with increasing altitude. Depending on the reference location on the Earth's surface, this negative temperature gradient may extend between 8 – 10 km in altitude, at which point a reversal of the gradient occurs and temperature increases with increased altitude, indicating the beginning of the stratosphere (Seinfeld and Pandis, 2006). A similar reversal occurs at the transition from the stratosphere to the mesosphere, and so on. Contrary to the varied temperature gradient at different altitudes, the change in atmospheric pressure with increasing altitude can be approximated as an exponential decrease (Jacob, 1999).

The five layers of the atmosphere are traditionally divided into two larger classifications: the upper and lower atmosphere. The division between the upper and lower atmosphere occurs at the top of the stratosphere, an altitude of approximately 50 km depending on geographic location (Seinfeld and Pandis, 2006). This research is focused on processes that occur in the lower troposphere, where NH_3 concentrations are highest and atmospheric chemistry involving NH_3 is most prevalent.

1.4.2 The Boundary Layer

Within the troposphere a further subdivision can be made to define the atmospheric boundary layer (ABL). The ABL is roughly given as the lowest 1-2 km of the atmosphere, depending on localized conditions, and is capped by an inversion layer (Kaimal and Finnigan, 1994). The ABL is the layer of the atmosphere which is most directly affected by the Earth's surface and responds rapidly (< 1 h) to surface forcing (Stull, 1988). Differential heating and cooling of the surface by solar radiation results in the establishment of convective currents that transport air and pollutants throughout the ABL. Closest to the surface (tens of meters), the establishment of these convective pathways does not occur as readily, resulting in a highly turbulent regime which does not achieve steady state. This lowermost region of the ABL is known as the surface layer (Seinfeld and Pandis, 2006).

Transport of pollutants (gaseous or particulate) through the atmosphere can occur between small (several meters) and large (several thousand meters) length scales. For the purposes of this research, the measurement of atmospheric transport within the surface boundary layer, at length scales of tens of meters, is of primary interest. This is conventionally referred to as "microscale" atmospheric transport, and the study of phenomena occurring at such scales is known as "micrometeorology" (Seinfeld and Pandis, 2006; Stull, 1988).

1.4.3 Advective and Turbulent Transport

The movement of atmospheric constituents and pollutants is driven by advective and turbulent fluxes. Turbulent fluxes are generally dominant over advective fluxes for vertical transport in the lower troposphere except during highly stable atmospheric conditions. For horizontal transport the opposite case holds where advective fluxes are the dominant means of transport (Jacob, 1999). Surface transport by winds can be divided into three subcomponents:

mean wind, waves, and turbulent eddies (Stull, 1988). The frequency of fluctuations in surface transport varies for each component, with mean wind having the slowest frequency of fluctuations, followed by waves, and finally turbulence with the highest frequency of fluctuations. A representation of surface transport composed of these subcomponents is presented in Figure 1.4 (Kaimal and Finnigan, 1994).

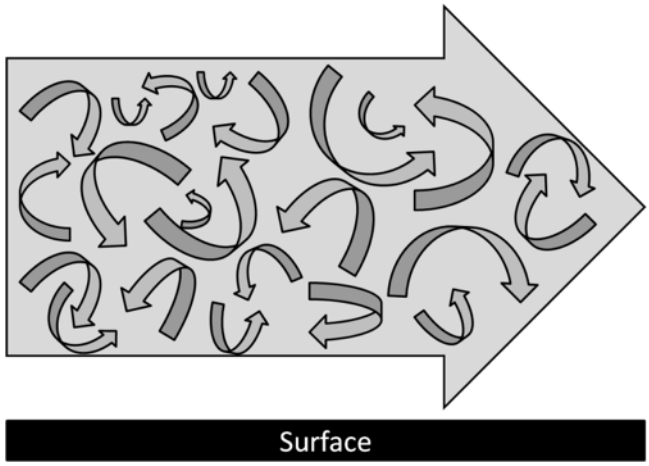

Figure 1.4: Depiction of bulk surface transport (large arrow) comprised mean wind, waves, and turbulent eddies (smaller arrows within large arrow, adapted from Kaimel and Finnigan, 1994).

Eddies vary in size and energy, with higher energy larger eddies typically occurring further from the Earth's surface (Kaimal et al. 1972). Given a stationary sampling point, the wind direction will change in three dimensions as eddies pass. Generally, eddies that contribute to scalar fluxes have a frequency of 5 Hz or less, although this frequency is dependent on measurement height (Kaimal and Finnigan, 1994; Bowling et al. 1998). Turbulent eddies within the surface layer are responsible for the microscale vertical transport of PM and trace gases toward and away from the surface. As such, an understanding of the turbulent movement within the surface layer is critical to accurately measure and predict the flux of pollutants at the microscale.

1.4.4 Stability

Atmospheric stability is determined by a comparison of the environmental and adiabatic lapse rates, where the environmental lapse rate is the actual rate of temperature change within the atmosphere and the adiabatic lapse rate is the vertical rate of temperature change of an adiabatic parcel of air. Using such variables, it is possible to determine if a parcel of air displaced from its original position will continue to move in the direction of displacement (unstable conditions), return toward its original position (stable conditions), or remain at the position to which it was displaced (neutral conditions) (Jacob, 1999; Seinfeld and Pandis, 2006).

The stability of the atmosphere is most commonly estimated using the Pasquill Stability Class method. This method allows for the estimation of stability class based on solar radiation (during the day), cloud cover fraction (during the night), and near-surface wind speed, typically measured at 10 m above the ground. Pasquill's method allows for six stability classes: extremely, moderately, or slightly unstable, neutral, and slightly or moderately stable (Seinfeld and Pandis, 2006).

Atmospheric stability can also be determined experimentally by the method proposed by Obukhov in 1946, and further expanded by Monin and Obukhov in 1954. The Monin-Obukhov length, *L*, is the height above the ground at which mechanical shear forces and buoyant forces contribute equally to the production of turbulence in the atmosphere (Kaimal and Finnigan, 1994; Seinfeld and Pandis, 2006). Below the Monin-Obukhov length, shear forces dominate turbulence production. Buoyant forces are predominant above height *L*. The Monin-Obukhov length is defined as:

$$L = -\frac{u_*^2 \bar{\theta}}{kgT_*} \qquad \text{Equation 1.1}$$

where overbars indicate time averaging, u_* is friction velocity, $\bar{\theta}$ is mean potential temperature, k = 0.4 is the von Karman constant, g is acceleration due to gravity, and T_* is the scaling temperature (Leuning, 2000; Seinfeld and Pandis, 2006):

$$T_* = -\frac{\overline{w'\theta'}}{u_*} \qquad \text{Equation 1.2}$$

where primes denote deviations from the mean and w is the wind velocity component in the vertical direction. It is useful to define the three-dimensional (3D) wind velocity components *u, v,* and *w,* along the orthogonal axes *x, y,* and *z*, representing streamwise, lateral, and vertical wind speed, respectively (Baldocchi et al., 1988). The friction velocity, then, is:

$$u_* = \frac{k\bar{u}(z_m)}{\ln(z_m/z_o)} \qquad \text{Equation 1.3}$$

where z_m is a measurement height within the surface boundary layer (commonly 10 m) and z_o is the surface roughness length (Seinfeld and Pandis, 2006).

The Monin-Obukohv length must be determined experimentally from field measurements, made at height z_m. According to Monin and Obukhov's 1954 hypothesis, the dimensionless atmospheric stability parameter, ζ, is determined as a function of z_m and L:

$$\zeta = \frac{z_m}{L} \qquad \text{Equation 1.4}$$

A negative value for the stability parameter indicates an unstable atmospheric condition, while a positive value indicates a stable atmosphere (Leuning, 2000).

1.5 Micrometeorological Turbulent Flux Measurements

To respond to the need identified within the literature and by the USEPA SAB (2011) to better understand the bi-directional exchange of NH_3 from agricultural crop production, it is necessary to measure NH_3 flux over agricultural cropland. Limited measurements of NH_3

emissions restrict the ability to evaluate closure between measurements and models used to simulate NH_3 exchange between the atmosphere and Earth (Balasubramanian et al., 2017) and the direct and indirect effects of such emissions (Myhre et al., 2013, Appel et al., 2011). Existing models (Bash et al., 2010) and measurements using accumulation methods (Myles et al., 2011; Walker et al., 2013) suggest that NH_3 emissions are not temporally uniform and are influenced by local environmental conditions that can change on the order of minutes.

Measurement of NH_3 flux to the atmosphere is challenging because NH_3 is readily absorbed by water and is reactive with acidic species in the atmosphere (Sutton et al., 2007). Further, NH_3 and NH_4^+ often exist simultaneously in the gaseous, particulate, and aqueous phases, where partitioning varies with environmental conditions such as temperature and relative humidity (Norman et al., 2009). This has led to the development of many different NH_3 flux measurement techniques, including enclosure and micrometeorological methods (Norman et al., 2009).

Micrometeorological flux measurement methods include mass balance (Denmead et al., 1977), the flux-gradient (FG) method (Duyzer, 1994), eddy flux/eddy covariance (EC) (Baldocchi et al., 1988), the modified Bowen ratio (Walker et al., 2006), eddy accumulation (EA) (Desjardins et al., 1972), and relaxed eddy accumulation (REA) (Businger and Oncley, 1990). When compared to enclosure methods for quantifying flux, micrometeorological methods have the advantage that they capture spatially averaged land–atmosphere gaseous exchange over large areas (> 100 m^2) without altering ambient conditions (Sommar et al., 2013). EC and FG approaches require the availability of a precise (± 10% precision), fast-response (> 10 Hz) sensors to measure the constituent of interest (e.g., NH_3 concentration, Phillips et al., 2004). The

EA and REA methods are attractive for the quantification of NH_3 fluxes because they do not rely on fast-response sensors to measure NH_3 concentration (Myles et al., 2011).

Many reported measurements of NH_3 flux from agricultural crop systems rely on chemical adsorption and/or accumulating methods to quantify flux, resulting in temporal resolution of hours or days (Myles et al., 2007; Walker et al., 2013). The mass balance method has been used to measure NH_3 flux from agricultural fields (Denmead et al., 1977). However, it is not straightforward to use in practice, as accurate measurements require that sampling equipment be placed in the center of a circular plot, which is not commonly available in production scale agricultural fields (Baldochi et al., 1988).

Low concentrations of NH_3 previously observed at agricultural sites (i.e., as low as 0.3 $\mu g\ m^{-3}$ two weeks after fertilization; Walker et al., 2013) limit the suitability of fast-response detectors due to detection limits (0.10 $\mu g\ m^{-3}$ NH_3 at 10 Hz with total accuracy of 0.14 $\mu g\ m^{-3}$ NH_3 ± 10 %; Miller et al., 2014). The FG method can yield sub-hourly temporal resolution of NH_3 flux and has been used to measure NH_3 fluxes over unfertilized agricultural fields (Myles et al., 2011) and a variety of fertilized crops including grassland (Spindler et al., 2001; Sutton et al., 2001; Milford et al., 2009), corn (Harper and Sharpe, 1995), triticale (Loubet et al., 2012), and wheat (Personne et al., 2015). However, measurements at sub-hourly timescales have not been previously reported for typical agricultural practices in the Midwest.

Recent advances have resulted in several demonstrations of fast-response, closed EC methods for measuring NH_3 flux from cattle feedlots (Sintermann et al., 2011; Ferrara et al., 2014). However, such methods are limited by reactivity of NH_3 in sample lines and inlets, thereby affecting their high-frequency response and resulting in underestimation of NH_3 flux (Ferrara et al., 2014). Open-path EC methods are a promising alternative to improve fast-

response measurement as they avoid the potential interference from sampling lines. Such a method was used for measurement of NH_3 flux at cattle feedlots, with a limit of detection for NH_3 flux of 1.3 ± 0.5 ng m^{-2} s^{-1} over a 30 min average (Sun et al., 2015). However, the exposed optics make long-duration measurement (i.e., > 1 day) in an open agricultural field challenging due to fouling of the optical cell by airborne dust and insects (Miller et al., 2014).

Meyers et al. (2006) and Walker et al. (2013) reported measurements of NH_3 collected above corn canopies using REA and the modified Bowen ratio, respectively. In both cases the researchers observed that the first month following fertilizer application exhibited the most dynamic variation of magnitude and temporal emission of NH_3. Walker et al. observed that total NH_3 emissions were consistent with emission factors for UAN solutions with urease inhibitors, but that the temporal emission profile – characterized by two large emission pulses – may not be well represented by current soil process models.

Improved temporal resolution of measurements during the early crop growing season are needed to better understand the variability of NH_3 emission and to quantify the benefit of urease inhibitors on reducing NH_3 volatilization at the field scale. Further, existing process-based models to describe surface-atmosphere exchange of NH_3 at sub-hourly timescale require field-scale measurements at similar timescales for closure evaluation (Génermont and Cellier, 1997; Personne et al., 2009; Garcia et al., 2012). Walker et al. (2013) suggested that existing NH_3 models may be least suited to accurately predict emissions during the first month after crop fertilization, when emission intensity is highest and most variable.

1.5.1 The Conservation Equation and Eddy Flux

Micrometeorological flux measurement techniques are based on the conservation equation, stating that the rate of change of a constituent of interest at a fixed point is in

equilibrium with advection, turbulent convergence or divergence, molecular diffusivity, and any source/sink contributions (Baldocchi et al., 1988), expressed as:

$$\frac{\partial \bar{C}}{\partial t} = \left[-\bar{u}\frac{\partial \bar{C}}{\partial x} - \bar{v}\frac{\partial \bar{C}}{\partial y} - \bar{w}\frac{\partial \bar{C}}{\partial z}\right] + \left[-\frac{\partial \overline{u'C'}}{\partial x} - \frac{\partial \overline{v'C'}}{\partial y} - \frac{\partial \overline{w'C'}}{\partial z}\right] + D + S \qquad \text{Equation 1.5}$$

where the left-hand side represents the time (t) rate of change of the concentration of a chemical constituent (C) and the right-hand side is the sum of the mean horizontal and vertical advection (first bracketed term), mean horizontal and vertical divergence or convergence of turbulent flux (second bracketed term), molecular diffusion (D), and the source or sink contribution (S). Flux convergence is defined as the accumulation of the constituent of interest in a control volume because the flux entering the control volume is greater than the flux leaving the control volume. Flux divergence is the opposite case.

As described by Baldocchi et al. (1988), by applying the following five assumptions:

1. Uniform and level surface
2. Uniform air density
3. No sources or sinks above the surface
4. Turbulent flux is dominant of molecular diffusivity
5. Mean turbulent covariance is constant within the surface layer

Equation 1.5 can be arranged to describe the mean turbulent flux of material over an area:

$$\bar{F} \approx \overline{w'C'} \qquad \text{Equation 1.6}$$

where the mean vertical turbulent flux of a constituent of interest, $\bar{F}$, is approximated by the mean covariance of instantaneous vertical wind speed and concentration. Flux is directed downward when $\bar{F} < 0$, and is directed upward when $\bar{F} > 0$. Equation 1.6 is key in micrometeorological measurements and describes in general terms the classical formula for the mean vertical turbulent flux, or "eddy flux," of any constituent of interest that can be accurately

measured at > 10 Hz (Burba, 2013). It is applied in many different scenarios and forms the basis for calculating the instantaneous flux of gases such as CO_2, CH_4, and NO_2, as well as determining sensible and latent heat flux and evapotranspiration.

It is important to note that while Equation 1.6 provides a simplified method for determining vertical turbulent flux of many constituents of interest, the assumptions required to arrive at this simplified equation introduce inherent measurement error. Such errors have been reported on the order of 10 to 20%, depending on the particular situation and geophysical environment (Wesley and Hart, 1985). Therefore, considering the specific geophysical characteristics of an experimental site is important in successfully measuring eddy flux (Burba, 2013). Further, the assumption that no sources or sinks exist above the surface means that this approach can only be used to measure mean fluxes *above* a plant canopy, and cannot be used to elucidate source and sink distribution within the canopy.

1.5.2 Eddy Accumulation

Desjardins (1972; 1977a; 1977b) first proposed a method that allowed for the use of slower response or accumulating detection methods in combination with high-speed 3D wind velocity measurements to calculate mean eddy flux. From Equation 1.6, the instantaneous vertical flux, F_{inst}, at a given point is:

$$F_{inst} = w_{inst} C_{inst} \qquad \text{Equation 1.7}$$

where the subscript "*inst*" refers to "instantaneous" measurements having measurement frequencies of at least 10 Hz. Desjardins expanded this expression by introducing a term, *N*, that represents the number of times an air parcel travels upward or downward across an arbitrary discrete vertical distance, ℓ. Expanding Equation 1.7 in this manner results in:

$$F_{inst} = \frac{d\ell}{dN}\frac{dN}{dt} C_{inst} \qquad \text{Equation 1.8}$$

By summing and averaging the updraft and downdraft components, where the updraft component is positive and the downdraft component is negative, the total mean flux through distance $d\ell$ over time dt can be calculated:

$$\bar{F} = \frac{d\ell}{dN}\frac{1}{t}\left(\sum_{k=1}^{N\uparrow} C_{k\uparrow} - \sum_{j=1}^{N\downarrow} C_{j\downarrow}\right) \qquad \text{Equation 1.9}$$

where $C_{k\uparrow}$ is the concentration during discrete updraft events $k = 1$ to upward N ($N\uparrow$) and $C_{j\downarrow}$ is the concentration during discrete downdraft events $j = 1$ to downward N ($N\downarrow$).

Desjardins' EA method is useful when there is a need to measure trace atmospheric gases for which instantaneous sampling equipment is not available. High frequency measurements of vertical wind direction by a sonic anemometer are used to identify updrafts and downdrafts. Desjardins (1977a) proposed the use of two sampling "reservoirs" – one for samples collected during updrafts and a second used during downdrafts. In this method, a logic circuit analyzes data from the vertical anemometer in real time and switches the collection reservoir based on vertical wind direction. Flow rate to each sampling reservoir is maintained proportional to vertical wind velocity so that at the end of sampling the concentration in each reservoir is proportional to $\overline{w^{\uparrow}C}$ and $\overline{w^{\downarrow}C}$ where $\overline{w^{\uparrow}}$ and $\overline{w^{\downarrow}}$ are mean vertical wind velocity during updrafts and downdrafts, respectively (Businger and Oncley, 1990).

While the EA method is conceptually attractive, it is difficult to implement in practical field applications (Businger and Oncley, 1990). Hicks and McMillen (1984) performed a numerical analysis of the EA method and observed that a number of technical challenges exist in its implementation, particularly with respect to the high level of accuracy required in the calculation of $\overline{w^{\uparrow}C}$ and $\overline{w^{\downarrow}C}$ (Businger and Oncley, 1990). The need to actively adjust the

collection reservoir flow rate to be proportional to vertical wind speed is technically complex and difficult to implement in the field (Businger and Oncley, 1990).

1.5.3 Relaxed Eddy Accumulation

Recognizing the potential benefit of the EA method, Businger (1986) suggested that a "relaxation" of the method could allow for real-world implementation and reduce the technical challenges associated with the method. Businger and Oncley (1990) provided the framework for a simplification of Desjardins' EA method. By incorporating a calibration coefficient, Businger and Oncley were able to effectively eliminate the need for proportional updraft and downdraft sampling rate required by the EA method, resulting in the practical approach known as REA.

Relaxation of the EA method simplifies the approach by using the statistical REA coefficient, β, in place of proportional sampling. This allows for a constant flow rate to the collection reservoirs when actuated, reducing the technical difficulty of implementing the method. With this simplification, the method only requires mean concentration for the updraft and downdraft reservoir, $\overline{C^{\uparrow}}$ and $\overline{C^{\downarrow}}$, respectively. Implementing these simplifications, the mean vertical flux can be calculated:

$$\bar{F} = \overline{w'C'} = \beta\sigma_w\left(\overline{C^{\uparrow}} - \overline{C^{\downarrow}}\right) \qquad \text{Equation 1.10}$$

where σ_w is the standard deviation of the vertical wind velocity. The REA coefficient was first proposed by Businger and Oncley (1990) and fully derived by Baker (1992) using a linear regression and the biserial correlation method of Pearson (1909) and Treloar (1942). Baker (1992) demonstrated that the REA coefficient was a statistical parameter derived from the relative probability of two statistical classes: updraft and downdraft sampling conditions. The theoretical expectation of β is 0.627 when the probability density function follows an ideal Gaussian frequency distribution and the relationship between turbulent fluctuations of *w* and

transport of the constituent of interest is linear (Sakabe et al., 2014). This is in agreement with observations by Businger and Oncley (1990) and others (described below) that $\beta \approx 0.6$ through most of the convective boundary layer.

Further theoretical and experimental studies have found that β can vary significantly even at a single site. Meyers et al. (2006) reported values ranging from 0.32 – 0.98 during a 35-day study over a single fertilized corn canopy. Others (Pattey et al., 1993; Gao, 1995; Milne et al., 1999; Ammann and Meixner, 2002) have reported many intermediate values within the range of 0.52 (Andreas et al., 1998) to 0.62 (Katul, 1994). These results demonstrate that a fixed value of β cannot be defined and β therefore needs to be calculated for each experiment. Further, Sakabe et al. (2014) recommend that changes in atmospheric stability should also be considered when calculating the REA coefficient to minimize errors.

It is known that β is dependent on the atmospheric stability parameter, defined previously in Equation 1.4 (Sakabe et al., 2014). Because β is dependent on the proportion of updraft and downdraft velocities, atmospheric stability at the time of measurement may impact the calculated value of β (Gao, 1995). To increase the updraft and downdraft concentration difference and to reduce the switching frequency of the valves, the use of a "dynamic deadband" was proposed (Bowling et al., 1999). In practice, the deadband is a dynamic value that must be exceeded by the absolute value of the up or downdraft velocity to trigger valve switching (Grönholm et al., 2008). The deadband is referred to as "dynamic" because it is continuously recalculated during an experiment as a function of σ_w.

In practice, β is determined by calculation from measurements of flux of another scalar, such as temperature or water vapor, which can be measured with fast response instruments (Oncley et al. 1993; Bowling et al., 1998). This method relies on spectral similarity, an

assumption that the surrogate scalar is transported by the same turbulent updrafts and downdrafts that transport the constituent of interest (Wyngaard and Coté, 1972; Bowling et al., 1999). Using temperature, *T*, as a surrogate scalar flux, Equation 1.10 may be rearranged such that:

$$\beta = \frac{\overline{w'T'}}{\sigma_w\left(\overline{T^{\uparrow}} - \overline{T^{\downarrow}}\right)} \qquad \text{Equation 1.11}$$

where $\overline{w'T'}$ is sensible heat flux, $\overline{F_H}$, and $\overline{T^{\uparrow}}$ and $\overline{T^{\downarrow}}$ are the mean temperature of updrafts and downdrafts, respectively. Such measurements can be readily obtained using a 3D sonic anemometer at frequencies > 10 Hz to determine β for a specific experimental scenario. Katul et al. (1996) calculated β using the surrogate fluxes of H_2O, O_3, and CO_2 and observed that the associated difference in the flux calculated using REA when compared to that calculated using a traditional EC method were 2.3, 3.3, and 3.9%, respectively. Therefore, it is understood that the representative surrogate scalar used in the determination of β does not have a significant impact on resultant REA-based flux measurements (Katul, et al., 1996; Bowling, 1998).

REA has been used for analysis of many different compounds including isoprene (Bowling et al., 1998; Zhu et al., 2000; Graus et al., 2006), monoterpenes (Christensen et al., 2000), volatile organic compounds (Park et al., 2010), particulate sulfate (Myles et al., 2007) and NH_3 (Zhu et al., 2000; Myles et al., 2007). Depending on the constituent of interest, different collection reservoirs and analysis techniques are used. Results have been reported using Tedlar, Teflon, and Curlam bags, denuders with different coatings, and various types of solid adsorbents (Bowling et al., 1998). Further, the REA method has been evaluated against the more direct EC method of flux measurement and has been observed to have suitable accuracy (within 5%) when measuring surface-air exchange fluxes of CO_2 (Pattey et al., 1993) and biogenic volatile organic compounds (Gallagher et al., 2000).

Reported measurements of bi-directional NH_3 flux using REA are limited in the literature. Zhu et al. (2000) described the first use of REA for quantifying NH_3 flux above a corn canopy using denuders as the sampling reservoir. They reported that the method was suitable for this purpose, and observed that NH_3 fluxes were closely correlated with incoming radiation. Further field campaigns using REA to quantify NH_3 flux were reported in several different regions and land uses including a wastewater treatment plant tertiary sprayfield in Syndey, FL (Myles et al., 2007) and fertilized grassland in Braunschweig, Germany (Hensen et al., 2009).

1.5.4 Flux Footprint

When implementing a flux measurement method, the measurement location must be carefully considered to ensure that collected data accurately characterize the environment of interest. An air parcel containing concentration C is emitted from the surface and transported both horizontally and vertically until it reaches a discrete measurement location. The distance of horizontal transport from the point of emission to the point of measurement is referred to as the fetch distance, x_f. Fetch is a function of surface roughness, measurement height, and meteorological conditions (Burba, 2013). A general rule of thumb for evaluating the suitability of a measurement plot is to use a 100:1 ratio of fetch to measurement height (Businger, 1986). Although this is often used for estimating maximum fetch, theoretical evaluation by Leclerc and Thurtell (1990) suggests that the rule of thumb can underestimate maximum fetch during highly stable atmospheric conditions and over smooth surfaces (Hsieh et al., 2000).

While fetch represents the horizontal distance traveled by a particular air parcel, it is also useful to quantify the total area that contributes to an integrated flux measurement. Theoretical calculation of this area, known as the flux footprint, is used to estimate the total area that contributes to a flux measurement. The cumulative flux contribution observed from horizontal

upwind distance x at measurement height z_m is known as the cumulative flux footprint, $f(x, z_m)$, and is calculated using the method described by Hsieh et al. (2000):

$$f(x, z_m) = \frac{1}{k^2 x^2} A z_u^P |L|^{1-P} \exp\left(-\frac{1}{k^2 x^2} A z_u^P |L|^{1-P}\right) \quad \text{Equation 1.12}$$

where A and P are model-specific similarity constants and z_u, is a characteristic model length scale derived from the Monin-Obukhov length, L, and x. The upwind distance that contributes most to the measured flux, x_{peak}, can be estimated as:

$$x_{peak} = \frac{A z_u^P |L|^{1-P}}{2k^2} \quad \text{Equation 1.13}$$

Cumulative flux footprint is typically reported as percentage contribution of total measured flux from distance x. An example graphical representation of flux footprint is presented in Figure 1.5 as both cumulative flux contribution (top) and percentage of flux contributed at each upwind distance (bottom). Figure 1.5 is provided for clarity in describing flux footprint and is not specific to this experiment (note: this figure should be understood only as an example of one possible distribution).

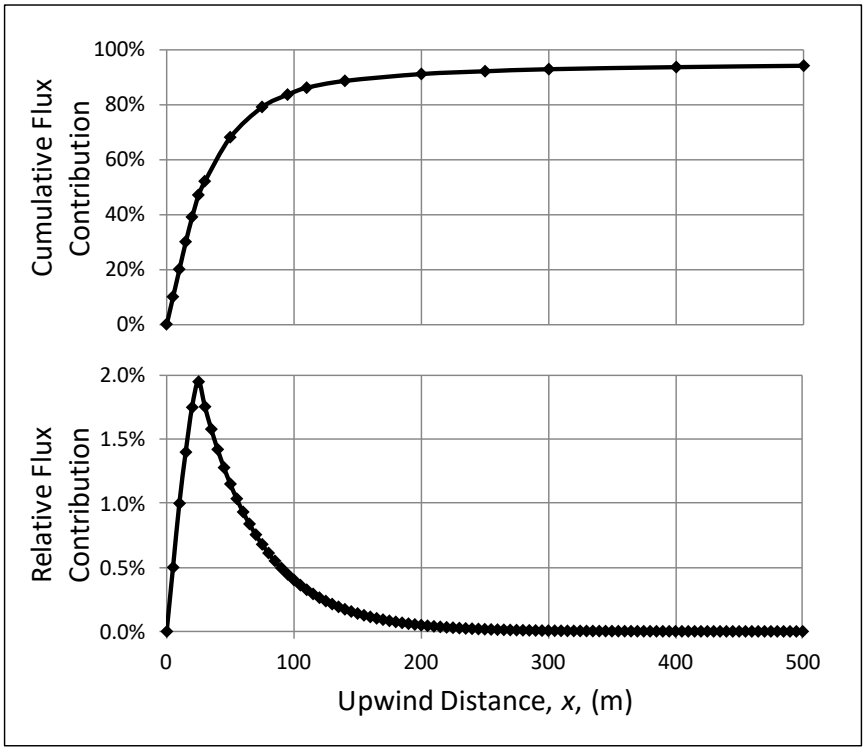

Figure 1.5: Example plots of cumulative (top) and relative (bottom) flux contribution as a function of upwind distance *x*.

As observed from the top plot in Figure 1.5, the 70% flux footprint distance is 55 m, meaning that 70% of the total measured flux originated from within a radius of 55 m of the measurement location; the peak upwind contribution distance, x_{peak}, is 25 m. The area under the curve of the bottom plot in Figure 1.5, when integrated from zero to infinity, will yield 100%.

1.6 Modeling Biosphere-Atmosphere Ammonia Exchange

Characterizing spatial and temporal heterogeneity associated with NH_3 fluxes from chemical fertilizer application under various environmental conditions is essential for development of representative emissions inventories for air quality modeling (Appel et al., 2011). While flux measurements can support such efforts, measurement studies are geographically sparse and limited to short study periods (< 2 months) (USEPA, 2011; Walker et

al., 2013). It is therefore important to develop NH_3 emission models and utilize limited measurement data to evaluate closure between model and measurement results.

Different modeling approaches have been developed to estimate NH_3 emissions and fluxes from agricultural cropland. Temporal variability of flux has previously been estimated using a coupled approach with approximate historical planting and harvesting dates with average values for fertilizer application and field management practices (Goebes et al., 2003). Shorter time scale (< 1 day) variability is estimated using with empirical relationships of hourly temperature and wind speed (Gyldenkærne et al., 2005), inverse modeling approaches (Paulot et al., 2014), and semi-empirical (Cooter et al., 2012) or process models (Balasubramanian et al., 2015).

Process-based models estimate NH_3 emission or flux by simulating the underlying biogeochemical processes that regulate the biosphere-atmosphere exchange of NH_3. Examples of process-based models include SURFATM-NH_3 (Personne et al., 2009), which simulates the bi-directional exchange of NH_3 with vegetation, Volt'air-NH_3 (Génermont and Cellier, 1997; Garcia et al., 2012), which simulates NH_3 fluxes from bare soil, and the DeNitrification DeComposition (DNDC) model (Li et al., 1992), which simulates NH_3 fluxes from agroecosystems. Such models can be implemented for a variety of environmental conditions, and are well suited to upscaling of emission from site to regional scale (Cuddington et al., 2013).

DNDC was originally developed to simulate the evolution of CO_2, N_2O, and N_2 in agricultural soils and predict the subsequent emission of gaseous N_2O to the atmosphere (Li et al., 1992). The model has since been further developed to include methods for predicting NH_3 flux based on spatially and temporally distributed biogeochemical processes in the agroecosystem (Li, 2000). At the site scale, DNDC has been used to study impact of crop-

rotation and tillage on crop yields (Farahbakhshazad et al., 2008), greenhouse gas fluxes (Gopalakrishnan et al., 2012), NH_3 fluxes from fertilized cropland (Balasubramanian et al., 2015, 2017), and nitrate leaching into water bodies (David et al., 2009).

DNDC uses six submodels to predict biogeochemical processes: soil climate, crop growth, decomposition, denitrification, nitrification, and fermentation (Gilhespy et al., 2014). Each submodel has specific required input parameters that can be user supplied (Gilhespy et al., 2014). If no input parameters are supplied, the model will use default values in many cases. Because it is capable of accounting for local weather and soil conditions, the use of DNDC for estimating NH_3 flux from fertilized cropland to the atmosphere may provide improved temporal estimates when compared to other modeling approaches.

1.7 Research Objectives and Significance

The overall goal of this research is to increase understanding of NH_3 emissions from intensively managed agricultural ecosystems in the Midwest US. Specifically, my contributions to this goal are divided into three objectives, which are described more fully below: (1) quantification of NH_3 emissions over a corn canopy in Central Illinois using REA; (2) inter-comparison of 4 h NH_3 flux measurements using REA with 0.5 h measurements from an FG system; and (3) evaluation of closure with DeNitrification DeComposition modeling estimates of NH_3 emissions using field measurements – specifically, quantifying flux of NH_3 in a spatially inhomogeneous study domain (i.e., a domain with variation in crop type and field management practices).

My work is part of a broader field of research on emission, fate, and transport of NH_3 at the biosphere-atmosphere intersection, broadly separated into four major research themes: (1) the effect of NH_3 on the global Nitrogen Cycle (Appel et al., 2011; USEPA SAB, 2011); (2) the role

of NH_3 in formation of secondary pollutant aerosols and other adverse environmental effects (Li et al., 2016; Bullard et al., 2017); (3) field-scale measurements and new methods to quantify atmospheric NH_3 concentration and bi-directional flux (Walker et al., 2013; Miller et al., 2014; Sun et al., 2015); and (4) development of improved NH_3 emission models, including bi-directional flux modeling (Pleim et al., 2013; Flechard et al., 2013; Balasubramanian et al., 2015). Together, this field of research seeks to better understand the role and impact of NH_3 in the environment and provide data to inform future regulatory and mitigation strategies.

1.7.1 Objective 1: Measurement of Season-Long Ammonia Emissions using Relaxed Eddy Accumulation

Walker et al. (2013) stated that new measurements are needed to better understand the biosphere-atmosphere exchange of NH_3. Consistent with the need identified by the USEPA SAB (2011), Walker et al. specifically called for field measurements throughout the duration of the growing season – with particular focus on the period from planting until peak leaf area index (LAI). Objective 1 addresses this need through a season-long field campaign to measure NH_3 flux above an experimental field plot planted with corn during 2014. This objective provides results important to more fully understand NH_3 emissions by characterizing the temporal variability of emissions throughout the season. Objective 1 is comprised of four sub-objectives.

1.7.1.1 Objective 1a: Design and validate REA system for the field campaign

Prior to the intensive field campaign described in Objective 1b, a REA measurement system was designed and assembled at the Illinois State Water Survey (ISWS) and tested at the Illinois Climate Network (ICN) site on the ISWS campus to provide quality assurance of the experimental setup and to mitigate issues that could result in bias, errors, or data loss. Initial troubleshooting was completed and all instruments and sensors were calibrated against standard

methods or ICN data collected at the same site. Because this research seeks to measure NH_3 flux immediately after planting through the duration of the season, it was important to have all troubleshooting completed before the growing season began. *Objective 1a is important for proper quality control to confirm that all software and hardware was correctly calibrated and working prior to the field campaign.*

1.7.1.2 Objective 1b: Measure NH_3 Flux at the Energy Farm using REA

Using the REA method, 4 h mean atmospheric NH_3 concentration and bi-directional NH_3 flux were measured over a fertilized corn field in Central Illinois for the duration of the 2014 corn-growing season. These data were used to develop a better understanding of NH_3 exchange throughout the corn-growing season, focusing particularly on the period from planting to peak LAI, identified by Walker et al. (2013) as an under-measured period of crop development. *Objective 1b represents the first study of above-canopy NH_3 flux from an intensively managed corn field in the Midwest US for the duration of the corn-growing season and provides new data describing the temporal variation of NH_3 flux.*

1.7.1.3 Objective 1c: Develop Footprint Correction Method for Integrated Flux Measurements

Micrometeorological flux measurement methods rely on the assumption of spatial homogeneity across the measurement footprint (Baldocchi et al., 1988). However, localized factors such as soil pH, soil moisture, and crop type have been shown to effect NH_3 flux from agricultural ecosystems (Bennett et al., 2013). Fast-response micrometeorogolical methods account for this by excluding data where the measurement footprint exceeds an area of relative homogeneity (e.g., when multiple crop types contribute to a measured flux). However, the process of excluding data is not straightforward with accumulating methods such as REA

because a single data point may represent multiple measurement hours. Further, accumulating measurement methods typically result in fewer data (e.g., one 4 h accumulating measurement is equivalent to 144,000 10 Hz measurements over the same time period), meaning exlusion of a single accumulated measurement is a larger loss relative to the overall data set. Hence, methods to quantify uncertainty and correct accumulating measurements due to an inhomogenous study domain are important. *Objective 1c presents new methods for quantifying the relative contributions from multiple, different agricultural fields, in accumulated flux measurements due to an inhomogenous study domain and for correcting such measurements with a coupled measurement-model approach.*

1.7.1.4 Objective 1d: Comparison of NH_3 Flux Results in Central Illinois with Other Studies

Because the spatial extent of NH_3 flux measurements is limited (Section 1.3.4), it is important to compare new flux measurements with the limited results presented in the literature. As previously mentioned, there is only one study of NH_3 flux over a corn canopy where measurements are reported for the period immediately after fertilization through full canopy development (Walker et al., 2013). The study plot used by Walker et al. was located in North Carolina and differed from common field-management practices in Illinois. Specifically, the study plot in Walker et al. was fertilized twice, once before and once after planting, as compared to a typical Illinois farm-management practice of a single fertilizer application immediately before planting. *Objective 1d compares NH_3 flux measurements in Central Illinois with measurements by Walker et al. to investigate the effect of different field management practices. This objective helps to inform future NH_3 flux measurements and to understand the spatial extent*

of NH_3 flux measurements required to adequately evaluate emission inventories and NH_3 flux models.

1.7.2 Objective 2: Inter-comparison of Relaxed Eddy Accumulation and Flux-Gradient Measurement Methods

Comparative studies of measurement techniques are important to understand the benefits and limitations of different methods (von Bobrutzki et al., 2010). The REA system described in Objective 1 was operated concurrently with an FG system, designed and operated by the National Oceanic and Atmospheric Administration (NOAA) Air Resources Laboratory Atmospheric Turbulence and Diffusion Division (ATDD). The FG system measures NH_3 flux in 0.5 h averaging intervals, while REA averages over a 4 h interval. Objective 2 represents the first comparative study of NH_3 flux above a fertilized corn canopy in the US as measured by concurrent use of a REA and a FG system and is comprised of two sub-objectives.

1.7.2.1 Objective 2a: Quantify NH_3 Flux using the FG Method[*]

Objective 2a represents the first implementation of the FG method to quantify NH_3 flux over a corn canopy in Central Illinois. *This objective is important because it provides new, higher temporal resolution (0.5 h) measurements of NH_3 flux that are required to evaluate process-based models describing NH_3 flux from agricultural ecosystems, such as Volt'Air-NH_3*

[*] ***A brief note on my specific contributions to objective 2a:*** NOAA designed and constructed a FG system to quantify NH_3 flux at the Energy Farm during the 2014 corn-growing season. I provided significant technical and field support to deploy and operate the FG system during the season. NOAA completed all initial calculations of NH_3 flux using the FG system before providing data to me. I worked closely with NOAA colleagues on data quality and we collaboratively developed the flux data set presented here. All subsequent analysis is my own.

and SURFATM-NH_3. Further, this objective provides the first reported measurement of diurnal NH_3 flux over a corn canopy in the Midwest.

1.7.2.2 Objective 2b: Inter-compare REA and FG Measurement Methods

Measurements using the REA and FG methods were inter-compared and evaluated for closure based on the methods of previous measurement inter-comparisons presented in the literature (VonBobrutzki et al., 2010; Walker et al., 2013). Results were compared to investigate agreement between maximum emission and timing, overall pattern of NH_3 flux, and observed flux variability. An analysis of cost and complexity for both measurement methods was performed. *Objective 2b provides new data comparing NH_3 flux measurements at a single site using 0.5 h and 4 h temporal resolution. Such data are important to understanding the temporal extent of measurements required to capture features of biosphere-atmosphere NH_3 flux profiles and guide future measurement and model developments.*

1.7.3 Objective 3: Evaluation of Closure Between DeNitrification DeComposition Model for NH_3 Flux and Relaxed Eddy Accumulation Measurements[*]

There is a need for increased measurement of fine resolution (1 km radius) NH_3 emissions combined with collection of ancillary data to improve the accuracy of emission estimates for air quality models (Cooter et al., 2010; Flechard et al., 2013). Validation of emission models has been identified as a research need to improve air quality models (Sutton et al., 2007). Objective 3 addresses both of these needs by using NH_3 flux measurements, coupled

[*] ***A brief note on my specific contributions to work described within Objective 3.*** All DNDC model runs were completed by Srinidhi Balasubramanian alone. I worked collaboratively with Ms. Balasubramanian and colleagues at UIUC, ISWS, and NOAA to develop input data sets described in Objective 3a, specific modeling cases and methods for footprint evaluation in Objective 3b, and methods for closure evaluation in Objective 3c.

with measurement of ancillary environmental parameters, to evaluate closure between REA measurements and a DNDC NH_3 flux model. Results from this objective are important to enable future up-scaling of modeled NH_3 fluxes using DNDC from the site to the regional scale.

Results from Objectives 1 and 2 were used to inform and evaluate modeling efforts by other University of Illinois at Urbana Champaign (UIUC) Department of Civil and Environmental Engineering students. Objective 3 focuses on the evaluation of NH_3 emission estimates using the DNDC model and development of a new method to evaluate closure between modeled and measured results. Objective 3 is composed of three sub-objectives.

1.7.3.1 Objective 3a: Development of Input Datasets for DNDC Model Runs

Objective 3a couples measured environmental parameters and above-canopy NH_3 flux measured at the Energy Farm with a DNDC model to predict NH_3 flux from fertilized cropland. Specifically, measurements of precipitation, solar radiation, wind speed, soil moisture, leaf wetness, and soil heat flux combined with detailed information of Energy Farm management practices such as fertilizer and herbicide application rates, tillage method, and planting density were developed as model inputs for estimation of NH_3 flux using DNDC. *Objective 3a develops a new baseline data set for an NH_3 emission model with improved temporal and spatial resolution compared to existing NH_3 emission models.*

1.7.3.2 Objective 3b: Develop Method for Closure Evaluation

To effectively evaluate model/measurement closure, data representative of a single study domain are required. In practice, this is challenging unless measurements are performed in a large study plot (> 3 km x 3 km). In the case of NH_3 measurements, the need for a large study plot is further complicated by the relatively high power requirements (120 V, > 15 amps) for REA or FG measurement equipment, thereby limiting the options for available research plots.

Flux measurements are commonly conducted in smaller (< 1.5 km x 1.5 km) study plots to provide ready access to equipment and power (Myles et al., 2007; Myles et al., 2011; Walker et al., 2013). As such, it is important to develop methods to evaluate model/measurement closure for cases where measurements are not collected in a spatially homogenous study domain. *Objective 3b presents a new method to evaluate model/measurement closure when spatially homogenous NH_3 flux measurements are not available.*

1.7.3.3 Objective 3c: Evaluation of Closure Between Modeled and Measured Results

This objective focuses on implementation of the closure evaluation method developed in Objective 3b and provides statistical analysis for model/measurement closure. *Objective 3c provides important new information about the ability of DNDC to estimate early-season NH_3 flux profiles and highlights practical challenges of model/measurement closure evaluation with recommendations for improvement.*

CHAPTER 2: MEASUREMENT OF SEASON-LONG AMMONIA FLUX USING THE RELAXED EDDY ACCUMULATION METHOD*

2.1 Research Motivation and Significance for Objective 1

Measurements of NH_3 flux to the atmosphere from anthropogenic activities are important for understanding the links among emission sources and transformation and fate of NH_3 in the atmosphere (Galloway et al. 2008). NH_3 emissions from the use of chemical fertilizers in agriculture are not well quantified (Bash et al., 2010; Walker et al., 2013), limiting the ability to accurately predict environmental and economic impacts. This uncertainty also affects the quality of evaluations of models designed to predict NH_3 emissions (Paulot et al., 2014; Balasubramanian et al., 2015), secondary pollutant formation (Gilliland et al., 2006), deposition of nitrogen species (Appel et al., 2011), and estimation of anthropogenic climate forcing (Myhre et al., 2013).

EC approaches to quantify flux require the availability of a precise (± 10% precision), fast-response (e.g., 10 Hz) sensor to measure concentration of the constituent of interest (Phillips et al., 2004). The eddy correlation and REA methods are attractive for the quantification of NH_3 fluxes because they do not rely on fast-response sensors to measure NH_3 concentration (Myles et al., 2011). However, a drawback to these methods is that they are labor intensive, and temporal resolution is limited by the need to acquire adequate NH_3 mass in the sampling reservoirs for quantification in the laboratory.

REA provides the ability to quantify trace gas fluxes based on conditional measurement of gas concentrations at a constant sample flow rate (Businger and Oncley, 1990). REA has been

* Reproduced in part with permission from A.J. Nelson, S. Koloutsou-Vakakis, M.J. Rood, L. Myles, C. Lehmann, C. Bernacchi, S. Balasubramanian, E. Joo, M. Heuer, M. Vieira-Filho and J. Lin (2017) Season-long ammonia flux measurements above fertilized corn in central Illinois, USA, using relaxed eddy accumulation, *Agr. Forest Meteorol*., 239, 202–212

used to measure fluxes of trace gases to the atmosphere with temporal resolution on the order of hours when gas concentrations cannot be measured instantaneously (Baker et al., 1992). The REA method requires the use of an empirically derived REA coefficient (β) to describe the relative contributions to flux of turbulent updrafts and downdrafts (Baker et al., 1992).

This chapter presents results from a study to quantify above canopy NH_3 concentration and flux from fertilized corn in an intensively managed agricultural ecosystem in the Midwest US. The study was conducted for the entire 2014 corn-growing season (day of year, DOY, 115 – 273) using the REA method. Measurements were also made at the same location over fallow land in March 2015 to characterize background NH_3 fluxes and concentrations after frost and before any fertilization activities. This research seeks to provide a better understanding of land-atmosphere NH_3 exchange due to fertilized corn and to quantify such exchange in an environment where field management practices and their timing are highly variable. Emphasis was placed on the period from planting to peak LAI, an important under-measured period for NH_3 emissions during crop development (Walker et al., 2013). The four-hour measurement interval used in Objective 1 provides improved information about shorter-term (< 1 day) NH_3 emission intensity from corn in the Midwest US. These measurements are important to improve understanding of how managed agricultural ecosystems impact air quality, contribute to the global Nitrogen Cycle, and to evaluate current NH_3 emission models. ***Objective 1a*** focuses on the design and validation of the REA system for use in the field campaign, ***Objective 1b*** is the measurement of NH_3 flux at the Energy Farm using the REA method, ***Objective 1c*** develops a new method for footprint correction of integrated flux measurements, and ***Objective 1d*** compares NH_3 flux measurements in Central Illinois with other reported NH_3 flux results.

2.2 Methods

2.2.1 Objective 1a: Implementation of REA Method

2.2.1.1 Setup and Calibration of Equipment Prior to Field Campaign

The REA system was setup, tested, and validated at ISWS, located at 2204 Griffith Dr., Champaign, IL 61820. This location was selected for the preliminary work because of the availability of an indoor high-bay area where equipment was assembled and calibrated during the winter months. Following indoor assembly and verification that the sensors were wired and operating correctly, the sampling equipment was moved outside to the secure ICN site at the south end of the ISWS campus (40° 5’ 02.1” N, 88° 14’ 24.9” W).

The ICN site was located in an open clearing free of trees or other vertical obstructions with sod groundcover. A tree line borders the site on the east, west, and south at a distance of 150 m, 30 m and 45 m, respectively. Buildings of the ISWS campus border the site to the north, with the nearest building (single story) located 65 m away.

Equipment was mounted to a stainless steel instrumentation tripod (model CM-120, Campbell Scientific, Logan, UT), extendable to a full height of 6.1 m. The tripod was leveled and staked into the ground using two 0.3 m long galvanized stakes at each of the three tripod feet. A lightning rod was fixed to the top of the tripod and connected to a 1.2 m copper grounding rod with 4 AWG stranded copper cable to provide Earth ground. The tripod was stabilized with guy wires extending from the top of the mast to each of the three tripod feet. A schematic of the instrumentation tripod with the REA system and environmental instrumentation is presented in Figure 2.1.

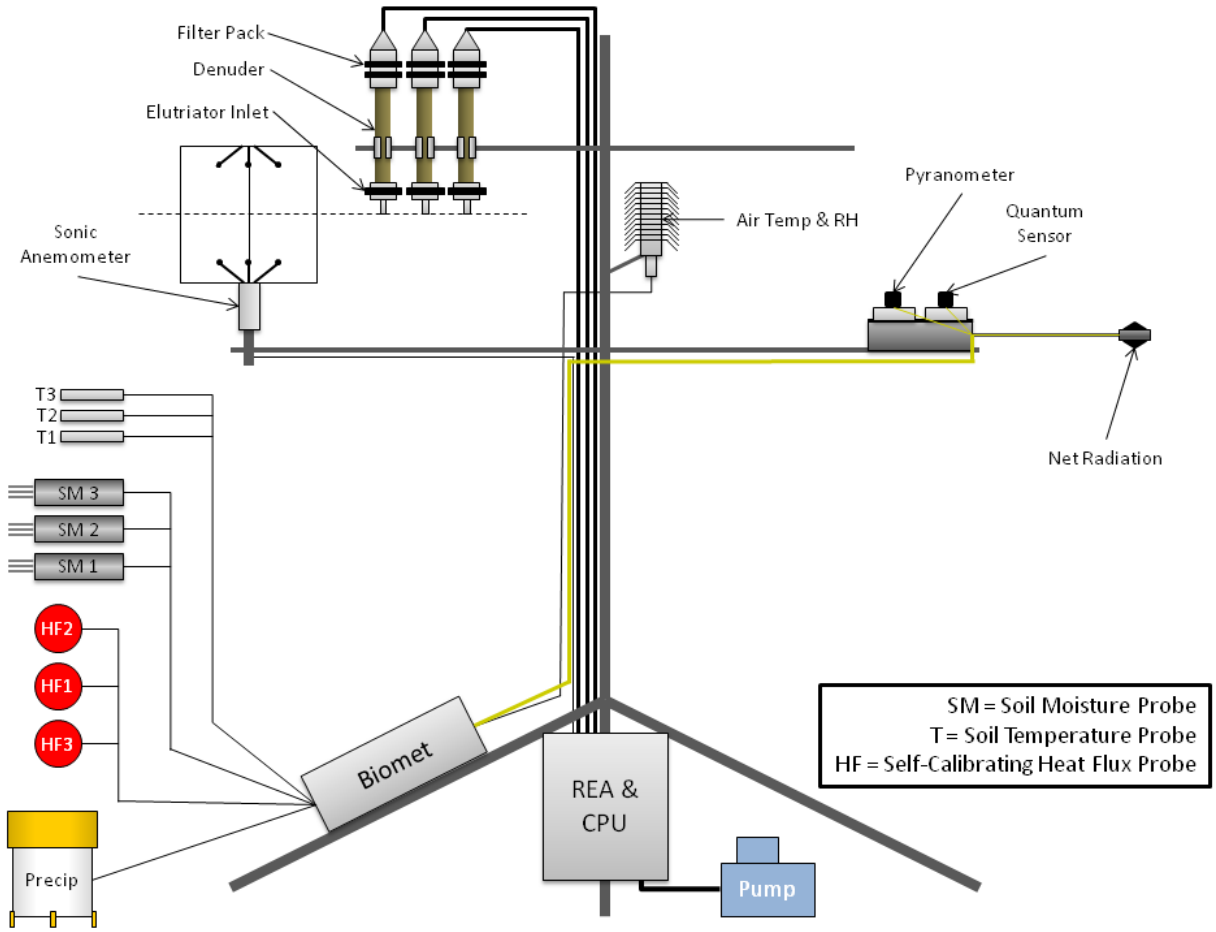

Figure 2.1: Schematic of the sampling tower including the relaxed eddy accumulation (REA) system sensors for measuring environmental parameters.

2.2.1.2 Measurement of Environmental Parameters

Atmospheric temperature, relative humidity (RH), precipitation as rain, photosynthetically active radiation (PAR), global solar radiation, soil temperature, soil moisture content, net radiation, and soil heat flux were measured using a Biomet system (model 102, LI-COR, Lincoln, NE) with an integrated data logging system. Resolution and accuracy of the instruments included in the Biomet, where available from the manufacturer, are listed in Table 2.1.

Parameter	Instrument	Resolution	Accuracy
Ambient temperature	Humidity and Temperature sensor (Vaisala HMP155) with radiation shield (RM Young 41005-5).	Not available from manufacturer	-80 to +20 °C: ±(0.226 - 0.0028 x T) °C +20 to +60 °C: ±(0.055 + 0.0057 x T) °C
Relative humidity	Humidity and Temperature sensor (Vaisala HMP155) with radiation shield (RM Young 41005-5).	0 to 40 %RH ±0.6 %RH 40 to 97 %RH ±1.0 %RH	+15 to +25 °C: ±1 %RH for 0 to 90 %RH ±1.7 %RH for 90 to 100 %RH -60 to -40 °C: ±(1.4 + 0.032 x reading) %RH -40 to -20 °C: ±(1.2 + 0.012 x reading) %RH -20 to +40 °C: ±(1.0 + 0.008 x reading) %RH +40 to +60 °C: ±(1.2 + 0.012 x reading) %RH
Net solar radiation	Net Radiometer (Kipp & Zonen NR Lite2)	10 µV/W/m²	< 1%
Solar radiation	Pyranometer Sensor (LI-COR LI-200SL-50)	90 µA per 1000 W m^{-2}	< ±5%
Photosynthetic Photon Flux Density	Quantum Sensor (LI-COR LI-190SL-50).	5 µA per 1000 µmol s^{-1} m^{-2}	< ±5%
Precipitation	Rain/Precipitation gauge (Texas Electronics TR-525USW)	0.1 mm	1.0 % up to 50 mm/hr
Soil temperature	Thermistor (LI-COR 7900-180)	Not available from manufacturer	-20 to +50 °C: 0.5 °C
Soil heat flux	Heat flux plate (Huskeflux HFP01SC)	± 3 % reading	-30 to +70 °C: 50 µV/Wm2

Table 2.1: Description, resolution, and accuracy of instruments used to measure environmental parameters with the Biomet system.

The Biomet system was wired in the indoor field staging area at ISWS between December 2013 and March 2014. The system was moved to the outdoor ICN site on March 7, 2014, where preliminary data were collected. Open space in the cable pass-through holes at the bottom of the enclosure was filled with loosely packed plastic kitchen scrubbing pads to keep out dirt, debris, bugs, and rodents. The enclosure was mounted to the leg of the tripod with U-bolts, and 14 AWG solid core copper wire was used to connect the enclosure grounding lug to the tripod grounding lug.

RH and temperature measurements were collected using a non-aspirated humidity and temperature probe (model HMP155, Vaisala, Vantaa, Finland) equipped with a multi-plate radiation shield (model 41003 R.M. Young Company, Traverse City, MI). The sensor with radiation shield was mounted to the measurement tripod using a band clamp and was located at the same height as the REA measurement equipment (described in a subsequent section). The HMP155 has an operating temperature range from -40 °C to +65 °C and operating humidity range of 0% to 100% RH and was manufacturer-calibrated prior to delivery. During long-term operation (> 1 month), the sensor was checked monthly to make sure the radiation shield was free of debris and that no contamination was present on the sensor probe.

Precipitation was monitored with a tipping bucket rain gauge (model TR-525M, Texas Electronics, Dallas, TX). Because this field campaign was focused on measuring NH_3 exchange during summertime crop growth, a heater was not used for the precipitation gauge since all precipitation was anticipated as rain. The precipitation gauge was mounted on a horizontal cross arm extending 1.5 m from the tripod mast and maintained at a minimum height of 15 cm above any vertical obstructions (e.g., crops, other sampling equipment). The gauge was calibrated by the manufacturer prior to delivery and was leveled using the integrated bubble level. During

long-term operation, the screen in the funnel of the rain gauge was checked weekly for obstructions. The funnel was removed on a monthly basis to clear the tipping bucket of accumulated dirt, bugs, and other debris.

PAR, defined as electromagnetic radiation with wavelength of 400 nm to 700 nm (Biggs et al., 1971), was quantified as photosynthetic photon flux density (photons per time per surface area) using a quantum sensor (model LI-190SL, LI-COR, Lincoln, NE). Global solar radiation was measured with a silicon photodiode pyranometer (model LI-200, LI-COR, Lincoln, NE). Net radiation, the balance between solar and reflected surface radiation, was measured with a net radiometer (model NR Lite 2, Kipp & Zonen, Bohemia, NY). All radiation sensors were supplied with factory calibration from the manufacturer that was valid for the duration of the field campaign.

The quantum sensor, pyranometer, and net radiation sensors were attached to the tripod using a radiation sensor mount (model 7900-350, LI-COR, Lincoln, NE). The arm of the net radiation sensor was oriented to the south, and care was taken that no shadows were cast over the sensors or the surface area measured by the net radiometer. The radiation sensors were leveled using the integrated bubble level on the net radiometer and sensor mount. Radiation sensors were cleaned on a monthly basis using deionized (DI) water and a microfiber cloth, as recommended by the manufacturer.

Soil temperature was measured with thermistors (model 7900-180, LI-COR, Lincoln, NE) and soil heat flux was measured with self-calibrating heat flux plates (model HFP01SC, Hukseflux, Manorville, NY). Three each of thermistors and self-calibrating heat flux plates were used. Holes were dug with a straight-sided spade to a depth of 5 cm. Care was taken to remove the soil in a single sample. The holes were evenly distributed at three points on a circle with

radius of 4 m, centered beneath the tripod. In each hole, a soil heat flux plate was inserted into the soil on the smooth-sided edge of the hole at a depth of 5 cm. A thermistor was inserted into the opposite side at a depth of 5 cm. At least 10 cm of the lead wire was coiled and placed in the bottom of the hole to mitigate heat transfer through the wires before replacing the soil and tamping it in place by foot.

Soil moisture was measured with soil moisture probes (model ML2x, Delta-T, Cambridge, UK). Three moisture probes were co-located with the soil temperature and heat flux sensors. Probes were inserted at a 70° angle relative to the soil surface until the plastic base was in firm contact with the soil surface.

All sensors described in this section were wired to a centralized datalogger (model XLite 9210, Sutron Corp., Sterling, VA). The datalogger was installed in a weatherproof enclosure, and sensors were connected to the input/output modules using manufacturer-provided wiring. The enclosure was grounded to the tripod ground lug with 12 AWG stranded copper wire. The datalogger was connected via serial connection to a computer running Windows 7, and specific manufacturer-provided sensor calibration data were input using the supplied XTerm software. Data were collected at a rate of one sample per minute and stored on an internal flash drive in the datalogger. A photograph of the datalogger layout inside the weatherproof enclosure is provided in Figure 2.2.

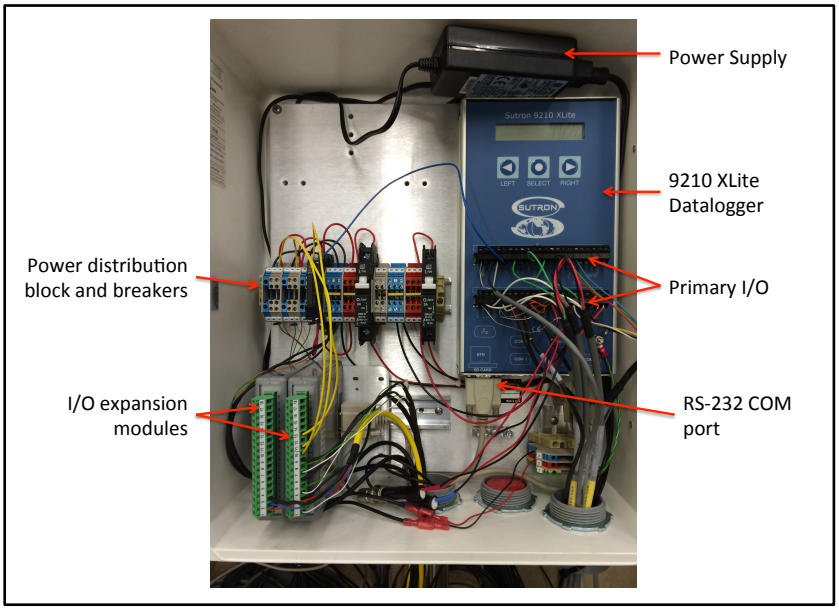

Figure 2.2: Photograph of the Biomet data logger, power distribution block, and I/O expansion modules inside the weatherproof enclosure.

The REA system and Biomet were setup at the ICN site on March 7, 2014 (Figure 2.3). The centerline of the anemometer was 3.75 m above the soil. This height was selected as a typical value for validating the operation of the equipment. The anemometer was oriented according to manufacturer instructions, with one arm of the transducer cage oriented to magnetic north. The Biomet was operated continuously from March 8 to March 17, 2014. Data were collected from the Biomet datalogger on March 17 by downloading to a laptop computer.

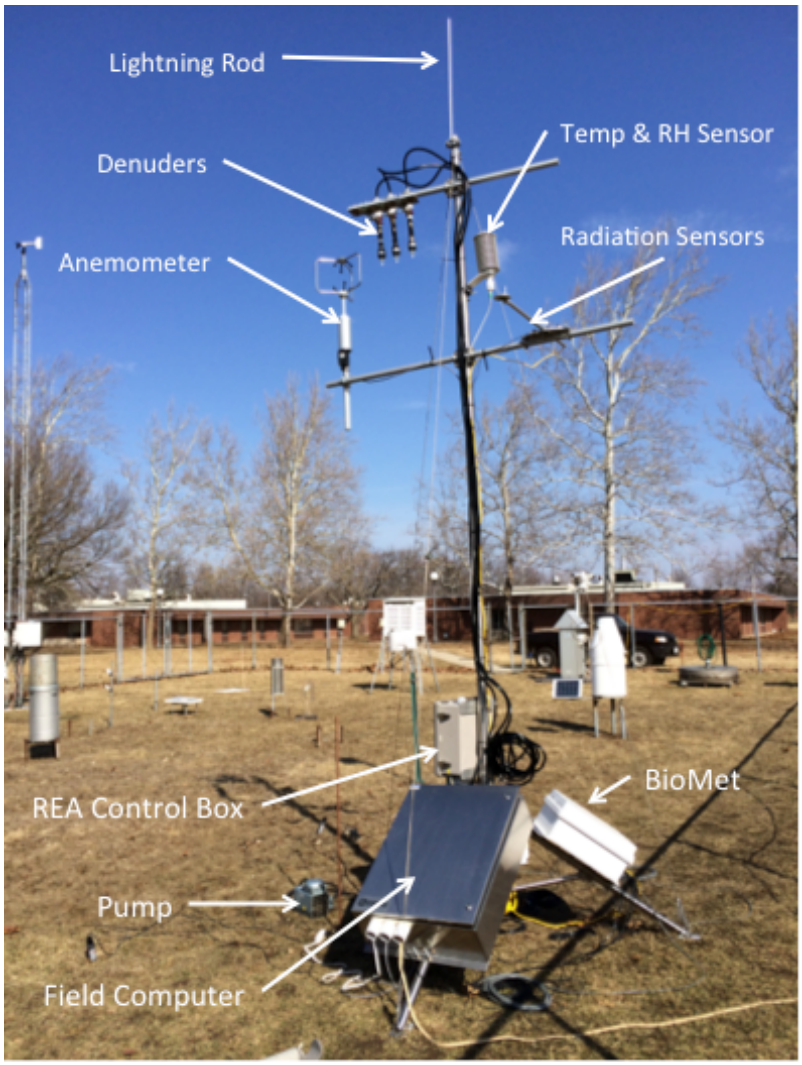

Figure 2.3: Photograph of the Relaxed Eddy Accumulation (REA) system and Biomet deployed at the Illinois Climate Network (ICN) site.

Environmental data were averaged over 30 min time intervals and mean values were plotted. Because soil temperature, moisture content, and heat flux were measured in triplicate, mean values from each sensor location were further combined to present a 30 min mean average of the triplicate measurement.

2.2.2 Objective 1b: Measurement of NH_3 Flux at the Energy Farm Using REA

2.2.2.1 Experimental Field Site Description

The field campaign took place during the 2014 corn-growing season at the UIUC Energy Biosciences Institute (EBI) Energy Farm in Urbana, IL. Illinois is located in the flat terrain geographical region known as the Midwest and belongs to the Midwest NCA climate region. The lack of mountains and distance from the ocean (> 1000 km) result in wide extremes of temperature and precipitation that can occur over days, weeks, months, and years, while all seasons have potential for damaging winds (USDOC-NOAA, 2013).

The Energy Farm (described by Zeri et al., 2011) was subdivided into four different 200 m x 200 m research plots. Research plots to the west, north, and east were planted with miscanthus, switchgrass, and a mixture of 28 different native prairie species, respectively (Zeri et al., 2011). A private field due south of the study plot was planted with corn during the last week of April 2014. The private field extended south 800 m to the next road and was separated from the experimental field plot by a 15 m wide dirt and grass track.

The southeastern most plot of the Energy Farm, hereafter referred to as the study plot, was planted with corn and was the location for this research (40° 3’ 46.209” N, 88° 11’ 46.0212” W, 220 m above sea level). A detailed record of farm activities occurring at the site, including planting date, fertilizer and herbicide type and application rate and date, and crop yield was maintained by EBI personnel. These data are important for overall quality control and the ability to accurately interpret results. The study plot was serviced with two 20 A, 110 VAC circuits. Based on Champaign, IL ICN data (located 4.4 km northwest of the Energy Farm) from 1979 to 2009, the mean annual temperature at the site was 11.1 °C and mean annual accumulated rainfall was 1,041.7 mm (Zeri et al., 2011). ICN data from February 1989 through 2013 (data for mean

wind direction was not available prior to February 1989) was used to determine the mean wind direction of 192.5° (ISWS, 2017). Figure 2.4 depicts the wind rose at the study plot during the 2014 growing season and its neighboring fields.

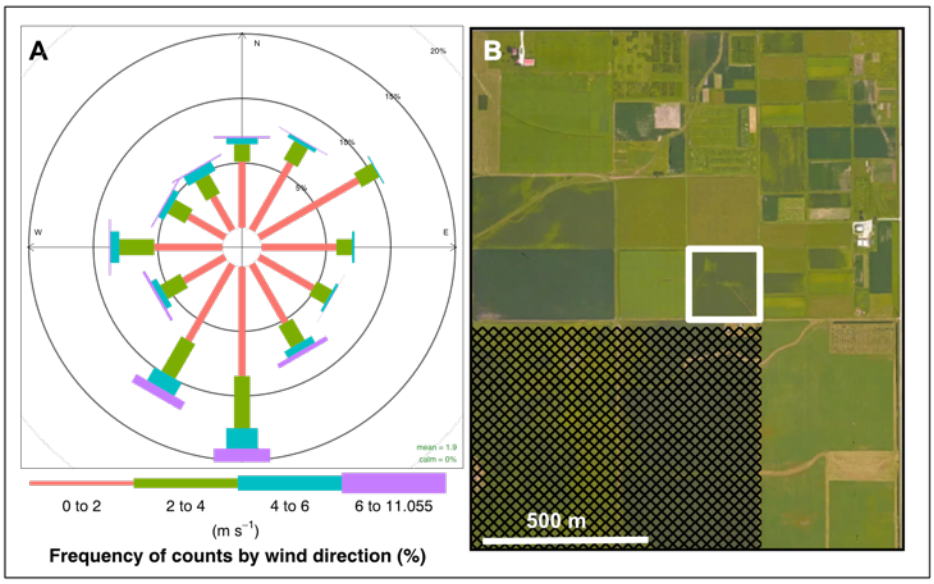

Figure 2.4: a) Wind rose during 2014 growing season at the study plot (DOY 115 – 273). b) Satellite view (Google Maps, 2016) of the study plot (outlined in white) and neighboring fields. Crosshatched areas correspond to neighboring fields that were also planted with corn.

Site selection was influenced by a number of factors: (1) management practices at the study plot were representative of conventional farm management practices in the area (e.g., chisel plow tilling, fertilization, and herbicide application) and historical records dating to 2008 were readily available; (2) on-site meteorological data were available from 2009 through the 2014 growing-season from another study that used eddy covariance for measurements of CO_2 and water vapor fluxes (described first in Zeri et al., 2011); (3) ready access to the site was available for installation; and (4) protection of instrumentation due to activities in the field was accommodated. Considering the fetch of the study plot (100 - 140 m), the scope of the study, logistics associated with NH_3 flux sampling, and challenges with access to third party property, this study plot was selected as the best site to meet the objectives of this research.

Canopy height, h_c, was measured twice weekly following crop emergence. The study plot was divided into four quadrants and four plants were measured at the center of each quadrant for a total of 16 measurements. Total growing degree days (GDD) – defined as the sum of average daily low and high temperatures minus 50 °F – was calculated and used to predict crop growth stage (Nafziger, 2014). Additionally, growth stage was evaluated once weekly by visual inspection as described by Abendroth and Elmore (2014). Prof. Carl Bernacchi's Environmental Plant Physiology Group (UIUC Department of Plant Biology) measured LAI weekly using a nondestructive plant canopy analyzer (model LAI-2200, LI-COR, Lincoln, NE)

2.2.2.2 Field management practices

The study plot was planted with a corn-corn-soybean crop rotation from 2008 through 2014. Soybeans (variety Asgrow® A3555, Monsanto, St. Louis, MO) were cultivated at the study plot in 2013. Standard agricultural practices for Central Illinois were used at the study plot. Diammonium phosphate, potash, and lime were applied using variable-rate technology to achieve the desired whole-farm soil fertility goal (pH: 6.0; 50.4 kg-P ha^{-1}; 336 kg-K ha^{-1}). The study plot was sprayed with 168 kg-N ha^{-1} as 28% UAN fertilizer containing a urease inhibitor (Agrotain®) and 7.0 L ha^{-1} pre-emergent herbicide (Lumax®, Syngenta: Basel, Switzerland), and immediately tilled, in the morning of May 6, 2014 (DOY 126). Corn (Dekalb® DKC64-69, Monsanto: St. Louis, MO) was machine-sown with 76 cm row spacing in the afternoon of May 6, 2014 at a seeded population of 86,000 plants ha^{-1}. Hand planting was used around the sampling equipment at the center of the study plot. Herbicide (Roundup® Powermax, Monsanto: St. Louis, MO) was applied as needed to control grass and broadleaf weeds prior to emergence. The same herbicide was applied to the entire plot on June 6, 2014 (DOY 157) at 1.6 L ha^{-1}. The neighboring cornfield was fertilized with 201 kg-N ha^{-1} on March 26, 2014 (DOY 85; 33 kg-N

ha^{-1} as 28% UAN and 168 kg-N ha^{-1} as 82% anhydrous NH_3) (personal communication with EBI Energy Farm manager).

2.2.2.3 Relaxed Eddy Accumulation System

The REA System and Biomet were transported to the Energy Farm in April, 2014. All equipment was setup in the same manner described in Section 2.2.1.2. Due to the un-level nature of the recently tilled field and loose pack of the top soil, concrete pavers (20 cm wide, 40 cm long, 5 cm high) were placed beneath each of the measurement tripod feet. Holes were drilled through the pavers and stakes were driven through the tripod feet and pavers into the soil. For additional wind protection, guy wires were extended from the top of the tower to the ground at a radius of 5 m from the center of the tripod. All wires for buried sensors were run through 2.5 cm inner diameter (ID) polyvinyl chloride (PVC) pipe to protect against tripping and damage from rodents, animals, and other equipment.

A REA control box was used to control gas flow and switching denuders during updraft, downdraft, and deadband conditions. The control box was similar to the one described in Meyers et al. (2006). The REA control box contained a mass flow controller (MFC) (model GFC371, Aalborg, Orangeburg, NY) and a sampling manifold with three solenoid valves (model 2W13W-9DB-A6C5, Snap-Tite Inc, Erie, PA). An integrated logic board controlled switching of the solenoid valves. Quick-disconnect fittings were used for connecting a rotary vane vacuum pump (model 0523, Gast Manufacturing Inc., Benton Harbor, MI) to the sampling manifold (Figure 2.5). Gas flow rate through the denuders was fixed at 20.0 L min^{-1} using the MFC.

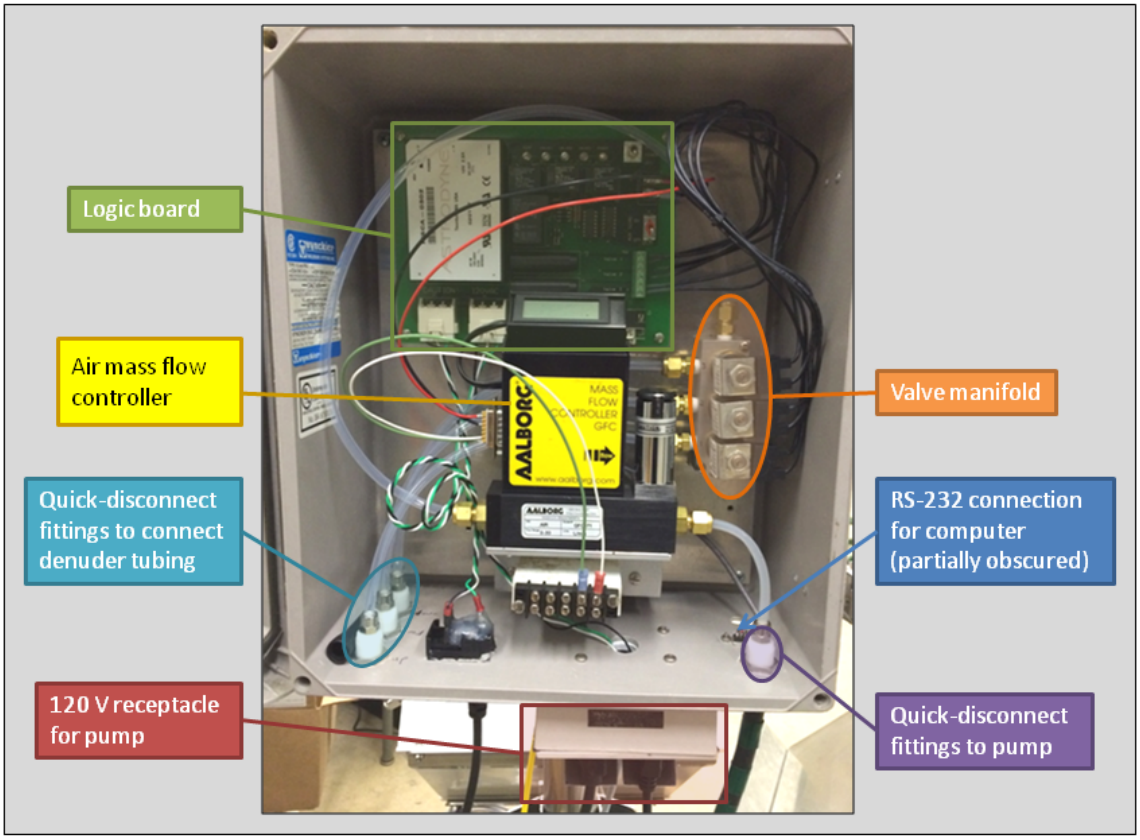

Figure 2.5: Photo of the custom-built REA control box provided by ATDD. Individual system components are highlighted for clarity.

The REA control box was connected via RS-232 to a field computer running Ubuntu and mounted in a stainless steel enclosure (model ENC 24/30S, Campbell Scientific, Logan, UT) mounted to a leg of the measurement tripod. The computer ran the open source REA control program, SONIC.C, developed by ATDD for use with the REA control box (Available online: ftp://ftp.atdd.noaa.gov/pub/dumas/software/sonic/). The most up-to-date version of the REA control program, Version 2.6.2, was used.

A three-axis ultrasonic anemometer (model 81000RE, R.M. Young Company, Traverse City, MI) measured *u*, *v*, and *w* at 10 Hz. Data were recorded using the field computer. Care was taken to mount the anemometer as close to vertical as possible to reduce error caused by off-axis

mounting. SONIC.C software rotated the anemometer coordinate system to align with meteorological coordinates and correct for tilt.

A dynamic deadband was implemented using a 5 min moving boxcar average to calculate the sampling threshold $\pm 0.3\ \sigma_w$. The use of a deadband serves to increase the difference between measured concentrations during updraft and downdraft conditions and reduce switching frequency of the valves (Bowling et al., 1999; Meyers et al., 2006). The deadband is a threshold value of vertical wind velocity that must be exceeded to trigger valve switching (Grönholm et al., 2008). Because the use of a dynamic deadband scales β based on atmospheric conditions, it allows the REA system to compensate for atmospheric non-stationarity that may occur during a multi-hour run (Grönholm et al., 2008). Corrected values of w_i were calculated in real time and compared to the sampling threshold once per second. Based on this analysis, the appropriate valve was actuated in the REA control box, following the conditions described in Table 2.2.

Condition	Sample Reservoir
$w_i < -0.3\sigma_w$	Downdraft
$-0.3\sigma_w \leq w_i \leq +0.3\sigma_w$	Deadband
$w_i > +0.3\sigma_w$	Updraft

Table 2.2: Definition of updraft, downdraft, and deadband conditions based on SONIC.C calculation of the dynamic deadband, 0.3 σ_w.

SONIC.C software recorded wind speed and temperature data at 10 Hz to a hard drive in the field computer. Further, the software calculated mean updraft, deadband, and downdraft temperature and σ_w in 30 min intervals to facilitate calculation of the REA coefficient and mean turbulent flux. All relevant parameters recorded to the field computer are described in Table 2.3.

Parameter	Symbol
Total updraft, deadband, and downdraft time (min)	$t_{\uparrow}, t_{\leftrightarrow}, t_{\downarrow}$
Vertical, streamwise, and lateral wind speed (m/s)	w, u, v
Standard deviation of vertical wind speed (m/s)	σ_w
Sonic temperature (°C)	T
Mean (30 min) updraft, deadband, and downdraft temperature (°C)	$\overline{T_{\uparrow}}, \overline{T_{\leftrightarrow}}, \overline{T_{\downarrow}}$

Table 2.3: Parameters for all relevant data recorded to the field computer via the SONIC.C software.

Three-channel annular glass denuders (model URG-2000-30x242-3CSS, URG Corp, Chapel Hill, NC) were selected for measuring trace NH_3 concentration. Denuders were fitted with glass elutriator inlets (model URG-2000-30K, URG Corp, Chapel Hill, NC) designed to remove particles with diameter ≥ 2.5 μm at 20 L min^{-1} (all flows are specified at standard conditions unless stated otherwise). Inlets were attached to the upstream end of denuders using a #30 coupler with a built-in Teflon impaction plate (model URG-2000-30P, URG Corp, Chapel Hill NC). Two-stage 47 mm Teflon filter packs (model URG-2000-30FG, URG Corp, Chapel Hill, NC) were utilized to collect PM for later analysis of particulate ammonium, nitrate, and sulfate by ATDD and to prevent damage to the solenoid valves and pump (Figure 2.6).

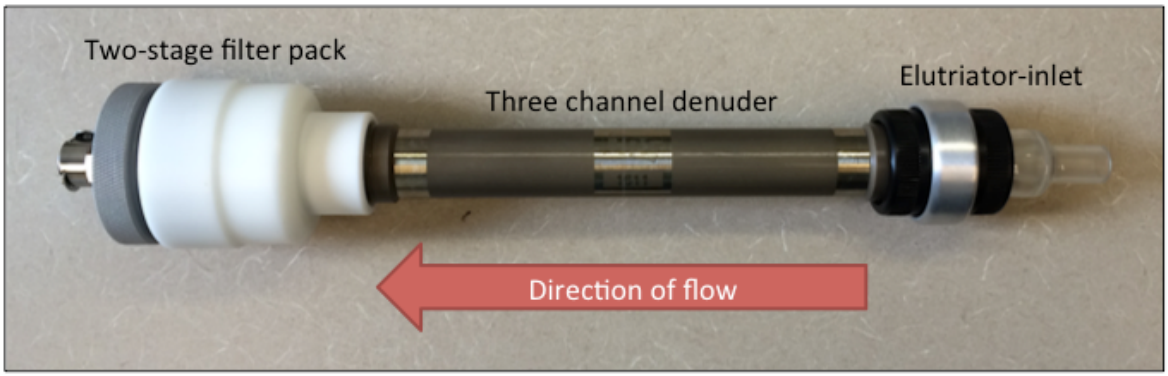

Figure 2.6: Photograph of REA denuder assembly comprised of an elutriator inlet, three-channel annular denuder, and a two-stage filter pack.

The inlet-denuder-filter systems (hereafter referred to as “denuder assemblies”) were positioned such that the elutriator-inlets were at the same height as the anemometer centerline,

defined as the vertical midway point between the upper and lower ultrasonic transducers. The denuder assemblies were oriented along a horizontal sampling axis, which passed through the centerline of the anemometer and was oriented perpendicular to the prevailing wind direction for the site (192.5°) (Figure 2.7).

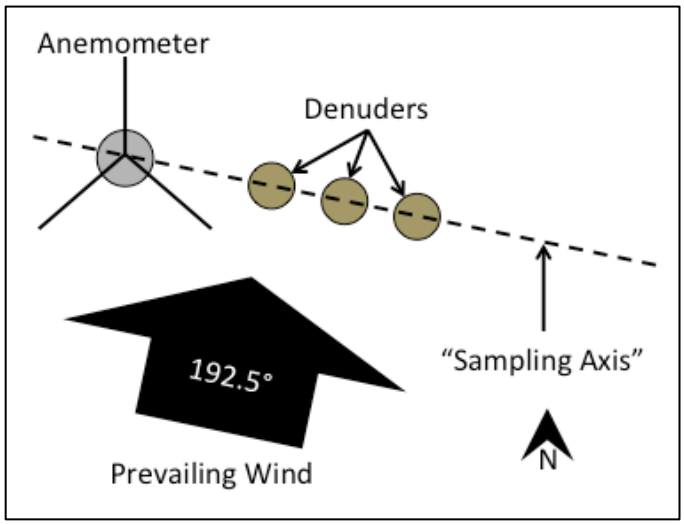

Figure 2.7: Schematic of top view of anemometer and denuder orientation and positions with respect to magnetic north and the prevailing wind direction.

Denuder assemblies were connected to the REA Control Box using 6.35 mm ID black PVC tubing (McMaster Carr, Chicago, IL) to supply controlled gas flow. Tubing for each assembly was 6 m in length and fitted with quick-disconnect ends. Care was taken to loosely coil excess tubing at the base of the measurement tripod without causing kinks. A mounting bracket was designed using broom handle clamps to fasten denuder assemblies, facilitating accurate vertical positioning. Four broom handle clamps were attached to an aluminum plate mounted vertically to the upper tripod cross arm using U-bolts. The mounting mechanism and vertical alignment of the denuder assemblies and anemometer is shown in Figure 2.8.

Figure 2.8: Photograph showing vertical position of denuders relative to sonic anemometer.

Four denuders were used for each REA sampling run: one each for updraft, deadband, and downdraft conditions and one as a field blank. The field blank denuder assembly was not actively sampled, but the inlet was exposed to the atmosphere during the REA sampling run to quantify NH_3 exposure caused by passive diffusion, advection, and denuder handling.

The complete REA sampling system is shown in Figure 2.9. Measurement height, z_m, was 2.0 m prior to corn emergence to reduce the probability of soil aspiration in the denuder assemblies. Measurement height was adjusted from 2.0 m to 4.5 m depending on canopy height (h_c) to avoid overestimating source/sink contributions from any single canopy element (Raupach, 1994).

Figure 2.9: REA sampling system (June 2014).

REA sampling runs were performed throughout the 2014 corn-growing season (as weather allowed) with focus on daily sampling during the first month after fertilization when peaks in NH_3 emissions have been measured in experiments at a location in North Carolina (Walker et al., 2013). Sampling did not occur during precipitation events because the aspiration of water into the denuders would affect the measurement accuracy. Samples were collected as often as possible during the first 30 days following fertilization. The sampling plan for the remainder of the season was scheduled to align with growth stages V5, V10, V15, VT, R3, and R6, depicted in Figure 2.10 (UI, 2009). However, adjustments to this schedule were required due to precipitation events and high winds (resulting in large flux footprint).

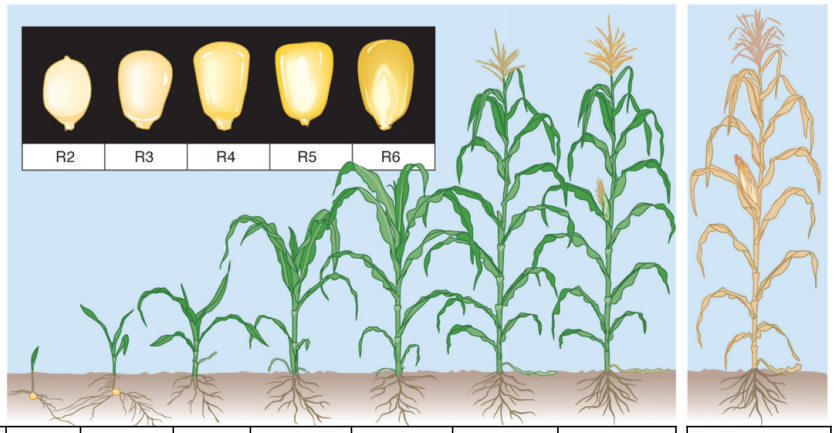

Growth Stage	VE	V1	V3	V7	V10	VT	R1	R6
GDD	115	155	315	635	845	1,350	1,400	2,700

Figure 2.10: Depiction of corn growth-stages and approximate growing degree days (GDD) needed to reach each stage. (Figure partially reproduced with modification from UI, 2009)

Sample duration was guided by the analytical detection limit for NH_4^+ and typical ambient NH_3 concentrations in the area. REA runs occurred from 07:30 – 11:30 am and 12:00 – 16:00 pm local time. These times were selected to represent average daily meteorology, to mitigate the effect of daytime atmospheric non-stationarity, and to avoid sampling during diurnal stability transitions at dawn and dusk. No nighttime samples were collected as the REA method is not expected to perform well in a stable boundary layer (Fotiadi et al., 2005).

2.2.2.4 Laboratory Preparation and Analysis of Denuder Assemblies[*]

All denuders were coated, extracted, and analyzed at the NADP Central Analytical Laboratory (CAL) by experienced CAL staff according to NADP Standard Operating Procedures (SOP) PR-4074.1 (NADP, 2012) and AN-4022.1 (NADP, 2014). Final assembly of the elutriator-inlets, denuders, and filter packs was not done by CAL staff but was carried out using CAL facilities.

[*] ***A brief note on my specific contributions to Section 2.2.2.4:*** NADP staff completed all coating and extraction of denuders. I, collaboratively with Dr. Marcelo Vieira-Filho, cleaned and assembled all denuders, elutriator inlets, and filter packs.

The CAL uses thoroughly validated quality assurance measures to reduce the potential for contamination of denuders during preparation and extraction. Denuders were handled in a clean air hood (model PVLF-72, Air Science USA LLC, Fort Myers, FL) designed to provide an environment free of NH_3. NH_3 concentration within the hood and the lab area is monitored using two-week integrated diffusive NH_3 samplers (model Radiello 123-7, Supelco, Bellefonte, PA).

Whenever handling equipment, laboratory personnel wore two layers of gloves: one pair of latex-free vinyl gloves (model 19-041-189, Fisher Scientific, Pittsburgh, PA) were put on first followed by one pair of polyethylene gloves (model Poly-D FoodMates, Ansell, Melbourne, Australia). This procedure has been observed to result in the least cross-contamination of NH_3 due to chemical composition of gloves and individual body chemistry (NADP, 2013). All plastic bags used for storage and transport were made of low density polyethylene (series F4 Double Track, Elkay Plastics, Chicago, IL). Coating, exposure, and extraction dates for all denuders and filter packs were tracked using an established CAL database and sequentially numbered bar-coding system.

Denuders (uncapped) and caps were soaked for at least 24 h at room temperature in DI water (model Advantage A10 w/ QTUM0TEX1 cartridge, Millipore, Billerica, MA) in 13.2 L covered high density polyethylene (HDPE) buckets (model S-9942, Uline, Pleasant Prairie, WI) prior to coating for use. Denuders and caps were rinsed for at least 1 min under flowing DI water after soaking and immediately prior to use. Clean denuders were capped and transferred to a chemical fume hood for coating. Downstream caps were removed, and denuders were filled with a 5 wt% phosphorus acid solution (98%, extra pure, Acros Organics, Geel, Belgium) until the glass channels were fully covered in solution. Downstream ends were capped, and denuders were inverted several times before resting for 1 min. Downstream caps were removed and denuders

were drained with gentle shaking to remove excess solution. Upstream caps were then removed, and the denuders were attached to a drying manifold (model URG-2000-30H4, URG Corp, Chapel Hill, NC) and dried under flowing high purity nitrogen for at least 10 min. Dry denuders were removed from the manifold, immediately capped at both ends, and stored at 4 °C in plastic bags until needed.

For every 20 denuders prepared, at least one denuder was maintained as a laboratory blank. The blank denuder was prepared identically to those used in the field but remained at 4 °C from when it was prepared until immediately before extraction and analysis. These blank denuders were coated, extracted, and analyzed at the same time as the previously numbered denuder (e.g., blank denuder labeled number 20 was coated, extracted, and analyzed with field denuder number 19).

Elutriator-inlets and filter packs were fully disassembled and cleaned analogously to denuders prior to preparation and use. After rinsing, all parts were allowed to dry completely on fiberglass trays lined with Kimwipes® (Kimberly-Clark Professional, Roswell, GA) in the NH_3 free hood. Elutriator-inlets were then assembled, and upstream ends were covered with Parafilm® (Bemis NA, Neenah, WI). Elutriator-inlets were either immediately attached to coated denuders or stored at 4 °C in plastic bags until required.

Filter packs were assembled with 1 μm pore size polypropylene backed polytetrafluoroethylene filters (Cat. No. 7590-004, Whatman Limited, Maidenstone, UK) on the upstream filter stage and 0.8 μm pore size nylon membrane filters (Cat. No. 7408-004, Whatman Limited, Maidenstone, UK) downstream. Filters were applied under the NH_3 hood using clean tweezers (soaked in DI for > 24 h once per week and stored in the NH_3 free hood). Care was taken to orient the filters correctly with respect to the direction of flow. Filter packs were

assembled, Parafilm® was applied to the downstream quick-disconnect fitting, and they were either immediately attached to coated denuders or stored at 4 °C until needed.

Prepared elutriator-inlets, denuders, and filter packs were assembled in the NH_3 free hood and stored at 4 °C until used. Denuder assemblies were collected from the CAL and transported to the Energy Farm on the day of planned exposure. Generally, eight assemblies were collected on each planned sampling day, with four used for each REA run. If not immediately used, denuder assemblies were stored at 4 °C in a refrigerator located at the Energy Farm until needed. Denuders were replaced in clean plastic bags after exposure and immediately returned to storage at 4 °C. Specific methods for REA runs are provided in a subsequent section.

Denuders were extracted by CAL staff within five days of exposure. Exposed denuders were removed from the refrigerator and allowed to acclimate (while capped) for 1 h at room temperature on an open bench in the CAL and then transferred to the NH_3 free hood. Working with one denuder at a time, downstream caps were removed, and 20.0 ml of DI water was pipetted into each denuder. Caps were replaced, and denuders were inverted 10 times before being allowed to rest for 5 min. The DI water solution was then decanted into a clean 60 ml HDPE bottle (Cat. No. 2114-0002, Thermo Scientific Nalgene Products, Rochester, NY) rinsed three times with DI water prior to use. The extraction process was then repeated for all updraft, deadband, and downdraft denuders such that each denuder was extracted with a total of 40.0 ml of DI water. Lab blanks and field controls were extracted only once using 20.0 ml of DI water. After extracting all denuders, a DI water blank was prepared by pipetting 20.0 ml of DI water into an empty, clean 60 ml HDPE bottle. The DI water blank and all extracts were stored at -18 °C until analysis. Extracts were analyzed by CAL staff using a flow injection analyzer (FIA) (model Quik Chem 8500 Series 2, Lachat Instruments, Milwaukee, WI) according to NADP SOP

AN-0022 (NADP, 2008). The FIA instrument uses a colorimetric method for determination of ammonium ion in solution by reaction with phenate with a detection limit of 3 μg-NH_4^+ L^{-1} of extract solution.

2.2.2.5 Field Procedures for REA Sampling Runs

REA sampling runs lasted 4 h each and were divided into morning and afternoon runs, typically from 07:30 – 11:30 and 12:00 – 16:00 local time, respectively. Morning and afternoon sampling runs were performed on the same day when possible. The exact starting and ending times for each run varied depending on field conditions and equipment troubleshooting and were documented in a field notebook.

Four denuder assemblies were used for each REA sampling run: one each for updraft, deadband, and downdraft sampling conditions and a fourth used as a field blank. Denuder assemblies were transported from the Energy Farm refrigerator to the experimental field plot in plastic bags. Measurement height was adjusted as necessary prior to each REA sampling run such that $z_m > 1.34h_c$ to avoid overestimating source/sink contributions from any single canopy element (Raupach, 1994). The sonic anemometer was also adjusted for proper orientation if necessary. These steps were performed by either lowering the measurement tripod mast or accessing the sampling bracket and anemometer via ladder.

With double-gloved hands, described in Section 2.2.2.4, assemblies were carefully removed from bags and clipped into mounting brackets, taking care to vertically align inlets with the anemometer centerline. Parafilm® was removed from the downstream end of the updraft, deadband, and downdraft denuder assemblies and vacuum lines were attached. Parafilm® remained on downstream end of the field blank denuder assembly for the duration of the REA sampling run. Parafilm® was then carefully removed from the inlet of all four denuder

assemblies and the measurement tripod mast was returned to its vertical position (if it had been lowered).

Flow rate through the denuder assemblies was controlled at 20.0 L min^{-1} by the MFC in the REA control box. The MFC had a valid factory calibration for the duration of the field campaign and was verified monthly at 20.0 L/min using a piston meter (model DryCal DC2, Bios, Butler, NJ). Initial flow rate through each of the three denuder assemblies, as indicated by the digital display on the MFC, was recorded in the field notebook. If flow through any of the three assemblies deviated from the setpoint by more than ± 0.5 L min^{-1}, troubleshooting was performed to identify the cause and remedy the deviation. Flow through each denuder assembly, as indicated by the MFC, was recorded in the field notebook at the end of each run.

Exposed denuder assemblies were immediately removed from the mounting bracket, placed into clean plastic bags, and returned to a 4 °C refrigerator located at the energy farm. At the end of the sampling day all denuder assemblies were returned to the CAL. Assemblies were promptly disassembled in the NH_3 free hood with double-gloved hands. Denuders were capped with clean end caps and stored at the CAL at 4 °C for no more than five days until extraction. Filter packs were disassembled under the NH_3 free hood. Exposed filters were removed with clean tweezers, placed in labeled 50 mm petri dishes (polystyrene, BF Falcon, Franklin Lakes, NJ) and stored at -18 °C in plastic bags at CAL. Exposed filters were sent overnight in coolers to ATDD at three different times during the field campaign for analysis. Results from the filter analysis are not part of this research.

2.2.2.6 Data Management

Data from the field computer were copied to an external hard drive at the end of each 4 h REA sampling run, leaving all original files on the field computer. These data were then

transferred to two separate locations, one cloud drive accessible by other members of the research team, and a separate physical drive that was used as the primary storage location of raw, unaltered data. These raw data were further backed up to a separate cloud drive. Hence, all data files being actively worked with by the research team were physically and digitally separated from the original files to maintain data integrity. Further, raw data were stored in three different physical locations.

Data from the Biomet data logger were retrieved biweekly. Data were downloaded directly to a laptop computer, and immediately copied to a separate external hard drive. Copies were made analogously to those described above for REA data, and at no time were original data files altered or worked with directly.

Physical and digital records were maintained describing the date of preparation, use, and extraction for all denuders and filter packs such that any potential contamination could be traced back to the original prepared lot if necessary. As mentioned in Section 2.2.2.4, at least one unexposed blank was used for each lot of denuders prepared for further quality control and identification of contamination during preparation and/or extraction.

2.2.2.7 NH_3 Flux and Concentration Calculation

NH_3 concentration for each denuder ($C_{NH_3-denuder}$) was calculated using Equation 2.1.

$$C_{NH_3-denuder} = 0.944\frac{C_{NH_4^+}\ V_{extract}}{V_{REA}} \qquad \text{Equation 2.1}$$

where 0.944 is the ratio of the molecular weight of NH_3 to NH_4^+, $C_{NH_4^+}$ is the concentration of NH_4^+ in the denuder extract solution, $V_{extract}$ is the volume of deionized water used during extraction, and V_{REA} is the total volume of ambient air sampled through each denuder assembly. Knowing $C_{NH_3-denuder}$, for the up- and down-draft denuders, mean NH_3 flux during each

sampling run ($\overline{F_{NH_3}}$) was calculated using Equation 1.10. REA sampling runs were omitted from the results when β differed from the population mean by more than three standard deviations. Ambient NH_3 concentration (C_{NH_3}) measured with the REA method was calculated by summing $C_{NH_4^+}$ for each of the three actively sampled denuders. Laboratory and field blanks were used to screen for contamination in denuders.

Ambient NH_3 concentration was also measured using passive samplers (model Radiello® 123-7, Supelco: Bellefonte, PA), at the study plot. Passive samplers were used in accordance with NADP SOP SS-4070 for monitoring ambient NH_3 on a biweekly time interval (NADP, 2013). Further, results from the AMoN Bondville monitoring site for the duration of this study (NADP, 2017b) were used to assess atmospheric NH_3 concentration as measured by the REA method and Radiello® passive samplers with a well-established monitoring site. The Bondville site is located 13 km west of the study plot in a similar intensively managed ecosystem characterized as a rural location surrounded by corn and soybean cropland. Coefficient of variation (CV) was used to quantify variability in the sample population, where CV is the absolute value of the ratio of the standard deviation to the mean.

Uncertainty in the REA method arises from the use of the dynamic deadband and the response time of up- and down-draft valve switching, as well as from error introduced through the preparation and analysis of samples. While these sources of uncertainty are not quantified in this study, other studies have reported REA and EC measurements of CO_2 to have high correlation ($r^2 > 0.92$), with measurements from each system differing by no more than 20% (Oncley et al., 1993). Uncertainty due to laboratory preparation and extraction of denuders is expected to be relatively low when compared with error introduced due to the dynamic deadband and valve response time. The laboratory methodological detection limit for detection of NH_4^+

(0.017 mg L^{-1}) is quantified in the NADP CAL annual quality assurance report along with other statistics representing experimental error (NADP, 2018b).

2.2.3 Objective 1c: Flux Footprint Correction and Uncertainty Estimation

Local point measurements of NH_3 flux are important to improve understanding of processes that affect NH_3 emissions from fertilization and to contribute to upscaling of such measurements to regional scales using models (Balasubramanian et al., 2015). When upscaling, uncertainties may be introduced due to uncertainties in inputs such as land use maps, soil maps, varying meteorology or lack of farm management data at the farm level (Balasubramanian et al., 2015). Taking this into account along with challenges accessing plots with larger footprints and the scarcity of NH_3 flux measurements in the given region, we followed the rationale that as long as the primary footprint (> 90%) of measurements was over fields of fertilized corn, the goal of characterizing emissions from an intensively corn managed ecosystem was still met. In this research, that condition was fulfilled as the study plot was neighbored by a corn field > 900 m deep extending from $110° < \theta < 265°$ in the predominant wind direction.

Flux footprints were calculated for each REA sampling run according to Kljun et al. (2004) using the EddyPro software package (Version 5.1.1, LI-COR: Lincoln, NE). This method requires that friction velocity (u^*) exceeds a threshold value ($u^* \geq 0.2$ m s^{-1}), and the atmospheric stability parameter (ζ) falls within a certain range ($-200 < \zeta < 1$). When these assumptions did not hold, the method by Kormann and Meixner (2001) was used because of its applicability to a wider range of atmospheric stability and friction velocity. Flux footprint was calculated for the 10%, 30%, 50%, 70%, and 90% distances, where the NN% distance corresponds to the determined footprint radius, r, of the area that contributed NN% of the total measured flux. For example, if r = 150 m for a 90% footprint distance, then 90% of the total

measured flux was understood to originate from within a radius of 150 m. For cases where the 90% footprint distance exceeded the 100 m study plot radius (r_s) the relative fractional contribution to the measured flux from within r_s was estimated by interpolation considering the 10%, 30%, 50%, 70%, and 90% footprint distances.

The average wind direction (θ) was calculated for each REA sampling period and wind roses were generated in R (R Core Team, 2013) using the OpenAir package (Version 0.9-2, Carslaw and Ropkins, 2012) run in RStudio (Version 0.98.501, RStudio Team, 2018). For cases where the 90% footprint distance exceeded r_s, visual inspection of wind roses was used to determine whether contributing sources to the measured flux from outside the study plot were corn fields or mixed crop types. Samples were removed from further statistics calculations if at least one of two conditions was met: (1) contribution from within r_S was less than 50% or (2) the footprint contained crops other than fertilized corn.

Sommer and Jensen (1994) found the highest rate of NH_3 volatilization from fertilized soils occurred within the first 5-10 days following fertilization using wind tunnel studies. Hence, it was expected that the highest fluxes from all fertilized fields will occur during the period immediately following fertilization (i.e., one to two weeks). Because the neighboring field was fertilized 40 days before the study plot, positive flux from the neighboring field was expected to be relatively lower than the study plot immediately following fertilization of the study plot on DOY 126. To quantify the impact of such differences on measurements, emissions from the study plot (E_S) and the neighboring cornfield (E_N) were estimated using the DNDC model (Li, 2000; Balasubramanian et al., 2015). Modeled emissions were then used to characterize the percent difference (E_{diff}%) between E_S and the experimentally measured emission (E_M, comprised of contributions from E_S and E_N) using Equation 2.2:

$$E_{diff}\% = 100\left(\frac{E_S * R_S + E_N * R_N}{E_S} - 1\right) \quad \text{Equation 2.2}$$

where R_S and R_N are the relative fractional contributions to the measured flux from within the study plot and the neighboring plot, respectively. Hence, when $E_{diff}\% > 0$, $E_S < E_M$, indicating the experimental result overestimates the actual emission from the study plot. A parallel study (Objective 3) was completed to examine closure between NH_3 flux measurements from REA and predictions from the DNDC model and is described in Chapter 4 of this document.

2.3 Results and Discussion

2.3.1 Objective 1a: Equipment Setup and Calibration at ICN Site

Data collected during the preliminary trial run of the Biomet are presented in Figure 2.11. Vertical bars plotted for soil temperature, moisture content, and heat flux correspond to the standard deviation of the triplicate measurements. This dataset does not include measurements of PAR, global radiation, or precipitation as rain, as these parameters were not recorded during the sampling period due to sensor connectivity issues. This problem was remedied, and these sensors were subsequently confirmed to be in working order before measurements at the study plot.

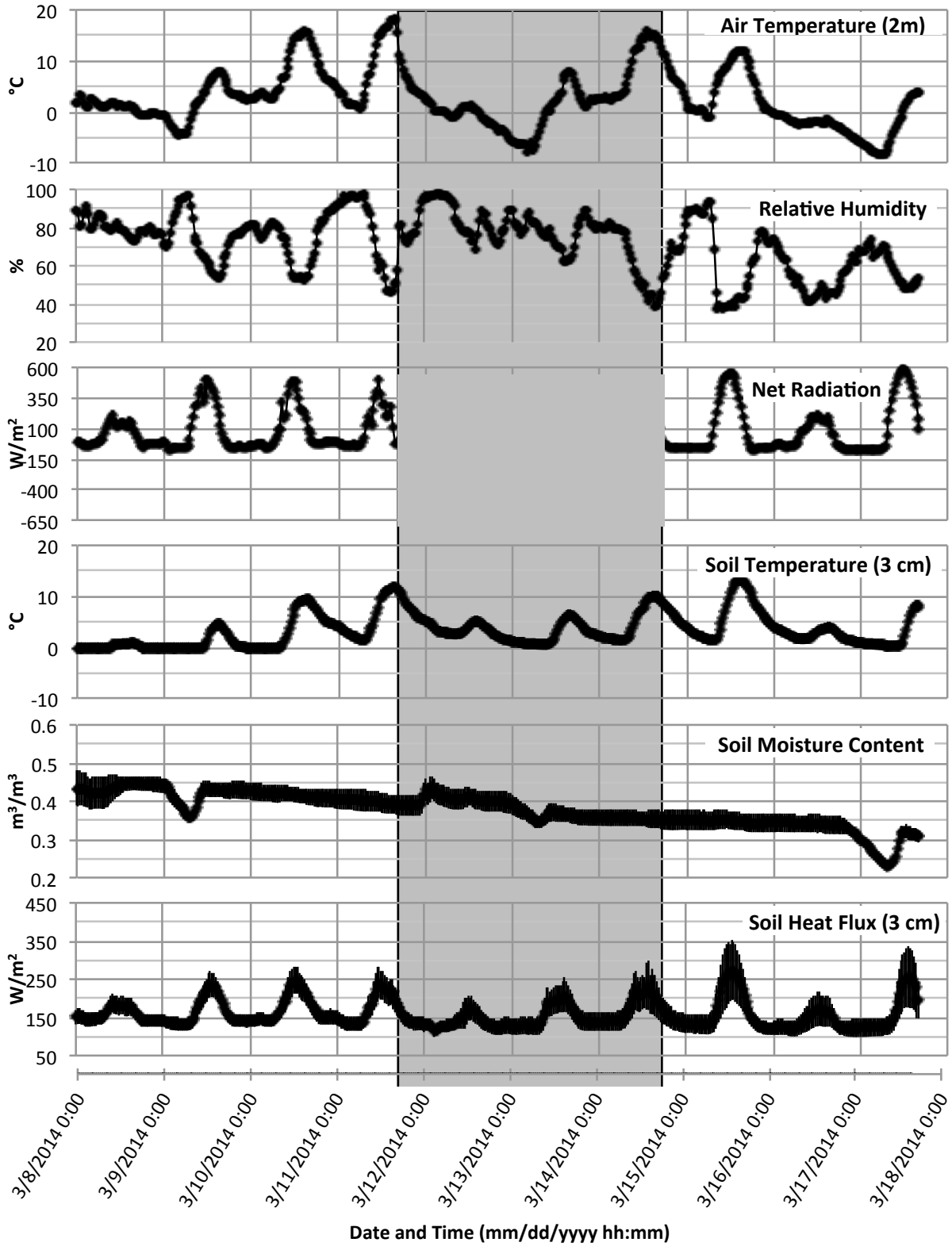

Figure 2.11: Environmental conditions during the preliminary data collection period. The area shaded in gray indicates when the instrumentation tripod was lowered for safety due to high winds.

During the preliminary sampling period, high winds (> 15 m s^{-1}) were forecast for the evening of March 11 extending through March 12. In the configuration used here, the tripod, with 6.1 m height, is rated to withstand winds up to 24 m s^{-1}, but out of an abundance of caution the tripod mast was lowered in advance of the forecast high winds. In Figure 2.11, the shaded area corresponds to the time when the tripod mast was lowered.

Lowering the mast in this manner is not expected to affect measurements of soil temperature, moisture content, or heat flux, as these sensors are located below the soil surface and are not influenced by the vertical position of the mast. However, net radiation measured during this time is understood to be inaccurate, as the net radiometer is attached to the mast and was therefore oriented parallel to the soil surface rather than perpendicularly when it was lowered. Therefore, these data have been omitted from the figure. Because the RH and temperature sensors were attached to the mast, they were in close proximity to the ground surface while the tower was lowered. This is expected to affect measurement of RH and air temperature during this time.

Daily observed maximum air temperature values ranged from -0.2 °C on March 16 to 18.2 °C on March 11. Due to a cold front passing through the region during March 15-16, the maximum observed temperature on March 16 was the first recorded reading at 00:01 hr (UTC -06:00). ISWS Water and Atmospheric Resources Monitoring (WARM) Program data were used for comparison with measured data collected with the Biomet system (ISWS, 2016). The WARM program reports daily maximum and minimum temperatures recorded at the ICN site. For the 10-day period, the mean maximum temperatures observed by the Biomet and the WARM program were between 8.8 °C and 9.1 °C, respectively. Using a two-tailed unpaired t-test at a 0.05 significance level, the observed maximum temperatures from both systems were not found

to be statistically different. Similarly, daily minimum temperatures were not found to be statistically different using a two-tailed unpaired t-test. After omitting suspect data (collected while the tripod was lowered), a negative correlation coefficient ($r = -0.72$) was observed between air temperature and RH. This is expected, as increased air temperature yields a higher water vapor capacity of an air parcel, thereby reducing RH.

Net radiation was calculated as the difference of incoming radiation and reflected radiation. Therefore, positive values of net radiation indicated incoming radiation was greater than reflected radiation. A diurnal cycle was observed for net radiation with a minimum during nighttime hours and elevated measurements during daytime hours, depending on cloud cover. Data on March 15 and 17 are similar because both days had minimal cloud cover. Data from other days are varied due to sporadic cloud cover, but generally exhibited a similar diurnal pattern. Due to an artifact from the experimental setup, it is believed that the reported net radiation values are underestimated. Space constraints at the preliminary research location required the tripod to be erected 2 m from a light colored artificial structure on the ground. This structure was observed to exhibit higher reflectivity than the sod surface. The increased surface reflection of this object reduced the overall net radiation value, as the radiometer was reading an artificially inflated value for reflected radiation. During the full field campaign, care was taken to make sure the sensor was positioned over a representative surface sample.

Soil temperature and soil heat flux both exhibited diurnal trends with minimum values occurring during nighttime hours and elevated values during daylight hours. When the tripod mast was in the upright position, a positive correlation ($r = 0.80$) was observed for soil heat flux and net radiation, as expected. Similarly, soil heat flux and soil temperature were both found to have a positive correlation with air temperature ($r = 0.75$ and $r = 0.83$, respectively), as expected.

2.3.2 Objective 1b: Results from REA Measurements at Energy Farm

2.3.2.1 Energy Farm Canopy Development

Cumulative GDD during the 2014 growing season was generally consistent with data from 2013 and the 10-year average from 2003 to 2013 (Figure 2.12). A warm spell occurring early in the growing season, DOY 147 – 154, resulted in a slight outpacing of historical GDD averages during 2014. However, a historically mild period during DOY 196 – 203 resulted in 2014 cumulative GDD at DOY 245 being similar to the 10-year historical average (2517 and 2492, respectively). The warm spell resulted in a rapid development of the canopy from DOY 147 – 168, reflected in the measured LAI.

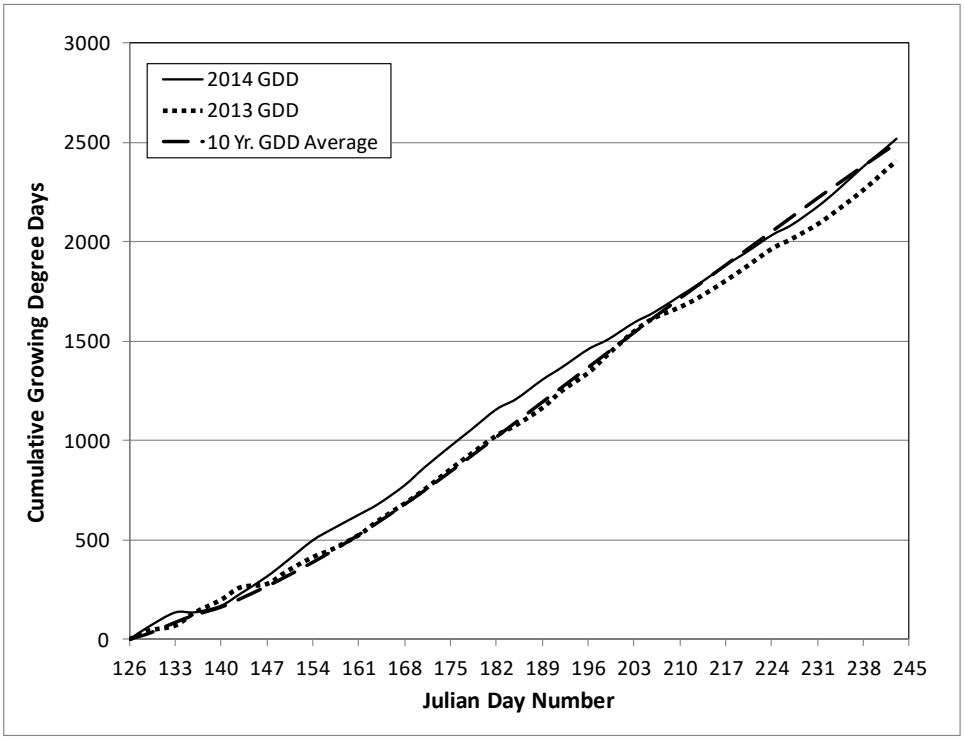

Figure 2.12: Comparison of cumulative growing degree days (GDD) at the Energy Farm in 2014 and 2013 and the 10 year average (2003-2013) based on Champaign Illinois Climate Network (ICN) data.

Plants were first visible on May 12 (DOY 132), six days after planting. Peak canopy height of 308 cm ± 10 cm was observed on July 25 (DOY 206). The mature canopy LAI was 6.1, measured on August 13 (DOY 225). The study plot was harvested on November 6 (DOY 310) with an average yield of 13.78 mt ha^{-1} (219.5 bu $acre^{-1}$), consistent with the average yield in Champaign County for 2014, 13.59 mt ha^{-1} (216.5 bu $acre^{-1}$) (USDA, 2017). Canopy development, as characterized by height and cumulative LAI is presented in Figure 2.13.

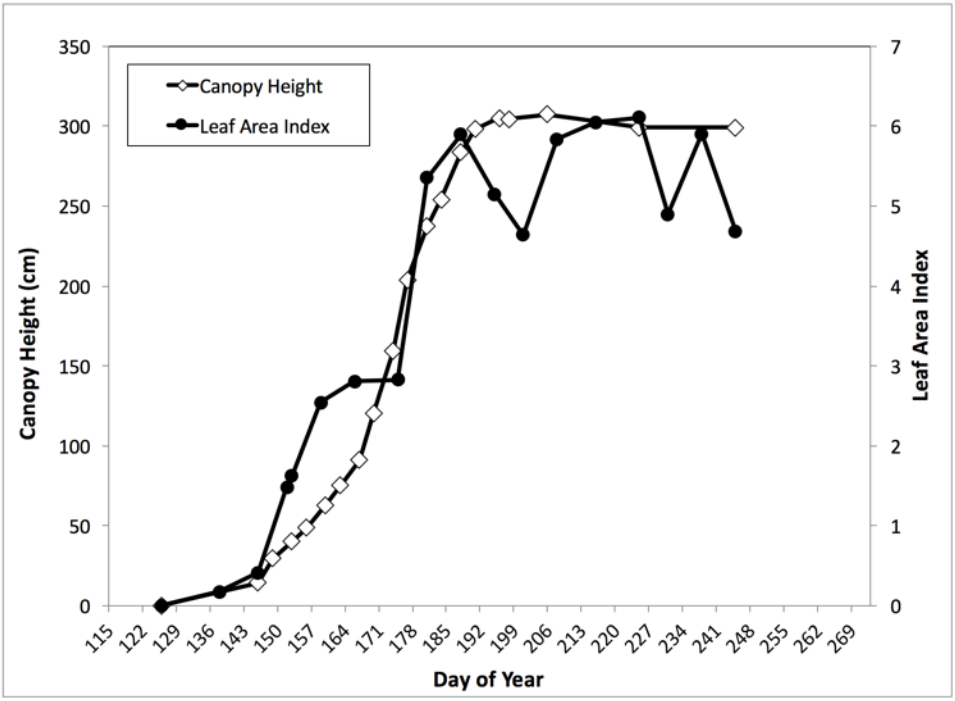

Figure 2.13: Canopy height (left axis) and leaf area index (LAI; right axis).

The decreased values of LAI observed on DOY 195 and DOY 201 are attributed to heavy rain and thunderstorms that caused damage to the canopy structure, followed by low temperatures contributing to slow canopy recovery. The ISWS reported heavy thunderstorms and 11.0 cm of rain in Champaign-Urbana, IL on DOY 192-193, followed by additional rain (1.3 cm)

on DOY 196 and abnormally low high temperatures (21.1 – 26.1 °C) for DOY 196-201 (ISWS, 2016).

2.3.2.2 Ammonia Concentration and Flux Measurements

Effort was taken to sample as frequently as possible during the first 14 days following planting (DOY 126-140). However, a gap in measurements from DOY 133 – 138 resulted from persistent rain during that time. The original experimental plan called for measurements at five vegetative growth stages (VE, V5, V10, V15, and VT). However, due to the rapid canopy development during DOY 147 – 181, the canopy matured faster than anticipated and it was not possible to sample during the V10 stage. Because of the time required to extract, clean, and recoat denuders following sampling on DOY 157-159 (V6), followed by a several days of precipitation, REA sampling runs were not performed again until stage V14.

Mean concentration and standard deviation of NH_4^+ for all denuder laboratory blanks was 0.034 ± 0.019 mg L^{-1}. Mean NH_4^+ concentration for field blanks was 0.043 ± 0.020 mg L^{-1}. For reference, mean NH_4^+ concentration across the full season was 0.144 ± 0.079 mg L^{-1} for up-draft denuders, 0.125 ± 0.056 mg L^{-1} for down-draft denuders, and 0.142 ± 0.102 mg L^{-1} for dead band denuders. Concentration of NH_4^+ in the laboratory DI water source was also measured each time denuders were extracted and was 0.0017 ± 0.0029 mg L^{-1} for the duration of the study. During the 2014 calendar year, the CAL instrument detection limit for NH_4^+ was 0.006 mg L^{-1}, and the method detection limit for NH_4^+ was 0.017 mg L^{-1} (NADP 2018b).

Results from the 39 REA sampling runs are presented in Table 2.4. Standard deviation of vertical wind speed (σ_w), average and maximum wind speed (u_{avg}, and u_{max}, respectively), θ, C_{NH_3}, NH_3 flux ($\overline{F_{NH3}}$), β, peak footprint contribution distance (*x_peak*), and 10%, 30%, 50%, 70%, and 90% flux footprint distances are presented as average values for each REA sampling

period. REA sampling runs are identified by DOY followed by -1 or -2 to denote morning and afternoon runs, respectively.

Day	Start	End	σ_w	u_{avg}	u_{max}	θ	C_{NH3}	$\overline{F_{NH3}}$	β	x_peak	x_10%	x_30%	x_50%	x_70%	x_90%
	(HH:MM)	(HH:MM)	(m s^{-1})	(m s^{-1})	(m s^{-1})	(deg)	(μg m^{-3})	(ng m^{-2} s^{-1})		(m)	(m)	(m)	(m)	(m)	(m)
115-1	8:10	12:01	0.52	7.40	13.16	318	7.22	-198.44	0.55	106.0	36.4	90.6	138.1	193.7	290.2
115-2	12:33	16:38	0.48	6.89	12.21	290	4.23	973.80	0.55	107.0	36.7	91.5	139.5	195.6	293.1
116-1	8:04	12:11	0.27	2.19	5.68	245	5.75	-99.16	0.58	99.8	36.4	87.4	133.3	188.7	294.4
116-2	12:21	16:24	0.33	2.86	7.22	70	8.11	634.30	0.60	95.5	34.6	83.2	126.9	179.2	276.4
126-2	17:27	19:40	0.50	4.89	9.56	121	0.88	-70.61	-1.19	62.7	21.5	53.6	81.8	114.7	171.8
127-1	7:47	11:57	0.45	6.03	10.91	203	2.20	399.27	0.55	66.4	22.8	56.7	86.5	121.4	181.8
127-2	12:10	16:19	0.54	6.38	12.44	180	3.75	275.72	0.57	67.2	23.1	57.4	87.6	122.9	184.1
128-1	8:02	12:05	0.51	7.54	13.44	200	3.38	284.33	0.61	66.6	22.9	56.9	86.8	121.7	182.4
128-2	12:15	16:16	0.57	8.00	14.27	188	3.47	293.58	0.57	67.3	23.1	57.5	87.7	123.0	184.3
129-1	9:59	14:02	0.54	7.67	13.24	234	6.00	642.17	0.41	66.7	22.9	57.0	87.0	122.0	182.8
130-2	12:38	16:43	0.33	2.02	6.67	270	3.92	474.74	0.56	61.5	23.9	59.4	90.6	127.1	190.4
131-1	9:12	13:17	0.42	5.67	10.12	186		682.15	0.58	65.8	22.6	56.3	85.8	120.3	180.3
132-2	12:41	16:49	0.53	7.63	13.56	190	1.87	799.60	0.49	62.2	21.4	53.2	81.1	113.7	170.4
133-1	10:22	13:17	0.40	4.79	8.58	282	2.14	191.26	0.57	61.3	21.1	52.4	79.9	112.1	168.0
138-2	12:56	17:01	0.31	2.11	6.24	159	1.23	212.80	0.60	52.2	17.9	44.6	68.0	95.4	142.9
157-1	7:31	11:58	0.30	1.71	5.31	140	2.50	-8.52	0.61	30.1	11.4	28.5	43.4	60.9	91.2
158-1	8:14	12:25	0.50	4.39	9.42	141	1.73	130.85	0.64	32.6	11.2	27.9	42.5	59.7	89.4
158-2	12:32	16:05	0.54	4.32	9.79	138	0.82	254.49	0.82	31.3	10.7	26.7	40.8	57.2	85.6
159-2	13:31	17:31	0.33	3.41	7.10	156	2.05	40.77	0.39	33.7	11.6	28.8	44.0	61.6	92.4
178-1	8:02	12:23	0.46	2.68	6.91	162	0.65	-36.62	0.79	18.2	6.3	15.6	23.7	33.3	49.9
178-2	12:29	16:39	0.52	2.56	6.98	166	1.97	14.31	0.69	17.9	6.2	15.3	23.4	32.8	49.1
179-1	7:34	11:36	0.53	3.00	7.71	181		71.21	0.74	18.0	6.2	15.4	23.5	32.9	49.3
179-2	11:42	15:52	0.58	2.96	8.17	173	0.61	-44.78	0.96	18.4	6.3	15.7	24.0	33.6	50.3
190-1	7:26	11:36	0.47	1.74	5.73	299	2.12	-113.29	0.66	25.4	8.7	21.7	33.2	46.5	69.7
190-2	11:45	15:55	0.59	2.14	7.34	286	0.48	-57.07	0.71	26.1	8.9	22.3	34.0	47.7	71.4
191-1	7:30	11:37	0.35	1.12	4.06	56	0.91	-30.60	0.57	25.8	8.8	22.0	33.6	47.1	70.6
191-2	11:43	15:59	0.43	1.29	5.58	51	0.26	84.95	0.55	26.2	9.0	22.4	34.2	47.9	71.8
213-1	7:49	11:47	0.24	0.53	3.10	126	1.54	100.86	0.51	14.1	7.8	19.5	29.8	41.8	62.6
213-2	11:48	15:48	0.31	0.84	3.38	183	1.83	-16.92	0.54	22.7	9.0	22.5	34.3	48.1	72.0
214-1	7:46	11:46	0.33	0.98	3.84	212	1.69	-27.59	0.59	24.6	8.4	21.0	32.1	45.0	67.4
214-2	11:52	15:56	0.32	0.71	3.55	121	0.63	-161.08	0.53	22.0	8.7	21.7	33.1	46.4	69.5
239-1	7:23	11:45	0.34	1.10	3.93	60	2.44	46.16	0.56	24.5	8.4	21.0	32.0	44.9	67.2
239-2	11:50	16:31	0.33	1.17	4.48	32	1.60	55.13	0.51	25.7	8.8	22.0	33.5	47.0	70.4
241-1	7:25	11:33	0.41	1.63	4.84	170	1.60	-16.42	0.24	25.5	8.8	21.8	33.2	46.6	69.8
241-2	11:39	15:43	0.41	1.45	6.20	172	1.07	6.63	0.40	24.7	8.5	21.1	32.2	45.2	67.7
273-1	7:38	11:48	0.57	2.06	6.57	33	0.75	-84.22	0.59	26.2	9.0	22.4	34.2	47.9	71.8
273-2	11:52	16:42	0.50	1.65	5.48	62	1.65	184.99	0.59	26.1	9.0	22.3	34.0	47.7	71.5
445_1	8:15	12:24	0.35	5.10	9.05	293	2.10	-246.01	0.57	108.0	37.1	92.3	140.7	197.4	295.7
445-2	12:33	16:42	0.39	4.91	9.52	65	2.59	98.20	0.53	110.1	37.8	94.1	143.6	201.4	301.7

Table 2.4: Relaxed Eddy Accumulation (REA) system measurements of standard deviation of vertical wind speed (σ_w), average wind speed (u_{avg}), maximum wind speed (u_{max}), average wind direction (θ), NH_3, concentration (C_{NH3}), flux ($\overline{F_{NH3}}$), empirical REA coefficient (β), peak footprint contribution (x_peak), and 10%, 30%, 50%, 70%, and 90% flux footprint distances. Samples are identified by day number with -1 for morning and -2 for afternoon samples. Day 445 corresponds to March 21, 2015.

The mean observed σ_w during all REA sampling runs was 0.43 m s^{-1}, consistent with values reported in the literature (Myles at al., 2007). One sample (DOY 126-2) was removed from further consideration based on the value of β. The observed mean and standard deviation of β was 0.58 ± 0.12, consistent with the theoretical expectation and other measurements presented in the literature (Table 2.5).

Author	Ecosystem	Reported β
Baker et al., 1992	Theoretical value	0.627
This study	Corn (entire growing season)	0.58 ± 0.12
Tsai et al., 2012	Marsh	0.57 ± 0.01
	Paddy	0.55 ± 0.01
	Lagoon	0.56 ± 0.01
Myles et al., 2007	Grassland	0.54 ± 0.12
Meyers et al., 2006	Corn (at planting)	0.58 – 0.70
	Corn (at peak LAI)	0.32 – 0.98
Zemmelink et al., 2002	Ocean	0.55 – 0.57
Zhu et al., 2000	Corn	0.413 – 0.518

Table 2.5: Summary of β values from this study and from the literature. Standard deviations are presented where available, otherwise maximum and minimum values are reported.

Season average and standard deviation (DOY 115-273) of C_{NH_3} from the REA method was 2.6 ± 2.0 μg m^{-3}. C_{NH_3} measured using the REA method (for combined updraft, deadband, and downdraft conditions), Radiello® passive samplers at the study plot, and Radiello® passive samplers at the Bondville AMoN site are presented in Figure 2.14 for DOY 115 – 248 in 2014.

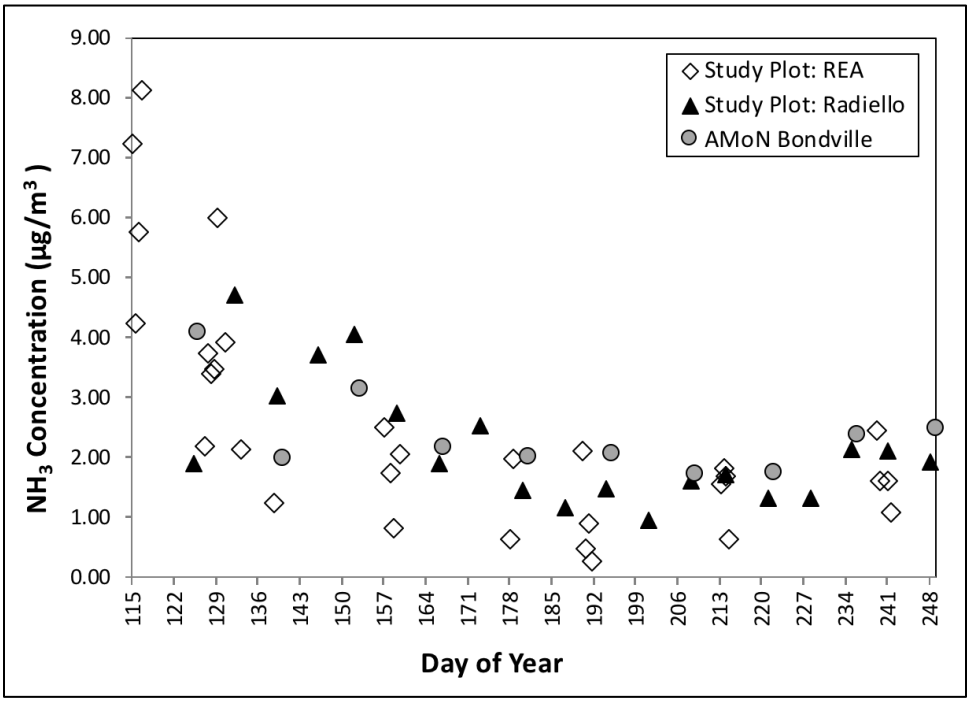

Figure 2.14: NH_3 concentration as measured at the study plot using REA and passive Radiello® samplers, and from the National Atmospheric Deposition Program (NADP) Ammonia Monitoring Network (AMoN) sampling site at Bondville, IL for DOY 115 - 248. Passive sampling occurred over two-week sampling periods.

The mean monthly profile of NH_3 concentrations as measured at the Ammonia Monitoring Network (AMoN) site at Bondville, Illinois from November 2007 through 2014 is presented in Figure 2.15. Measurements reported in this study occurred during the months of April through September, corresponding to months with historically elevated ambient NH_3 concentration near the study plot relative to winter months (Dec – Feb). Elevated NH_3 concentrations correspond to times of fertilizer application in the surrounding area (spring and fall applications), where fall applications are typically applied after soybean harvest in a corn-soybean rotation (Bullard et al., 2017).

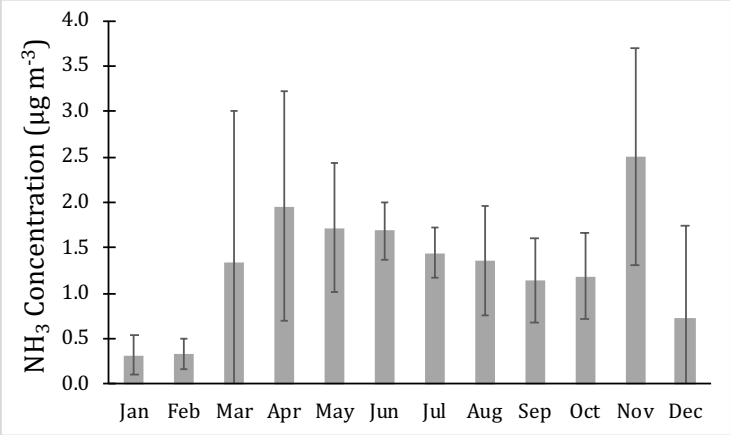

Figure 2.15: Mean monthly NH_3 concentration at the Ammonia Monitoring Network Bondville site, based on reported data from November 2007 through 2014. Error bars indicate standard deviation of measurements. For reference, measurements in this study occurred from April through September, 2014.

A high degree of variability was observed, with C_{NH_3} ranging from 0.26 µg m^{-3} on July 10 (DOY 191) to 8.11 µg m^{-3} on April 26 (DOY 116). This range is narrower than reported observations between 0.30 to 61.2 µg m^{-3} over a corn canopy at Lillington, NC, studied by Walker et al. (2013). Across all reported measurements, the REA denuder samples exhibited the highest CV (0.78), compared to CV = 0.46 for the passive samplers at the study plot, and CV = 0.31 for the Bondville site. The higher variability of measurements from the REA method is attributed to the shorter averaging time (4 h) when compared to the passive samplers (bi-weekly), thereby allowing the REA method to more readily capture temporal variation in C_{NH_3}.

A common trend in results from all three C_{NH_3} sampling methods was that the highest concentrations occurred during the beginning of the growing season (i.e., before June 1, DOY 152) when agricultural fertilization was occurring. Mean and standard deviation values for C_{NH_3} for the first two weeks following fertilization at the study plot from the REA system were 4.56 ± 1.96 µg m^{-3} while values for the remainder of the season were 1.46 ± 0.69 µg m^{-3}. The overall

temporal decreasing trend is consistent with other experimental observations (e.g., Walker et al., 2013).

Following a similar trend to that observed in C_{NH_3}, NH_3 fluxes were highest immediately following fertilization and planting (DOY 127 – 159). The remaining samples (DOY 160 – 273) had smaller NH_3 flux values, including 10 measurements of negative flux, indicating deposition to the surface (not including background measurements in March, 2015). Mean values of NH_3 flux, β, and ζ for each REA sampling run are presented in Figure 2.16.

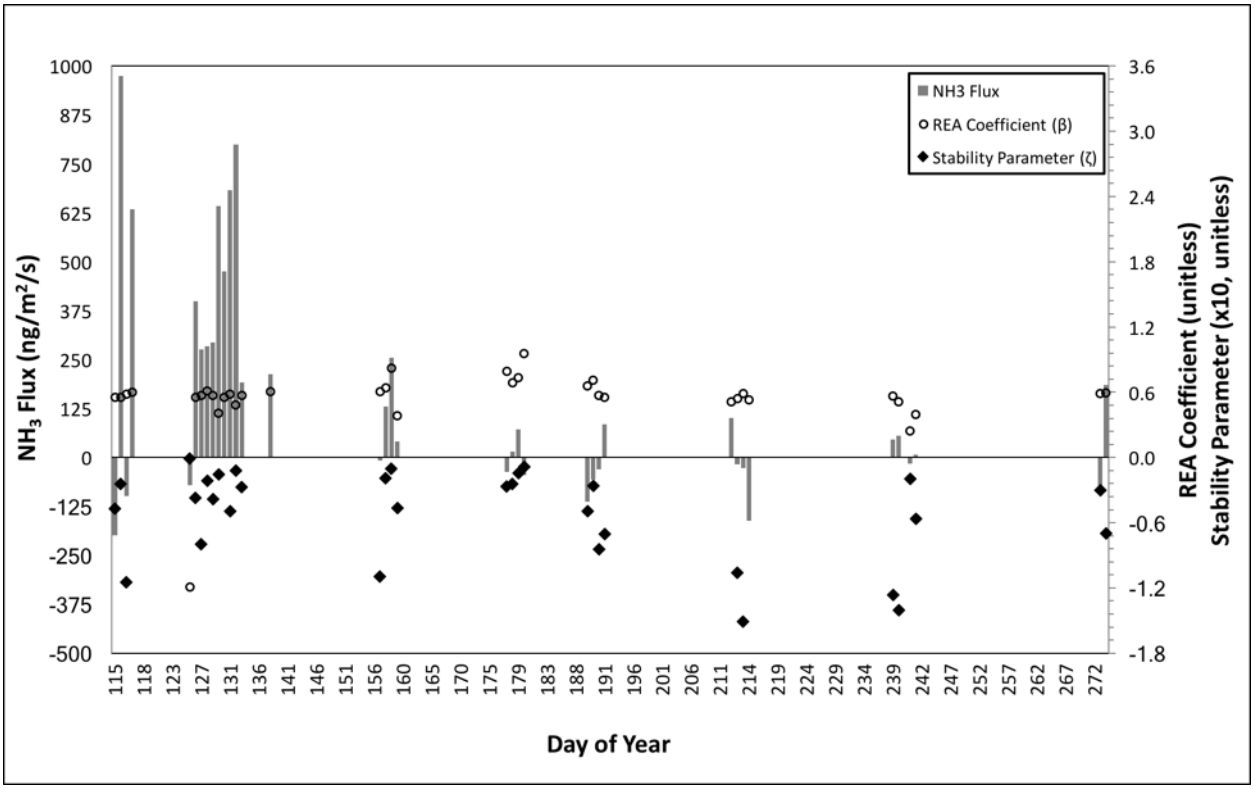

Figure 2.16: Mean values of NH_3 flux, β, and ζ values for all REA sampling runs collected during the 2014 growing season.

As discussed in Section 2.2.2.7, uncertainty in NH_3 flux measured with REA was not quantified here, however, others have reported REA measurements to agree with direct EC measurements within +/- 20% (Oncley et al., 1993). No statistically significant difference between morning and afternoon samples was identified using a t-test at the 95% confidence level

whether the test was performed on all qualified samples or separately for qualified positive and negative fluxes. 50% of the morning samples exhibited negative fluxes compared to 22% of afternoon measurements. Of all qualified samples, mean positive flux was 233 ± 203 ng m^{-2} s^{-1} in the morning and 260 ± 253 ng m^{-2} s^{-1} in the afternoon. Mean negative flux was -45.3 ± 38.6 ng m^{-2} s^{-1} in the morning and -78.4 ± 74.9 ng m^{-2} s^{-1} in the afternoon. A summary of NH_3 concentration, flux ranges, and REA coefficient values for the full growing season and two sub-periods is presented in Table 2.6. This table describes all results after eliminating outlier values as described above.

Period (DOY)	C_{NH3} (μg m^{-3})	σ_{CNH3} (μg m^{-3})	$\overline{F_{NH3}}$ *range* (ng m^{-2} s^{-1})	β (-)	σ_β (-)
All	2.6	2.0	-161, 800	0.58	0.12
127 – 159	2.70	1.38	- 8.5, 800	0.57	0.11
160 – 273	1.20	0.73	-161, 185	0.60	0.15

Table 2.6: Values of average ambient NH_3 concentrations and their standard deviations, ranges of qualified NH_3 fluxes, and average and standard deviation REA coefficients for the complete growing season, 32 days post planting (DOY 127-159), and the remainder of the 2014 growing season.

Correlation between NH_3 flux and environmental parameters was investigated for both sub-periods defined above. Good correlation of NH_3 flux with both wind speed (r = 0.54) and soil moisture (r = -0.75) was observed during DOY 127 – 159, while air temperature (r = 0.28) and soil temperature (r = -.02) were found to have weak correlation over the same period. No correlation with these parameters was found during DOY 160 – 273 ($r < |0.1|$ for all parameters). This result suggests that localized environmental conditions have a greater impact on NH_3 fluxes during the early season before canopy development.

Processes resulting in the bi-directionality of NH_3 flux exhibited during DOY 160 – 273 are not well understood. Walker et al. (2006) reported highest deposition rates when the canopy was wet, while temperature can affect stomatal resistance and compensation point which are

linked to concentrations of apoplastic NH_4^+ and H^+ (Wu et al. 2009). Additional targeted measurements are required to quantify the effect of the canopy and canopy evapotranspiration on NH_3 flux.

2.3.3 Objective 1c: Flux Footprint and Measurement Uncertainty

Figure 2.17 presents wind roses from two REA sampling runs where the 90% flux footprint distance exceeded the study plot boundary (182 m on DOY 127-1 and 168 m on DOY 133-1). The shaded areas of the wind roses correspond to values of θ where neighboring fields were comprised of mixed crop types.

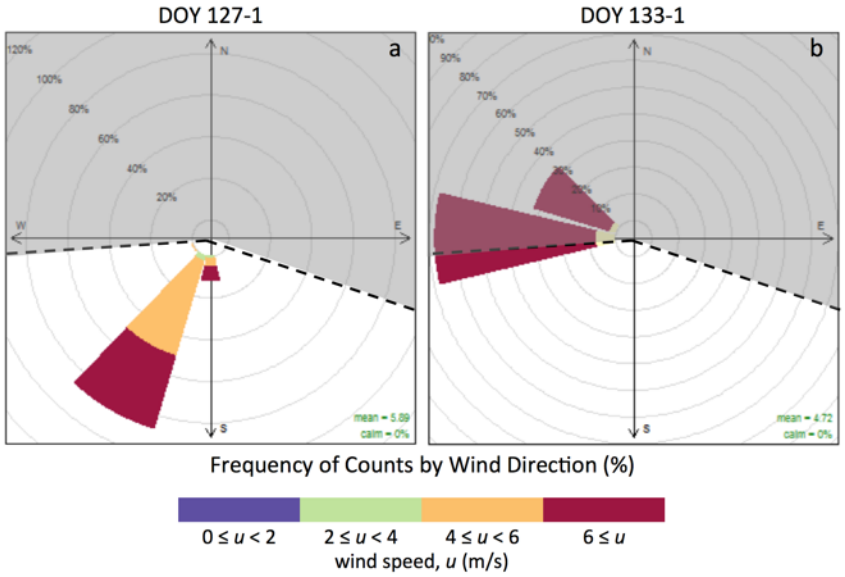

Figure 2.17: Wind roses for DOY 127-1, when the 90% footprint was contained within fertilized corn (a), and DOY 133-1 when the 90% footprint was outside the study plot and included a mix of crops (b). The shaded area corresponds to values of wind direction, θ, with mixed crop types.

The wind rose for DOY 127-1 shows that wind originated from the non-shaded area of the wind rose, indicating that corn was the contributor to the measured flux. However, on DOY 133-1 wind originated from the mixed crop area in the west to northwest direction ($285° < \theta < 315°$) 32% of the time in the 4 h period, and was distributed along the boundary of the corn and mixed crops the remaining 68% of the time ($255° < \theta < 285°$). In these example cases, DOY

127-1 was further evaluated to estimate the under-prediction of NH_3 flux, while DOY 133-1 was not considered for further statistical evaluation due to contributions by mixed crop types. An analogous process was used to evaluate footprint contribution for all REA measurements.

The largest footprints occurred during the pre-planting and post-harvest periods due to higher average wind speed and minimal plant canopy resulting in reduced surface roughness. Further, 90% footprint distances exceeded the boundary of the study plot during the first two weeks of sampling (DOY 126 – 138). As described above, one flux measurement (DOY 133-1) was removed from statistical consideration during this period due to contributions from non-corn crops. Ten REA sampling runs were identified between planting and harvest where the 90% flux footprint distance exceeded the boundary of the study plot but extended over the neighboring cornfield without passing by the nearby mixed crop areas. (Table 2.7).

Day (DOY)	E_S (kg-N ha^{-1} d^{-1})	E_N (kg-N ha^{-1} d^{-1})	R_S (%)	R_N (%)	E_{diff} (%)
126-2	0.21	0.09	61.8	38.2	- 21.8
127-1	0.38	0.09	58.4	41.6	- 31.8
127-2	0.38	0.09	57.7	42.3	- 32.3
128-1	0.51	0.10	58.2	41.8	- 33.6
128-2	0.51	0.10	57.6	42.4	- 34.1
129-1	0.61	0.09	58.1	41.9	- 35.7
130-2	0.57	0.08	55.7	44.3	- 38.1
131-2	0.70	0.09	58.9	41.1	- 35.8
132-2	0.68	0.08	62.3	37.7	- 33.3
138-2	0.26	0.03	72.8	27.3	- 24.1

Table 2.7: E_{diff} represents the difference between experimentally measured emission and emission originating from the study plot alone based on DeNitrification DeComposition (DNDC) model runs for environmental and field management conditions measured during the REA sampling runs where the flux footprint exceeded the boundary of the study plot but was entirely over neighboring cornfields. E_S and E_N are DNDC emission estimates from the study and neighboring plots, respectively. R_S and R_N are the relative contributions to total flux from the study and neighboring plots, respectively.

From Equation 2.2, measured flux during the ten sampling runs where the footprint exceeded the study plot was underestimated by 32% ± 5%. This value describes the difference between an ideal sampling case (i.e., one in which the study plot extends uniformly and infinitely

in all directions) and the actual case with non-uniform fields of finite size. Because the neighboring cornfield was fertilized 40 days earlier than the study plot, its expected peak NH_3 emissions occurred before any measurements at the study plot were made. Therefore, during the measurement period just after fertilization of the study plot, and in cases where the flux footprint extended over the neighboring corn field, the contributed flux from the neighboring field was lower than the flux contributed by the study plot alone, resulting in a lower average flux. Having established that DNDC can effectively capture spatial and temporal variation of NH_3 fluxes as a function of environmental and farm management parameters from the measurement-modeling comparison study by Balasubramanian et al., (2017), using DNDC modeled estimates provided a method to quantify uncertainty ranges for the field measurements.

2.3.4 Objective 1d: Comparison of NH_3 Flux in Central Illinois with Other Studies

As previously mentioned, Walker et al. (2013) studied a corn canopy in North Carolina using the modified Bowen ratio to measure NH_3 fluxes over two-hour averaging periods. They reported a similar temporal profile with highest emissions occurring in the first 30 days post-fertilization. The field studied by Walker et al. was fertilized (20 kg-N ha^{-1} as injected ammonium polyphosphate) and planted with corn from DOY 108 – 113. A subsequent side-dress application (134 kg-N ha^{-1} as UAN) was applied from DOY 145 – 149.

Walker et al. (2013) divided fluxes into two periods: the first 31 days following side-dress fertilizer application (DOY 149 – 180) and the remaining 32 days (DOY 181 – 213). Reported fluxes from Walker et al. (2013) are presented in Table 2.8 with results from this study presented in similarly divided time periods relative to the initial date of fertilization.

	Location	DOY	Days post- final fertilization	Mean Flux ± std. dev (ng m^{-2} s^{-1})	Max. Flux (ng m^{-2} s^{-1})	Min. Flux (ng m^{-2} s^{-1})
Walker et al. (2013)	Lillington, NC	149 – 180	0 – 31	339.2 ± 601.7	6906	-42.5
		181 – 213	32 – 64	61.4 ± 10.2	3125.4	-230.4
This study	Urbana, IL	127 – 159	1 – 33	359 ± 250	800	-8.5
		160 – 180	34 – 54	1.0 ± 54	71	-45
		160 – 273	34 – 147	-2.0 ± 91	101	-161

Table 2.8: Comparison of measured flux results from Walker et al. (2013) and this study. Results by Walker et al. were reported as two time periods following fertilization that occurred twice during the crop season. Data from this study have been similarly reported.

Though the general trend measured in this study is similar to results by Walker et al., the maximum positive flux reported by Walker et al. (6906 ng m^{-2} s^{-1}) is higher than in this study (800 ng m^{-2} s^{-1}), even if we correct for the underestimation predicted using DNDC modeling. Similarly, Walker et al. reported greater negative fluxes (-230.4 ng m^{-2} s^{-1}) compared to the corresponding time period in this study (-45 ng m^{-2} s^{-1}). The differences in measured maxima and minima between Walker et al. and this study may originate in differences in field management practices, measurement methods and averaging times, climatic and soil characteristics, and background conditions.

The effect of differing field management practices, (i.e., date of fertilizer application, method of application, and amount of fertilizer applied) is likely the largest contributing factor to differences in measurements between the two sites (Balasubramanian et al., 2017). The higher maximum flux at the North Carolina site is attributed to the use of a side-dress application of UAN. In contrast to the Energy Farm study plot, where liquid UAN was spray applied and tilled into the soil within 4 h of application, the side dress application at the North Carolina site applied liquid UAN directly to the soil surface without incorporation into the soil. This surface application is more favorable to volatilization of NH_3 because of direct exposure to solar radiation and higher soil temperatures at the surface (Watson et al., 1994). The difference in averaging time (1 h at North Carolina vs. 4 h at the Energy Farm) enables better quantification of

short-term peak fluxes at the North Carolina site that may otherwise not be resolved using a longer averaging interval. Because fertilization and planting dates are typically guided by soil and atmospheric temperature, climatic conditions are likely a lesser relative contributor to flux differences, though localized environmental conditions such as daily precipitation or cloud cover would have a contributing effect. However, such localized environmental impacts would exist between any comparison of field studies not conducted at the same site. While soil pH has been identified as having a significant impact on NH_3 emission potential (Balasubramanian et al., 2017), soils are typically managed to achieve a target pH. At the North Carolina site, soil pH was reported to range from 6.41 to 6.56, while the Energy Farm was managed to a target pH of 6.0 (actual soil pH measurements are not available from the Energy Farm).

We estimated NH_3 loss relative to fertilizer applied for the full corn growing season (Loss for the Full Season) and during the first 21 days after fertilization (Loss in the First 21 Days) using mean and median NH_3 flux values for each time period with timescale characterization similar to that reported by Walker et al. (2013) (Table 2.9).

	Loss for the Full Growing Season		**Loss in the First 21 Days**	
	Mean (%)	Median (%)	Mean (%)	Median (%)
Walker et al. (2013)	8.3	6.1	4.5	3.4
This study	10.9	4.7	4.6	3.7

Table 2.9: Comparison of integrated nitrogen loss from Walker et al. (2013) and this study for the full growing season (Loss for Full Season) and during the first 21 days after fertilization (Loss for First 21 Days).

Though different field management practices were used, both fields were treated with a urease inhibitor concurrently with fertilization. NH_3 loss during the periods presented in Table 2.9 is similar between these studies, with differences likely attributable to experimental error. NH_3 Loss in the First 21 Days after fertilization accounts for 79% of Loss for the Full Growing Season in this study compared to 56% as reported by Walker et al. This difference is attributable

to the longer duration of this study with more observations during low-emission periods and highlights the importance of early-season emissions in the overall NH_3 emission profile. Future research should continue to focus on this early-season period, when the largest loss of NH_3 occurs.

In considering these results with Walker et al. (2013), differences are also expected due to different field management practices. However, it is not straightforward to identify the relevant importance of such differences given that management practices, temporal resolution of measurements, and environmental conditions also have an effect. Quantification of the relative impact of such factors requires further detailed studies designed to control for such conditions. Such uncertainty could be resolved with systematic measurement studies that involve carefully controlled inter-comparisons in similar environments and measurement-modeling studies for a broad range of environmental conditions and farm management practices.

2.4 Summary and Conclusions

NH_3 flux above a corn canopy in Central Illinois was measured using REA for the duration of the 2014 corn-growing season, including additional post-season background measurements collected during March 2015. High variability (CV = 1.93) in NH_3 flux was observed throughout the season. Using median season-long flux measurements to estimate nitrogen loss, 79% of total loss was observed in the first 21 days post-fertilization. The greatest fluxes toward the atmosphere occurred in the first 30 days following fertilization when compared with the remainder of the season. Results from this field campaign exhibit a temporal pattern of emission similar to that reported by Walker et al. (2013) over a corn canopy in North Carolina, where highest emissions were observed during a 30 day period following fertilization. However, maximum and minimum fluxes reported by Walker et al. were both greater in magnitude than

those measured in this study (764% and 414%, respectively). Further studies are required to understand the cause of these differences in measured NH_3 emissions from fertilized fields and for measurement method inter-comparison.

This research represents the first reported measurements of NH_3 flux over a corn canopy in the Midwest National Climate Assessment climate region, where NH_3 emissions are dominated by chemical fertilizer application. Such measurements are important to improve understanding of NH_3 emissions from this important, yet understudied ecosystem, particularly in the Midwest. Further, the data presented in this study are needed to assess closure between measurements and models of NH_3 emissions for use in biogeochemical and chemical transport models to understand the impact of agricultural NH_3 emissions on air quality and the global Nitrogen Cycle.

CHAPTER 3: INTER-COMPARISON OF RELAXED EDDY ACCUMULATION AND FLUX-GRADIENT MEASUREMENT METHODS*

3.1 Research Motivation and Significance for Objective 2

This chapter presents an inter-comparison of NH_3 flux measurements above a corn canopy in Central Illinois, USA, using REA and FG measurement methods. This inter-comparison provides important understanding of closure between the FG method when compared with the REA method, which has been more extensively used for NH_3 flux measurement in varied ecosystems (Zhu et al., 2000; Meyers et al., 2006; Myles et al., 2007) and in Central Illinois (described in Chapter 2). Enhanced temporal resolution of NH_3 flux measurements provided by FG is important to improve understanding of the impact of localized environmental parameters on NH_3 flux intensity and to evaluate local and regional modeling of NH_3 emission (Flechard et al., 2013; Walker et al., 2013). Further, continuous NH_3 flux measurement is beneficial for characterizing diurnal patterns of NH_3 flux, which has not previously been reported in the literature for typical field-management practices in Illinois.

This research presents new 30 min averaged NH_3 flux measurements using the FG method and inter-compares these results with concurrent REA measurements of NH_3 flux over an intensively managed corn canopy in the Midwest US. These new measurements, and the inter-comparison of experimental methods, are important to enhance NH_3 emission model evaluations and to improve understanding of the impact of intensively managed agricultural ecosystems on air quality and the global Nitrogen Cycle. Given the dependence of NH_3 fluxes on multiple

* Reproduced in part with permission from A.J. Nelson, N. Lichiheb, S. Koloutsou-Vakakis, M.J. Rood, M. Heuer, L. Myles, E. Joo, J. Miller, and C. Bernacchi (2018) Ammonia Flux Measurements above a Corn Canopy using Relaxed Eddy Accumulation and a Flux-Gradient System. *Submitted to Agr. Forest Meteorol.* 2/12/18 (AGFORMET-D-18-00154)

parameters, this objective further highlights the need for increased spatial coverage and increased temporal resolution (e.g., < 1 h) of measurements to better understand the environmental impact of agricultural NH_3 emissions and for evaluation of models describing surface-atmosphere exchange of NH_3. ***Objective 2a*** describes the quantification of NH_3 flux at the Energy Farm using the FG method with an automated exchange mechanism. ***Objective 2b*** provides an inter-comparison of NH_3 flux measurements using the REA and FG methods and details an analysis of cost and complexity associated with each measurement method.

3.2 Methods

3.2.1 Objective 2a: NH_3 Flux Measurements[*]

Complete descriptions of the study plot and field management practices are provided in Sections 2.2.2.1 and 2.2.2.2, respectively. The REA system was setup in the afternoon on DOY 126, 4 h after planting of the study plot was complete. The FG system was setup over the following two days and was operational on DOY 129. The study plot was serviced with two 20 A electrical circuits, both of which were required to operate the computers and pumps associated with the measurement systems. The REA and FG systems were situated 5 m apart at the center of the study plot, fully surrounded by plants (Figure 3.1).

[*] ***A brief note on my specific contributions to objective 2a:*** NOAA designed and constructed the FG system to quantify NH_3 flux at the Energy Farm during the 2014 corn-growing season. I provided technical and field support to deploy and operate the FG system during this season. NOAA completed all initial calculations of NH_3 flux using the FG system before providing data to me. I worked closely with NOAA colleagues on data quality and we collaboratively developed the flux data set presented here. All subsequent analysis is my own.

Figure 3.1: The relaxed eddy accumulation (left tower) and flux-gradient (right tower) measurement systems were located 5 m apart in the center of the study plot.

3.2.1.1 Relaxed Eddy Accumulation System

The REA system used for this objective is described in Section 2.2. The system was operated intermittently throughout the growing season, with more sampling concentrated during the first 30 days following fertilization. REA samples were collected from 07:30 – 11:30 and 12:00 – 16:00 local time to represent average meteorological conditions and avoid sampling during atmospheric stability transitions at dawn and dusk. The REA system was not used to collect nighttime samples as it is not expected to perform well during highly stable atmospheric conditions (Fotiadi et al., 2005).

3.2.1.2 Flux-Gradient System

The FG technique is theoretically described by analogy to Fick's laws of diffusion, with an assumption that turbulent transfer is analogous to molecular diffusion. The turbulent flux is therefore proportional to the product of the mean vertical mixing ratio gradient and the vertical eddy diffusivity, K (Baldocchi at al., 1988). By assuming mass and energy are transported by the

same eddies, eddy diffusivities are assumed equal among scalars and heat in the atmosphere. Hence, the FG technique assumes that the eddy diffusivity of each tracer gas is identical to the measured eddy diffusivity of heat (Hicks and Wesely, 1978). Based on this assumption, K is determined directly by combining the measured eddy covariance flux of temperature (F_H) and gradient measurements of temperature and concentration. Thus, the NH_3 flux from FG (F_{FG}) is calculated using Equation 3.1:

$$F_{FG} = -K_H\left(\frac{\Delta C_{NH_3}}{\Delta z}\right) = F_H\left(\frac{\Delta C_{NH_3}}{\Delta T}\right) \qquad \text{Equation 3.1}$$

where K_H is the eddy diffusivity for sensible heat ($m^2\ s^{-1}$), ΔC_{NH3} is the difference in NH_3 concentration ($ng\ m^{-3}$) between two measurement heights, Δz is the vertical distance between the two measurement points (m) and ΔT is the corresponding difference in temperature (K). Eddy covariance measurements of temperature flux were used to determine K_H (Myles et al., 2011).

The FG system is graphically depicted in Figure 3.2. The vertical distance between the two measurement heights was kept constant (Δz = 1.3 m) with a lowest initial measurement height of z = 0.4 m above the ground prior to corn emergence. Sampling height was adjusted with an automated exchange mechanism (AEM) (REBS Inc.: Bellevue, WA). The AEM design was similar in principle to that described by Gay and Fritschen (1979). After emergence, measurement height was adjusted weekly such that z = 0.2 m and 1.5 m above the canopy.

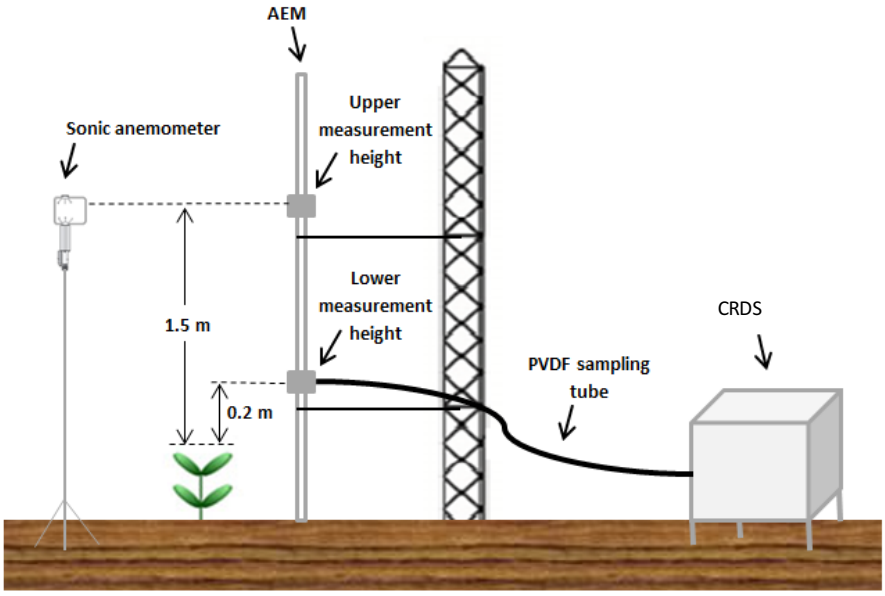

Figure 3.2: Schematic of the flux-gradient (FG) sampling system with an automated exchange mechanism (AEM), cavity ring down spectrometer (CRDS), and polyvinylidene fluoride (PVDF) sampling tube.

In order to determine K_H, the sensible heat flux was measured by eddy covariance using a sonic anemometer (model 81000 VRE, R.M. Young: Traverse City, MI) placed at 1.5 m above the canopy. Temperature and 3D wind speed (*u, v, w*; m s^{-1}) were measured with the sonic anemometer at 10 Hz using a custom Linux-based acquisition program developed by the NOAA ATDD (Oak Ridge, TN) (Meyers et al., 1996). Measurements of temperature at the lower and upper measurement heights were made with resistance thermometers (100 Ω Platinum Thermometer, Thermometrics Crop.: Northridge, CA) housed in aspirated radiation shields (model 43502, R.M. Young: Traverse City, MI) to minimize solar heating effects. 30 min average values of K_H were calculated using Equation 3.2:

$$K_H = -\frac{\overline{w'T'}}{(\Delta T/\Delta z)} \qquad \text{Equation 3.2}$$

where $\overline{w'T'}$ is the sensible heat flux (W m^{-2}), overbars represent 30 min averaging, and primes denote instantaneous deviation from the mean.

Concentration of NH_3 was measured using a cavity ring-down spectroscopy (CRDS) instrument (model G2103, Picarro Inc.: Santa Clara, CA) at the upper and lower measurement heights. The lower detection limit of this instrument for NH_3 is < 0.06 μg m^{-3} with an accuracy of (± 5 % of reading + 0.35 μg m^{-3}) at a 300 s averaging time. CRDS is a laser absorption technique, which measures the lifetime of photons reflected between two mirrors in an optical cavity and determines the sum of sample extinction between the cavity mirrors, enabling quantification of NH_3 concentration by the strength of near-infrared absorption. (Scherer et al., 1997). The advantage of this method is that it allows absorption measurements using very long optical path lengths (effective path length up to 20 km) while maintaining a closed optical cell to enable single point measurements and limit contamination (Moosmüller et al., 2005).

The CRDS instrument was connected to a rotary pump (model 0523, Gast Manufacturing Inc.: Benton Harbor, MI) sampling at 70 L min^{-1}. The CRDS and pump were housed in an air-conditioned enclosure unit in which the temperature was adjusted to 10 °C below ambient to prevent overheating. The CRDS was calibrated by the manufacturer, but before use an additional calibration was completed using a zero check and span adjustment according to manufacturer directions. The zero check was performed with ultrahigh purity nitrogen (99.999%) and the span adjustment was performed using 715.8 μg m^{-3} (1030 ppb) NH_3 (NIST-traceable reference gas; Air Liquide: Plumsteadville, PA).

An inlet tube was used to transfer air to the CRDS because it was housed in an enclosure and was situated in an agricultural field. Due to the high water solubility and polarity of NH_3, the choice of the sampling tube material was carefully investigated. Polyvinylidene fluoride (PVDF)

was selected for use as the tubing material based on an experimental study by Vaittinen et al. (2014) that found it to be the least adsorbent polymer of five tested. An 8 m PVDF sampling tube (25.4 mm OD, 22.2 mm ID, McMaster-Carr: Elmhurst, IL) was used for the inlet line. The sampling tube was warmed with heating tape to 5 °C above ambient temperature to prevent condensation and limit NH_3 loss. The sampling tube was attached to the AEM allowing vertical movement.

NH_3 fluxes were continuously monitored (24 h/day) during the first three months of the 2014 corn-growing season (DOY 129 – 212), starting two days after fertilization and planting. NH_3 concentrations were averaged over 30 min. Due to precipitation events that blocked the sonic anemometer, 1.5% of overall samples were not collected. Furthermore, data corrections were conducted due to increasing pressure drop across the CRDS internal filter over time due to aspirated particulate dust which contributed to increased response time. The response time of the FG system was measured at the beginning and end of the experiment, then corrected using the method of McCarthy (1973), based on a least squares exponential curve fit. The response time for the correction ranged from 4.8 min to 10.5 min. NH_3 data were smoothed to remove noise using a cubic spline filter. Data were further processed by removing measurements where the magnitude of the measured NH_3 flux exceeded the population mean by more than five standard deviations.

NH_3 flux was calculated in 30 min averages (FG_{30min}) using the FG method. Subsequently, 240 min average fluxes (FG_{240min}) were calculated from these data to compare with the timescale of REA measurements. FG_{240min} was calculated as a moving boxcar average, where averages were only calculated if FG_{30min} samples existed for the duration of the 240 min period.

3.2.1.3 Flux Footprint Analysis

Flux footprint was calculated for all REA and FG sampling periods using the EddyPro software package (Version 5.1.1, LI-COR: Lincoln, NE) (Nelson et al., 2017). Footprint was calculated for NN% = 10%, 30%, 50%, 70%, and 90% distances, where NN% distance corresponds to the calculated radius (r) of the area that contributed NN% of the total measured flux. The flux footprint calculation was used to select REA and FG samples where significant measured NH_3 flux originated from within the study plot (i.e., 70% and 90%). Samples were selected by comparing the 70% and 90% footprint distances corresponding to the shortest boundary of the study plot, r = 100 m. For example, if $r_{70\%} < 100$ m for a particular sample, it was selected for further analysis.

3.2.2 Objective 2b: Inter-comparison of REA and FG Measurements

All REA and FG measurements were compared to determine the total number of concurrent measurements after qualification using both the 70% and 90% footprint distance. For any 4 h REA measurement, an FG measurement was considered to be concurrent if there were at least 3 h of overlapping data. This data qualification procedure based on footprint analysis ensures that reported data are representative of fluxes from the study plot and mitigates the influence of NH_3 emissions from neighboring fields.

Data were analyzed to investigate correlation and closure between coincident F_{REA} and $F_{FG240min}$ data. The Pearson correlation coefficient ($Correl(REA, FG)$) was calculated for all coincident measurements using Equation 3.3:

$$Correl(FG, REA) = \frac{\sum(F_{FG240min} - \overline{F_{FG240min}})(F_{REA} - \overline{F_{REA}})}{\sqrt{\sum(F_{FG240min} - \overline{F_{FG240min}})^2 \sum(F_{REA} - \overline{F_{REA}})^2}} \quad \text{Equation 3.3}$$

A nonparametric Wilcoxon ranks sum test was also used to evaluate whether there was statistically significant difference among the two measurement methods at a 0.95 confidence level (Walker et al., 2013).

3.3 Results and Discussion

3.3.1 Objective 2a: NH_3 Flux Measurements using Flux-Gradient

3.3.1.1 Full-Season Flux Measurements

Full-season NH_3 flux measurements from the REA and FG methods are presented in Figure 3.3A. FG measurements in Figure 3.3A, reported as 30 min averages (FG_{30min}), are selected based on footprint according to the method described in Section 3.2.1.3.

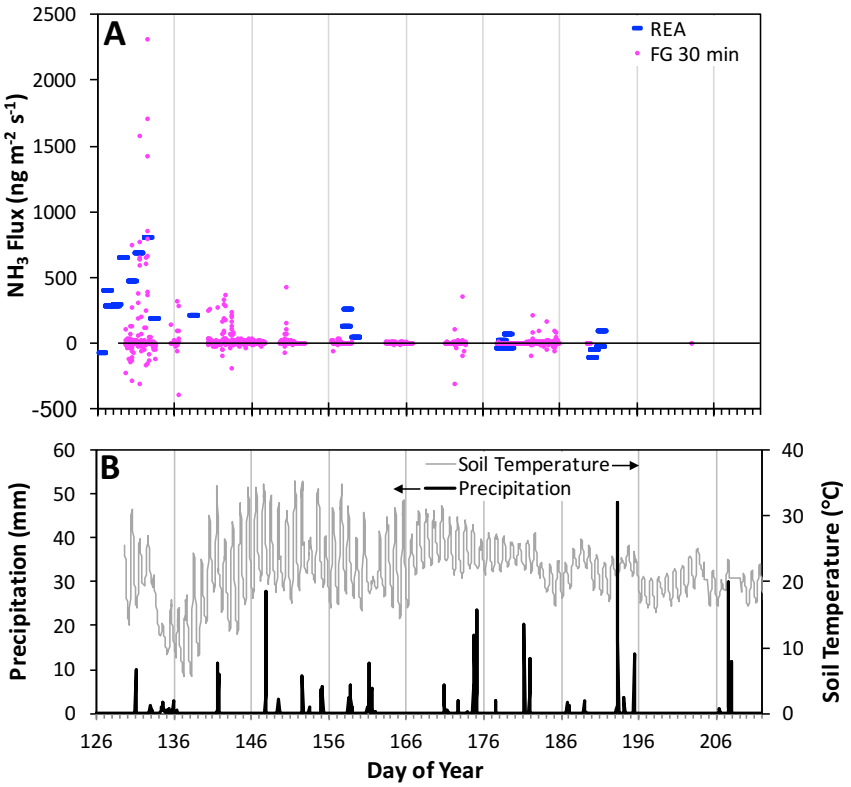

Figure 3.3: (A) NH_3 flux as measured using relaxed eddy accumulation (REA) and 30 min averaged flux-gradient (FG_{30min}) systems at the study plot for the full growing season (fertilization occurred on DOY 126). (B) Soil temperature (30 min average) and precipitation (30 min accumulated per event).

Mean soil temperature was 21.4 ± 4.4 °C, with lowest temperatures observed shortly following fertilization (DOY 133 – 140), when mean soil temperature was 13.5 ± 4.6 °C (Figure 3.3B). Total precipitation for all data reported in Figure 3.3B was 1082 mm as rain.

A summary of mean, maximum, and minimum NH_3 flux measured using REA and FG are presented in Table 3.1. FG results presented in Table 3.1 are divided into FG_{30min} and FG_{240min} data. Further, daytime and nighttime mean fluxes are provided for the FG method. REA results are not divided into daytime and nighttime measurements because REA was not used for nighttime measurements.

	NH_3 Flux (ng m^{-2} s^{-1})		
	REA	**FG_{30min}**	**FG_{240min}**
All data			
Mean	147 ± 284	23.9 ± 148	12.4 ± 73.2
Maximum	800	2312	1023
Minimum	-161	-400	-93
Daytime	- -	25.9 ± 93.5	17.0 ± 85.4
Nighttime	- -	-0.23 ± 0.23	0.1 ± 0.1
DOY 126 - 156			
Mean	431 ± 204	29.4 ± 169	24.0 ± 103
Daytime	- -	53 ± 159	34.4 ± 122
Nighttime	- -	-0.5 ± 9.0	0.4 ± 6.0
After DOY 156			
Mean	13.7 ± 99.2	0.8 ± 23.3	1.1 ± 7.1
Daytime	- -	1.4 ± 21.1	1.6 ± 7.7
Nighttime	- -	0.0 ± 2.0	-0.2 ± 1.8
Concurrent data			
Mean	205 ± 300	- -	110 ± 256

Table 3.1: Summary of all NH_3 flux measurements using relaxed eddy accumulation (REA) and flux gradient (FG) methods. FG_{30min} data correspond to 30 min average fluxes using FG, and FG_{240min} are 240 min averages. Data are further subdivided based on the first 30 days after planting (DOY 126-156) and the remainder of the season (after DOY 156), where DOY is "day of year".

Mean NH_3 fluxes over the entire growing season were 147 ± 284 ng m^{-2} s^{-1} and 23.9 ± 148 ng m^{-2} s^{-1} with REA and FG_{30min} data, respectively. The difference in mean flux measured with each system is attributed to the higher temporal resolution of the FG system, resulting in FG

measurements across more environmental and atmospheric conditions, including measurements of deposition during nighttime and more measurements during daytime

3.3.1.2 Early Season Emission and Impact of Timescales

A similar emission trend was observed using both measurement methods. That is, peak NH_3 emission occurred during the first 30 days after fertilization followed by lower emissions for the remainder of the corn-growing season. Figure 3.4 presents measurements using REA and FG_{30min} for the first 30 days following fertilization as well as precipitation and soil temperature data for the same time period.

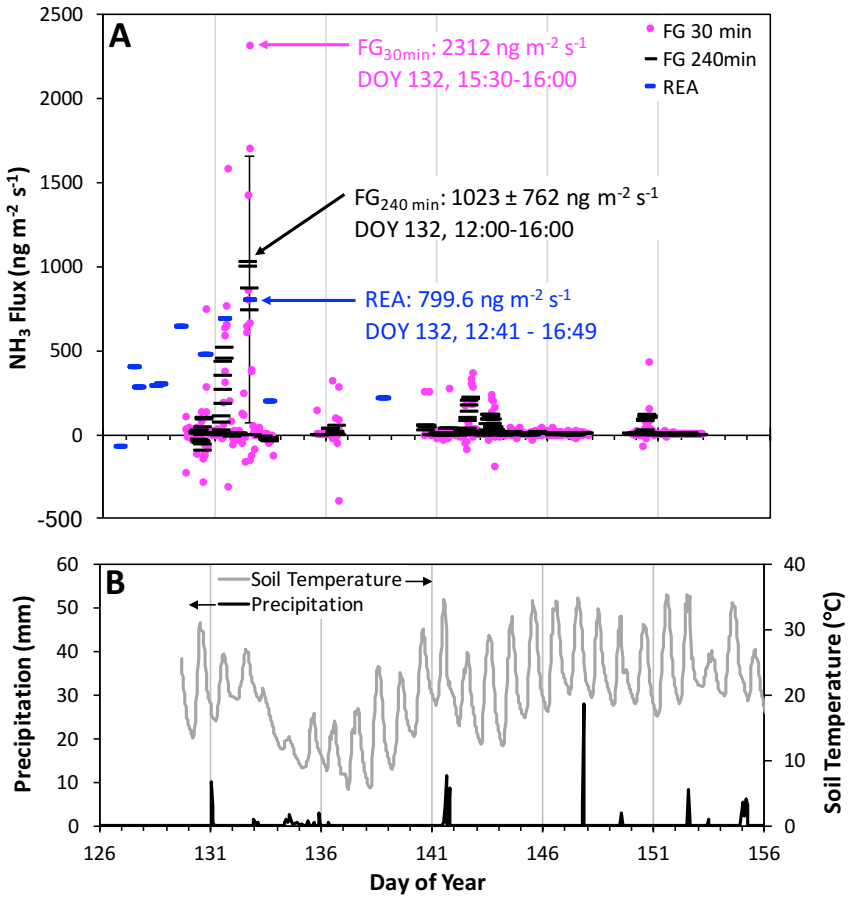

Figure 3.4: (A) Relaxed Eddy Accumulation (REA), 30 min flux-gradient (FG_{30min}), and 240 min flux-gradient (FG_{240min}) measurements of NH_3 flux during the first 30 days after fertilization. Error bars for the FG_{240min} maximum represent the standard deviation of eight averaged 30 min measurements. (B) Soil temperature and precipitation during the same period.

Maximum observed NH_3 emission was 800 ng m^{-2} s^{-1} with REA and 2312 ng m^{-2} s^{-1} with FG_{30min}. The REA emission peak was observed during the 12:41 – 16:49 averaging interval on DOY 132 while the FG_{30min} peak was observed on the same day during the averaging period at 15:30 – 16:00 (all reported as local time). While the averaging periods for both maxima overlap, results from the FG_{30min} measurements indicate a high amount of variability. FG_{30min} measurements ranged from -157 to 2312 ng m^{-2} s^{-1} between 13:00 and 17:00 on DOY 132 with standard deviation of 762. Though the net flux during this time period was positive, there was one FG_{30min} sample where deposition was observed (15:00 – 15:30). 10 mm precipitation as rain occurred on DOY 131, followed by a cold front, resulting in reduced soil temperature from a maximum of 30.9 °C in the afternoon on DOY 130 (Figure 3.4B) to a maximum of 13.2 °C in the afternoon on DOY 134. Soil temperature did not return to 30.9 °C until DOY 141 in the morning.

To further investigate the effect of averaging time on the observed variability of NH_3 flux, REA measurements were compared with FG measurements averaged to 240 min intervals (FG_{240min}). Maximum emission was again observed in the afternoon on DOY 132 for both systems, where max REA flux was 800 ng m^{-2} s^{-1} from 12:41 – 16:49 and FG_{240min} maximum was 1023 ± 762 ng m^{-2} s^{-1} from 12:00 – 16:00, reported as the mean FG_{240min} value with standard deviation of the eight averaged FG_{30min} measurements. No error bars are presented for REA or FG_{30min} measurements because each data point represents a single measurement. Error bars are presented for the FG_{240min} maximum because this data point represents an average of eight FG_{30min} measurements. Error bars are not shown for all FG_{240min} data to maintain clarity of the figure. The REA and FG_{240min} flux maxima are not statistically different at 95% confidence level, due to the high standard deviation of the FG_{240min} measurement. The FG_{240min} peak was shifted

earlier in the day by 0.75 h when compared to REA because emissions were generally higher earlier in the afternoon.

The maximum 240 min averaged fluxes measured in this study are consistent with values of midday flux of 700 ± 1100 ng m^{-2} s^{-1}, reported by Walker et al. (2013). However, the FG system is capable of resolving the early season emission trend in higher resolution than previously reported in the literature using accumulating NH_3 flux measurement techniques (Nelson et al., 2017; Walker et al., 2013). This increased temporal resolution provides new information about non-stationarity in the NH_3 emission profile, where short-duration emission pulses vary in intensity by multiple orders of magnitude within a 4 h period. Further, the FG method provides an advantage over accumulating methods in that higher time resolution measurements subject to footprint distances that exceed the field boundary can be readily removed. It is therefore possible to collect more data when surface roughness and canopy height are low, corresponding to larger footprint distances. Such data are important to more fully understand the mechanism and profile of NH_3 fluxes.

Two different periods of elevated NH_3 emission were measured using the FG system: the first occurring during DOY 130 – 132, and the second during DOY 140 – 143. The timing and occurrence of these two distinct periods are attributed to environmental conditions (i.e., precipitation and soil temperature) and the use of urease inhibitor during fertilization. Previous studies have found elevated NH_3 emission to be correlated with higher temperatures (Sharpe and Harper, 1995; Balasubramanian et al., 2017). The highest FG_{30min} emission (2312 ng m^{-2} s^{-1}) was observed in the afternoon on DOY 132. This was followed by intermittent precipitation beginning at 23:00 on DOY 132 through 12:30 on DOY 136 resulting in a total rainfall during this period of 55 mm. Soil temperature subsequently reduced from 22.5 ± 2.8 °C on DOY 132 to

a minimum of 11.6 ± 4.0 °C on DOY 137 (where temperatures are reported as average of 26 daytime measurements), and lower NH_3 emission was observed. Soil temperature then increased, reaching 24.4 ± 4.9 °C on DOY 140, concurrent with the second elevated emission period.

Beside meteorological parameters, the timing of the NH_3 emission peaks can be influenced by the properties of the applied fertilizer. Walker et al. (2013), observed two periods of elevated NH_3 emission following application of 134 kg-N ha^{-1} UAN with Agrotain®: one during the first week after fertilization (500 ng m^{-2} s^{-1}) and a second during the third week after fertilization (700 ng m^{-2} s^{-1}). Walker et al. attributed the emission profile to the effect of the urease inhibitor, where the first period is attributed to the NH_4^+ fraction of the UAN volatilizing as NH_3, and the second period corresponds to reduced effectiveness of the urease inhibitor, resulting in hydrolysis of urea to NH_4^+ and subsequent volatilization as NH_3.

The profiles reported here and by Walker et al. (2013) differ from those reported by Rawluk et al. (2001) and Engel et al. (2011) during focused studies on the effect of urease inhibitor. In seven of eight field trials using chamber measurement methods, Rawluk et al. reported an emission profile with two periods of elevated NH_3 emission in only one trial. Engel et al. (2011) reported NH_3 emission peaks occurring 20 – 40 days after fertilization across 12 field trials, and presented no cases in which a bi-modal pattern of emission was observed. It is important to note that the study by Engel et al. was conducted over cold soils (-2 to 5 °C), so the magnitude of the time delay is expected to be increased when compared with this study. However, both of these studies were conducted using integrated sampling methods, with averaging intervals of one to four days by Rawluk et al., and five to seven days by Engel et al. Due to the short duration (< 2 days) of the first elevated emission period reported both in results presented here and by Walker et al. (2013), it is possible that such a peak would not have been

observed using longer averaging intervals (i.e., days). Further research is required to quantify the effect of urease inhibitor at the field scale relative to local environmental conditions.

3.3.1.3 Diurnal NH_3 Emission

A dynamic deadband was used in the REA system to increase the relative measured concentration of NH_3 in up- and down-draft denuders (Bowling et al., 1999). This approach helps to more effectively resolve NH_3 flux during turbulent conditions but can result in reduced data quality during neutral and stable nighttime conditions. As such, the REA method as used in this field campaign is not a suitable approach to measure nighttime NH_3 fluxes (Fotiadi et al., 2005).

Conversely, the FG method does not rely on turbulent eddies to trigger conditional sampling during up- and down-drafts. This enables the FG method to quantify flux across a broad range of atmospheric stability, including nighttime conditions. Additionally, the shorter 30 min averaging period reduces the impact of atmospheric non-stationarity on data quality. A clear diurnal pattern of NH_3 flux was observed, in which the highest positive fluxes and greatest variability in flux (as characterized by standard deviation) occurred during daytime hours. Mean NH_3 flux and standard deviation for each 30 min period across all qualified measurements are presented in Figure 3.5.

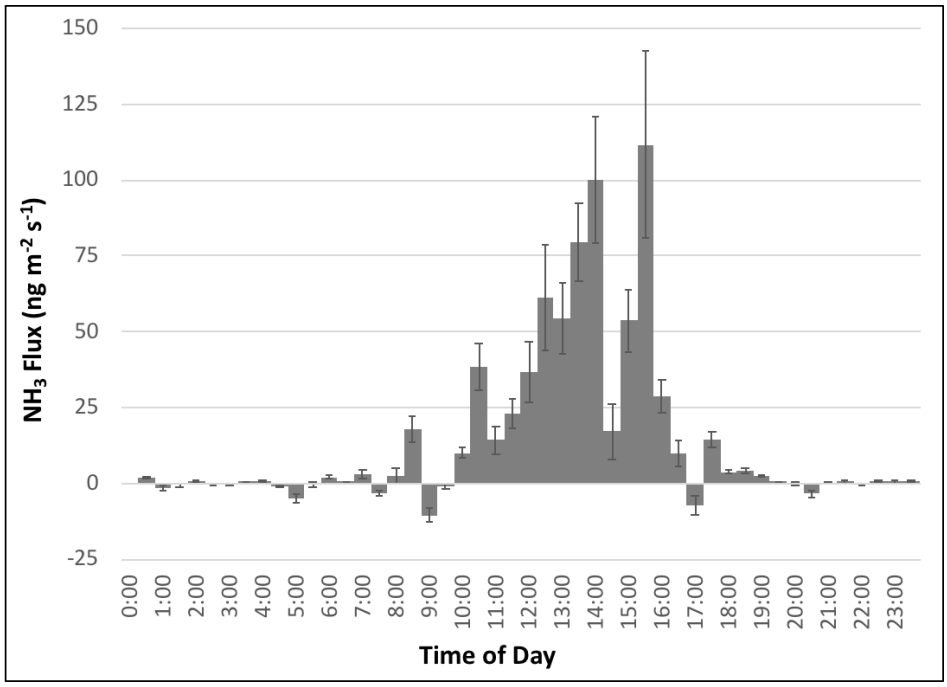

Figure 3.5: Diurnal pattern of NH_3 emission as measured using the flux-gradient method, where solid bars indicate mean NH_3 flux during each 30 min period and error bars represent standard error.

For the entire growing season, mean daytime FG_{30min} flux was 25.9 ± 93.5 ng m^{-2} s^{-1}, while mean nighttime flux was -0.23 ± 0.23 ng m^{-2} s^{-1}. When calculated for the first 30 days after fertilization (DOY 126 – 156), mean daytime flux was 53 ± 159 ng m^{-2} s^{-1}, compared to nighttime flux of -0.5 ± 9.0 ng m^{-2} s^{-1}. Following the first 30 days after fertilization, emission to the atmosphere was markedly lower during the daytime for the subsequent 30-day period (DOY 157 – 186), where daytime flux was 1.4 ± 21 ng m^{-2} s^{-1}, and 0.04 ± 2.1 ng m^{-2} s^{-1} during nighttime.

3.3.2 Objective 2b: Inter-comparison of REA and FG Measurement Methods

3.3.2.1 Inter-Comparison of Concurrent Measurements

After FG data qualification for $r_{90\%}$ < 100 m and $r_{70\%}$ < 100 m, remaining measurements were compared to determine total concurrent samples (Table 3.2).

	Number of Measurements (N)		
	Total	**$r_{70\%}$ < 100 m**	**$r_{90\%}$ < 100**
REA	39	23	22
FG	2782	1178	896
Concurrent (4 h)	10	10	7
Concurrent (30 min)	82	82	57

Table 3.2: Total number of relaxed eddy accumulation (REA) and flux-gradient (FG) measurements, remaining qualified measurements after using 70% and 90% footprint distance, and concurrent REA and FG samples, where "4 h" indicates measurements were concurrent during the entire 4 h REA interval and "30 min" indicates a coincident REA measurement occurred during a 30 min FG measurement.

The REA system was operated most regularly during the first 30 days after fertilization, as this was the period of greatest interest for NH_3 flux measurement (Nelson et al., 2017). Therefore, it was also expected that the most concurrent REA and FG measurements would occur during this part of the season. However, challenges associated with the operation of the FG system at the beginning of the season limited the total number of concurrent measurements during this period. For the 70% footprint condition, six concurrent measurements were collected between DOY 131-158, while three concurrent measurements were collected for the 90% footprint condition. Since the early-season period is of most interest for NH_3 emissions (Walker et al., 2013; Nelson et al., 2017), the 70% footprint condition was used for the purpose of method inter-comparison discussed in this section (Table 3.3).

DOY	$\overline{F_{NH3}}$ (ng m^{-2} s^{-1})		
	REA (Nelson et al., 2017)	**FG** ($r_{70\%}$ < 100 m)	**FG** ($r_{90\%}$ < 100 m)
131	682.1	379.1	
132	799.6	752.6	
133	191.3	-35.9	
157	-8.5	5.0	5.0
158_1	130.8	-0.2	-0.2
158_2	254.5	-0.5	-0.5
178_1	-36.6	-0.1	-0.1
178_2	14.3	-0.1	-0.1
179_1	71.2	0.04	0.04
179_2	-44.8	0.01	0.01
All	**205 ± 300**	**110 ± 256**	**0.6 ± 2.0**

Table 3.3: Summary of all concurrent relaxed eddy accumulation (REA) and flux-gradient (FG) measurements. REA measurements were footprint-corrected according to the method described in Chapter 2. FG measurements were averaged to a 4 h interval, after 70% and 90% footprint qualification, where _1 and _2 indicate morning and afternoon measurements, respectively.

$Correl(REA, FG)$ for all concurrent $r_{70\%}$ measurements, averaged to the 4 h REA averaging interval, was 0.91, indicating a strong correlation between the flux trends observed with both systems at the timescale of REA measurement. Measurements from both systems were in agreement using the Wilcoxon rank sum test at a 0.95 confidence level.

Later season REA flux measurements (i.e., after DOY 157) were lower when compared with DOY 126-157, with mean measured flux of 14 ± 99.2 ng m^{-2} s^{-1}. For concurrent samples during DOY 158-179, mean flux with REA was 57.3 ± 106 ng m^{-2} s^{-1}, compared to -0.50 ± 5.10 ng m^{-2} s^{-1} with FG_{240min}. The FG method did not further resolve flux variability with 30 min or 240 min measurements during this period ($\overline{FG_{30min}}$ = 0.8 ± 23.3 ng m^{-2} s^{-1}; $\overline{FG_{240min}}$ = 1.1 ± 7.1 ng m^{-2} s^{-1}).

3.3.2.2 Benefits and Limitations of Measurement Methods

The REA method has been well-documented in literature for use in measuring trace atmospheric fluxes of NH_3 from fertilized fields (Myles et al., 2007; Walker et al., 2013; Nelson et al., 2017). However, these field campaigns have either been focused on a short period (1 – 3 months) of the total growing season (Myles et al., 2007; Walker et al., 2013) or limited in total number of measurements (N = 35) across a full growing season (Nelson et al., 2017). This is largely due to the labor required to operate an accumulating system coupled with the need for subsequent laboratory analysis of samples. It is necessary when operating such a system to have personnel on site at the beginning and end of each measurement interval. Further, samplers must be prepared and extracted in a controlled laboratory environment and stored under refrigeration. While not insurmountable, these challenges add to the complexity of using a REA system, under realistic field conditions.

The FG system was designed for near-autonomous, continuous operation under field conditions, though visits were required on a weekly basis to adjust the AEM and reference sonic anemometer and to install a clean inlet. However, the complexity of the FG system led to additional downtime due to equipment malfunctions and required frequent maintenance and adjustment. The length of the sampling line, combined with repeated vertical movement of the AEM, resulted in kinking of the sampling line on multiple occasions. Challenges with the sampling line heater also resulted in condensation of water in the sample lines during periods of high relative humidity. Future research focused on technical improvements of the system could resolve some of these issues.

Though the complete REA system does require more regular field visits for operation, it benefits from being relatively inexpensive (< $10,000 equipment and installation costs) to deploy

in the field. When compared with the complete FG system (> $100,000 equipment and installation costs), the cost of deploying a REA system has significant advantages when seeking to measure NH_3 emissions from a diverse range of field conditions, crop types, and agricultural practices. However, for situations where it is desirable to obtain higher time resolution emission and deposition fluxes in the first several weeks after fertilization, the REA method cannot provide the high temporal resolution that is possible with FG.

3.4 Summary and Conclusions

This research presents the first inter-comparison of NH_3 flux measurements using the relaxed eddy accumulation (REA) and flux gradient (FG) methods in the Midwest US. This inter-comparison was conducted using measurements collected above an intensively managed corn canopy in Central, Illinois, USA, thereby providing important new data regarding NH_3 fluxes under meteorological conditions in this area. Use of the FG system enabled temporal resolution of early-season peak fluxes greater than those previously reported using accumulating measurement methods. Results from the REA and FG system were highly correlated, with Pearson correlation of 0.91 between the two systems, when measurements at the same averaging time (4 h) were compared.

The FG system resolved two distinct periods of elevated early-season emission (DOY 130 – 132 and DOY 140 – 143). This was made possible by the advantage of 30 min sampling and straightforward removal of data when large footprint conditions were observed. The ability to accurately quantify fluxes over the 4 h REA averaging interval was limited during the second elevated emission event due to high winds and low surface roughness. The two periods of elevated emissions are attributed to a combination of the effect of localized environmental conditions (i.e., precipitation and soil temperature) and nBTPT urease inhibitor. Further research

is needed to understand the extent of the impact of these factors on early-season emission and to improve evaluation of process-based models with increased temporal resolution (i.e., < 1 h).

Inter-comparison of the two measurement methods indicated that both methods are in good agreement with respect to 4 h average NH_3 fluxes. The FG system was able to resolve temporal variability in 30 min intervals that was not possible using the REA system. However, it was also sensitive to mechanical failure and extreme weather conditions, which resulted in loss of data during the corn growing season. The REA method is labor-intensive, and needs be supported by strict quality assurance and quality control procedures for measurement of the typically low ambient NH_3 concentrations. The integrated nature of REA sampling often necessitates long fetch that can be challenging to achieve in many field conditions. When taken with other measurement considerations such as cost of equipment and operation, it is clear that there are tradeoffs needing careful consideration before implementing the methods in different environments. It appears that further method development and inter-comparison in diverse climatic, topographical, and land-use environments are essential to assist improved understanding of the spatial and temporal variability of biosphere-atmosphere NH_3 flux from agricultural fertilizer application and to facilitate evaluation of numerical models describing NH_3 emission and air quality.

CHAPTER 4: EVALUATION OF THE DENITRIFICATION DECOMPOSITION MODEL FOR QUANTIFYING AMMONIA FLUX*

4.1 Research Motivation and Significance for Objective 3

There is a need for increased measurement of fine spatial resolution (1 km radius) NH_3 emissions combined with collection of ancillary data to improve the accuracy of NH_3 emission models which serve as inputs to regional air quality models (Cooter et al., 2010; Flechard et al., 2013). Biogeochemical models such as DNDC can be employed to characterize temporal trends of NH_3 flux by accounting for the biological, chemical, and physical processes that drive NH_3 exchange between the biosphere and atmosphere. Evaluation of closure between experimental measurements and modeled results is important to enable future research focused on modeling of NH_3 fluxes at a regional scale for input to air quality and chemical transport models. This process of expanding from site-scale to regional-scale modeling is known as upscaling. However, before upscaling of NH_3 flux models can be implemented more broadly, modeled outputs must first be evaluated in the context of experimental measurements at the site scale (i.e., a single farm). Objective 3 addresses this need by coupling site-scale NH_3 emission measurements with measurement of ancillary environmental parameters to evaluate closure with a DNDC NH_3 emission model.

Models such as DNDC parameterize pathways of evolution for different trace gas fluxes with different degrees of detail. It is therefore important to evaluate the model for each of its trace gas outputs under different environmental conditions, crops, and management practices in different localities (Bennett et al., 2013). Results from this research respond to the need of

* Reproduced in part and adapted with permission from S. Balasubramanian, A.J. Nelson, S. Koloutsou-Vakakis, J. Lin, M.J. Rood, L. Myles, C. Bernacchi (2017) Evaluation of DeNitrification DeComposition model for estimating ammonia fluxes from chemical fertilizer application, *Agr. Forest Meteorol*. 237–238, 123-134.

evaluating DNDC for NH_3 flux with experimental results, at a location in the Midwest US and are important to guide future efforts to: (1) further improve DNDC predictions; (2) facilitate quantitative estimates of NH_3 fluxes and associated uncertainties for use in emission inventories, and (3) test the model as a tool for upscaling NH_3 emissions from the site to the regional scale. Objective 3 is comprised of three sub-objectives. ***Objective 3a*** is focused on the development of input data sets from measurements collected at the Energy Farm and other available data sources. ***Objective 3b*** develops a new method to estimate closure between modeled and measured NH_3 flux using an inhomogeneous measurement study domain. ***Objective 3c*** evaluates closure between DNDC modeled NH_3 emissions and measurements described within Objectives 1 and 2.

4.2 Methods*

4.2.1 Objective 3a: Development of Input Datasets for DNDC Model Runs

DNDC (version 9.5, downloaded January 2014) models variations in trace gas fluxes at the site scale as a function of weather, soil, crop growth and field management practices (Li, 2000). Input data are used to model the evolution of soil climate and processes in the soils such as nitrification, denitrification and decomposition that produce trace gas fluxes. NH_3 fluxes are estimated within the decomposition sub-model. In the model, NH_3 flux is regulated by soil ammonium concentration (generated by the turnover of soil organic matter), soil pH, and ambient temperature (governing the partitioning of NH_3 between liquid phase in soil and gaseous

* ***A brief note on my specific contributions and those of my colleagues for work described within Objective 3.*** All DNDC model runs were completed by Srinidhi Balasubramanian alone. I worked collaboratively with Ms. Balasubramanian and colleagues at UIUC, ISWS, and NOAA to develop input data sets described in Objective 3a, specific modeling cases and methods for footprint evaluation in Objective 3b, and methods for closure evaluation in Objective 3c.

phase in soil pores). Volatilization of NH_3 to the atmosphere from soil pores is controlled by diffusion as a function of porosity and clay content (Li, 2000). NH_3 deposition is modeled based on atmospheric NH_3 concentrations and deposition velocity adjusted for LAI, crop nitrogen and leaf surface moisture (Li, 2000).

4.2.1.1 Layout of Study Plot and Neighboring Agricultural Fields

Measurements using the REA method at the Energy Farm study plot, described in Chapter 2, were used for the model evaluation presented in this Chapter. The surrounding agricultural fields are described in Figure 4.1, where plot 1 is the corn study plot described in Chapter 2. Surrounding plots were planted with miscanthus (*Miscanthus x giganteus*, plot 2), switchgrass (*Panicum virgatum* L., plot 3); and a mix of 28 native prairie species (plot 4) during the 2014 growing season. Privately owned corn fields (plot 5) were located to the south and southwest. Alfalfa fields (plot 6) were located southeast of the Energy Farm.

Figure 4.1: Layout of the Energy Farm in Urbana, Illinois (plots 1-4). Relaxed eddy accumulation and flux-gradient measurements occurred in plot 1 (fully described in Chapters 2 and 3). Adjoining plots were planted with miscanthus (plot 2), switchgrass (plot 3), mix of 28 native prairie grasses (plot 4). To the south of the Energy Farm, crops included corn (plot 5) and alfalfa (plot 6).

4.2.1.2 Modeling Scheme and Input Data

For the measurement-model comparison study, the 90% footprint of the REA tower at the measurement site was considered. The method for REA footprint correction is described fully in Section 2.2.3. For the cases when the 90% REA footprint exceeded the boundary of plot 1, contributions from the surrounding crops (plots 2-6) were also estimated by running DNDC with the parameters of the respective 'sites'. Plots 2-6 were only modeled with DNDC when 90% footprint distance exceeded the boundary of plot 1 and wind roses (described in Section 2.3.3) showed wind originating from the direction of a particular plot (e.g., if wind originated from the southwest, plots 1, 2, and 5 were modeled).

For each plot, input data were first obtained from field records or, where unavailable, from regional databases or literature. Daily ambient temperature, wind speed, precipitation, solar radiation and humidity for years 1999-2014 were obtained from the ICN site at Bondville (15 km west of plot 1) (ISWS, 2018). Local site measurements of temperature and wind speed substituted the ICN data when available (April to October 2014). Ambient NH_3 concentration (NADP, 2017b) and NH_4^+ wet deposition data were obtained from observations at Bondville (NADP, 2018). Soil pH, bulk density and soil organic carbon were obtained from Energy Farm records (communication with Energy Farm manager Timothy Mies and field research specialist Michael Masters). These data resulted from analysis of bulk soil with 5 cores taken at each plot in April 2014 at depths of 0 – 10 cm and 10 – 30 cm. Soil texture (loam), clay content and porosity were obtained from the Web Soil Survey (USDA, 2015a). Saturation field capacity (water filled porosity at saturation field capacity, henceforth referred to as field capacity) and wilting point were obtained from measurements reported by the ICN for the Bondville site

(ISWS, 2018). Crop type, fertilizer type, amount of nitrogen applied, and fertilization, harvest, and plating dates for all plots are provided in Table 4.1.

Plot #	Crop type	Fertilizer type	Application Rate (kg-N/ha)	Application Date (DOY)	Planting Date (DOY)	Harvest Date (DOY)
Plot 1	Corn	28% UAN	168	126	126	310
Plot 2	Miscanthus	urea	56	102	144	326
Plot 3	Switchgrass	urea	56	102	78	332
Plot 4	Restored prairie	None	-	-	149	324
Plot 5	Commercial corn	28% UAN	180	86	113	310
Plot 6	Alfalfa	None	-	-	113	-

Table 4.1: Field management practices for all modeled plots.

Default values from DNDC's crop library were considered for corn and soybeans, except for growing degree days, which were obtained from ICN Bondville data (ISWS, 2018). Crop parameters for switchgrass and miscanthus were added to the DNDC crop library based on Heaton et al. (2008). Harvest for switchgrass and miscanthus was assumed to occur the year after planting. Default values from DNDC's crop library were used for prairie grass and alfalfa. A corn-soybean rotation was considered for years 1999 – 2005 and fertilizer management practices were developed following seasonal nitrogen management data (Balasubramanian et al., 2015). Turnover of cropland to establish the Energy Farm in years 2006 – 2007 was modeled as fallow land. For years 2008 – 2014, planting and harvest dates, fertilizer type, application amount and timing, and tillage dates were obtained from Energy Farm records for all plots (personal communication with Energy Farm manager, Timothy Mies). These baseline inputs were used to initialize independent DNDC model runs for crop plots 1 – 6 to model daily NH_3 fluxes for the year 2014. To minimize impact of initial conditions, a spin up period of 15 years was used (Fumoto et al., 2008; Perlman et al., 2013).

4.2.2 Objective 3b: Closure Evaluation in Inhomogeneous Field Conditions

A new method was developed to evaluate closure between modeled results and measurements from an inhomogeneous study domain. This was required to account for fluxes from surrounding crops for time periods when the REA footprint extended outside plot 1 and to account for the difference in time resolution between model predictions (daily) and measurements (4 h). The 90% REA footprint was first calculated for each measurement period, as described in Section 2.2.3). If the 90% footprint was less than 100 m (the minimum distance from the REA tower to edge of plot 1), measured NH_3 flux was assumed to include contributions only from plot 1. Otherwise, fluxes from plots 2-6 were also accounted. For measurement periods with 90% REA footprints exceeding 100 m, the 30%, 50% and 70% footprints were additionally calculated, and interpolation was performed to identify the percentage of flux contribution to REA measurements at 100 m and 141 m, corresponding the nearest edge and farthest corner of the study plot to the measurement tower, respectively:

$$NN\% = 100((\mathrm{C1} * R^4) + (\mathrm{C2} * R^3) + (\mathrm{C3} * R^2) + (\mathrm{C4} * R)) \quad \text{Equation 4.1}$$

where C1, C2, C3, and C4 are empirically derived coefficients and R is the footprint radius (m).

Prevailing wind direction was determined using wind roses for each measurement period. Wind direction was used to identify which contributing plots to consider. Frequency of wind from each direction was used to adjust the modeled flux at the measurement site by weighing the contributing fluxes relative to the REA footprints. The estimated NH_3 flux at the study plot was then calculated based on contributions of the study plot and neighboring fields:

$$F_{NH3,total} = [f_{P1}(F_{NH3})_{P1}] + (1 - f_{P1}) \sum_{i=P2}^{i=P5} \{(wd)_i (F_{NH3})_i\} \quad \text{Equation 4.2}$$

where f_{P1} is the fractional contribution of flux to $F_{NH3,total}$, and $(wd)_i$ is the fraction of time that wind originated from the direction of plot *i*, as determined by analysis using wind roses.

Estimated NH_3 flux at the measurement site ($F_{NH3,total}$) is comprised of contributions from plot 1 ($P1$) and outside plot 1 (i.e., plots 2, 3, 4, 5). $(F_{NH3})_{P1}$ represents the modeled NH_3 fluxes using DNDC for plot 1. Similarly, $(F_{NH3})_i$ refers to modeled fluxes using DNDC for plots i={2, 3, 4, 5}. The contribution of fluxes from outside plots were weighed using the fraction f_{P1} and $(wd)_i$ as described below.

The fraction f_{P1} was estimated as follows: for measurement periods when REA footprint was smaller than 100 m, $f_{P1} = 1$. When REA footprint exceeded 100 m, f_{P1} was reduced by first estimating 10%, 30%, 50% and 70% REA footprints, then applying the interpolation described above to estimate the percentage REA footprint at 100m. For example, if REA footprint at 100 m was calculated as 60%, then $f_{P1} = 0.6$. (i.e., 60% of the measured flux originated from plot 1 and 40% originated from outside plot 1).

After calculating f_{P1}, the plots contributing to the measured flux were identified to calculate the fractional contribution from each plot due to wind direction ($(wd)_i$. Wind roses were developed for each measurement period to estimate prevailing wind directions and identify contributing crops. If there was only one contributing crop, $(wd)_i$ was set at 1. However, if prevailing wind directions resulted in fluxes from two or more crops, then $(wd)_i$ was determined by considering the frequency of wind speed and direction; e.g., if wind originated from the south (plot 5) 80% of the time, and from the east (plot 3) 20%, then $(wd)_5 = 0.8$ and $(wd)_3 = 0.2$.

Differences in temporal scales between modeled and measured NH_3 fluxes were bridged using concurrent continuous NH_3 flux measurements from the FG method described in Chapter 3. The aggregated NH_3 flux profile over the measurement period as a function of time is presented in Figure 4.2. Hourly percent flux was first calculated for each day using data in Figure 4.2. Then, the mean and standard deviation of hourly percent fluxes were calculated for the entire

measurement period that the FG system was operated. The resulting mean hourly temporal profile was applied to scale the modeled NH_3 fluxes from the daily to the hourly scale and aggregated over the hours corresponding to REA measurements.

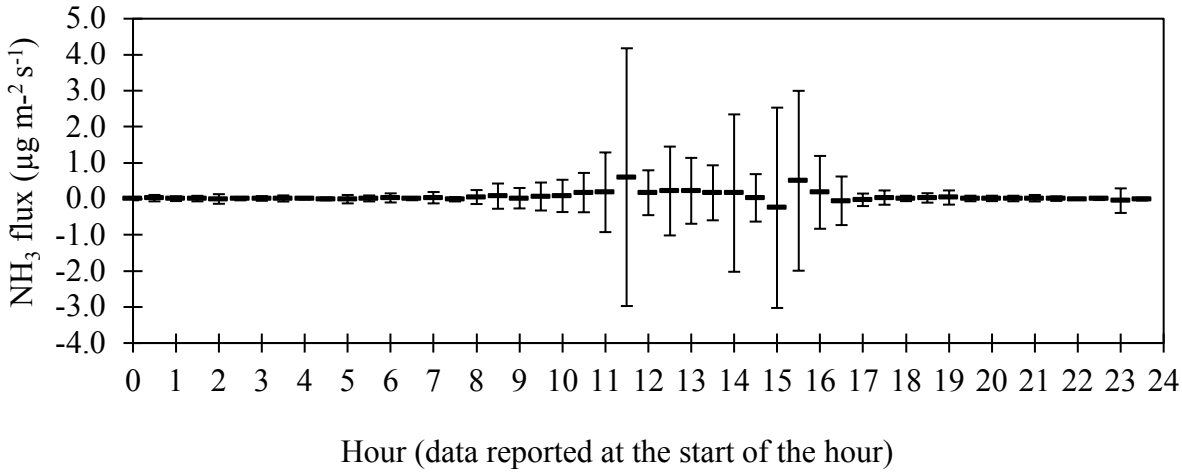

Figure 4.2: Distribution of mean hourly NH_3 flux and standard deviation based on flux gradient measurement data described in Chapter 3. Fluxes are averaged at an hourly scale and reported at the start of the hour.

Four scenarios were considered to obtain NH_3 flux outputs from DNDC:

(a) **'baseline'** – only fluxes from plot 1 were considered

(b) **'baseline_spatial'** – baseline NH_3 fluxes from plot 1 were adjusted for NH_3 fluxes outside plot 1 with REA footprint correction

(c) **'baseline_temporal'** – baseline NH_3 fluxes from plot 1 were scaled from day to the hour scale

(d) **'baseline_spatial_temporal'** – baseline NH_3 fluxes from plot 1 adjusted using both REA footprint and temporal scale corrections

4.2.3 Objective 3c: Evaluation of Closure Between Modeled and Measured Results

4.2.3.1 Statistics for Closure Evaluation

Closure was evaluated using analysis of association and analysis of coincidence. Analysis of association indicates how well trends in modeled and measured NH_3 fluxes are replicated while the analysis of coincidence estimates the differences in magnitude of modeled and

measured NH_3 fluxes (Smith and Smith, 2007). Association was analyzed using the sample correlation coefficient, r_a:

$$r_a = \frac{\sum_{i=1}^{i=n}(O_i - \bar{O})(P_i - \bar{P})}{\sum_{i=1}^{i=n}(O_i - \bar{O})^2 \sum_{i=1}^{i=n}(P_i - \bar{P})^2} \quad \text{Equation 4.3}$$

where, O_i is the i^{th} observation, $\bar{O}$ is the mean of i observations, P_i is the i^{th} prediction, $\bar{P}$ is the mean of i predictions, and n is the number of samples. When $r_a = 1$ a positive association of trends between measured and modeled values exists, while $r_a = -1$ indicates negative association. 'Significant' association is generally considered the condition when $r_a^2 \geq 0.8$ (Smith and Smith, 2007).

Coincidence was analyzed using the root mean square error, RMSE, described in Equation 4.4 and the Student's t-test, t, (Equation 4.5) to identify if differences in modeled and measured fluxes were statistically significant at 0.95 confidence level (Smith and Smith, 2007).

$$RMSE(\%) = \frac{100}{\bar{O}} \sqrt{\frac{\sum_{i=1}^{i=n}(O_i - P_i)^2}{n}} \quad \text{Equation 4.4}$$

$$t = \frac{\frac{\sum_{i=1}^{i=n}(O_i - P_i)}{n} \times \sqrt{n}}{\sqrt{\frac{\sum_{i=1}^{i=n}\left[(O_i - P_i) - \left(\sum_{i=1}^{i=n}\left(\frac{O_i - P_i}{n}\right)\right)^2\right]}{n-1}}} \quad \text{Equation 4.5}$$

4.3 Results and Discussion

4.3.1 Objective 3a: Field Conditions, Input Data Sets, and DNDC Model Outputs

Environmental and average climatic parameters for the site were calculated from multiple sources and are presented in Table 4.2 (with references to data sources) as the baseline for the study year, 2014.

Parameter	Baseline	Minimum-maximum values observed in Central Illinois
Air temperature (°C) (annual average)	9.44	Comparing measurements at the Energy Farm, Bondville & Willard stations [a]
Precipitation (cm) (annual average of daily precipitation)	0.3	Comparing measurements at the Energy Farm, Bondville & Willard stations [a]
Field capacity	0.36	0.33[b] - 0.44[a]
pH	5.16	4.42[c] – 6.7[d]
Soil organic carbon (kg C/kg soil)	0.035	0.015[e] – 0.045[d]
Tilling date	5 May	4th May – 6th May
Tilling depth (cm)	10	10[f] – 15[g]
Fertilizer application date	5 May	21st April[h] – 23rd May[h]
Fertilizer application depth (cm)	15	10[f] – 15[g]
Fertilizer application amount (kg-N/ha)	168	160[i] – 220[i]

[a] *Illinois State Water Survey*, 2015; [b] *Hollinger*, 1995; [c] Energy Farm records; [d] *USDA*, 2015b; [e] *Gopalakrishnan et al.,* 2012; [f] DNDC default value for chisel tillage; [g] *Simmons and Nafziger*, 2014; [h] *USDA*, 2010; [i] Observed values (1999-2014), USDA, 2015b.

Table 4.2 Range of input values observed in Central Illinois. For each input parameter, the minimum and maximum values were used in the modeling scheme provided in Section 2.2.1 to characterize uncertainty in modeled NH_3 fluxes at the measurement site for the year 2014.

A full description of crop development, yield, and ancillary environmental measurements is provided in Section 2.3.2. Ambient temperature and modeled NH_3 fluxes for crops in plots 1-6 for the year 2014 are shown in Figure 4.3a and b, respectively.

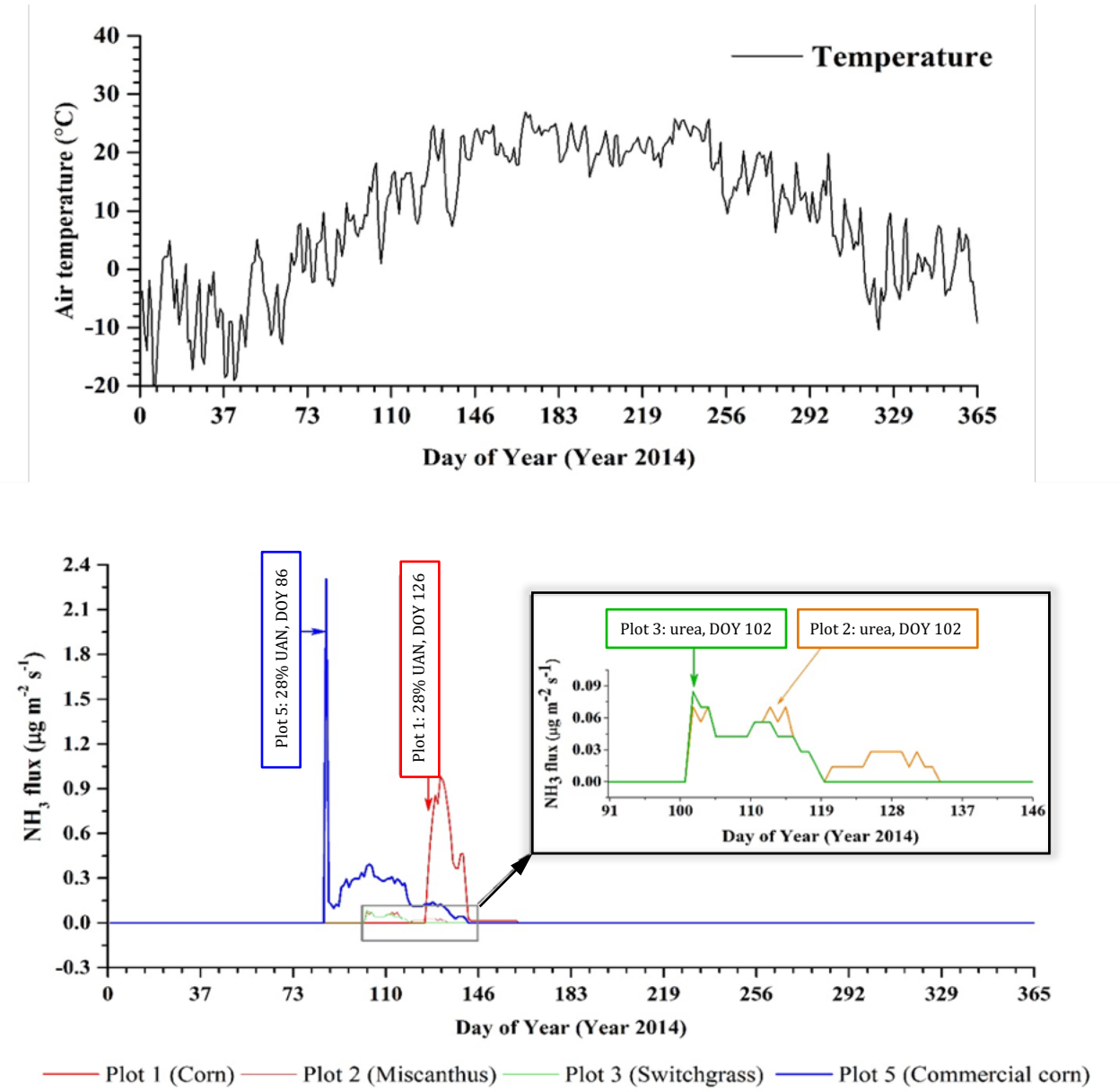

Figure 4.3: (a) Daily average ambient air temperature (ISWS, 2017) and (b) modeled NH_3 fluxes for crops located in plots 1, 2, 3 and 5, for year 2014. Inset indicates trends in modeled NH_3 fluxes for plots 2 and 3. Type of fertilizer and date of application are indicated with arrows, using same color as legend. No fertilizer was applied and hence zero NH_3 fluxes were modeled by DNDC in plots 4 and 6 in 2014. DNDC outputs are reported in kg-N ha^{-1} day^{-1} and converted to µg-NH_3 m^{-2} s^{-1}.

Largest modeled NH_3 fluxes occurred after fertilizer application for corn in plot 1 (7.13 kg-N ha^{-1} yr^{-1}) and plot 5 (9.22 kg-N ha^{-1} yr^{-1}). In contrast, NH_3 fluxes from miscanthus (plot 2, 0.79 kg-N ha^{-1} yr^{-1}) and switchgrass (plot 3, 0.57 kg-N ha^{-1} yr^{-1}) were considerably lower, while

modeled NH_3 fluxes were zero for prairie grass (plot 4) and alfalfa (plot 6). These differences are attributed to the differences in type, amount, and timing of fertilizer application.

Plot 1 was planted and fertilized on May 6th with 28% UAN, while plot 5 was fertilized on March 26th with a combination of 28% UAN (33 kg-N ha^{-1}) and 82% anhydrous ammonia (168 kg-N ha^{-1}) and planted on April 23rd (personal communication with EBI Energy Farm manager, Timothy Mies). Use of anhydrous ammonia in plot 5 resulted in a spike in fluxes within one day of fertilization, consistent with previous observations (Sommer et al., 2004). Positive NH_3 fluxes to the atmosphere continued for 55 days following fertilization. Similarly, NH_3 peak fluxes in plot 1 were observed shortly after fertilization application, however, they continued over a shorter period of 35 days post-fertilization. NH_3 flux following UAN application in plot 1 is of the same order of magnitude and display similar temporal trends as those reported by Jantalia et al. (2012), with peak fluxes observed 6 – 10 days following application.

4.3.2 Objective 3b: Estimation of Flux Contribution in an Inhomogeneous Field

Results from footprint contribution estimates using Equation 4.1 and associated empirical coefficients are presented in Table 4.3 for all days where 90% footprint contribution exceeded 100 m.

						NN%	
DOY	C1	C2	C3	C4	C5	R = 100 m N,S,E,W	R = 141 m NE,NW,SE,SW
126-2	1.57E-09	-7.63E-07	1.07E-04	1.23E-03	3.12E-02	61.8%	81.5%
127-1	1.25E-09	-6.43E-07	9.54E-05	1.16E-03	3.12E-02	58.4%	78.6%
127-2	1.19E-09	-6.20E-07	9.31E-05	1.15E-03	3.12E-02	57.7%	77.9%
128-1	1.24E-09	-6.38E-07	9.49E-05	1.16E-03	3.12E-02	58.2%	78.4%
128-2	1.19E-09	-6.18E-07	9.29E-05	1.15E-03	3.12E-02	57.6%	77.9%
129-1	1.23E-09	-6.33E-07	9.44E-05	1.16E-03	3.12E-02	58.1%	78.3%
130-2	1.04E-09	-5.61E-07	8.71E-05	1.11E-03	3.12E-02	55.7%	76.1%
131-2	1.30E-09	-6.60E-07	9.71E-05	1.17E-03	3.12E-02	58.9%	79.0%
132-2	1.62E-09	-7.82E-07	1.09E-04	1.24E-03	3.12E-02	62.3%	81.9%
133-1	1.72E-09	-8.16E-07	1.12E-04	1.26E-03	3.12E-02	63.2%	82.6%
138-2	3.28E-09	-1.33E-06	1.55E-04	1.48E-03	3.12E-02	72.7%	89.6%

Table 4.3: Estimation of flux contribution (NN%) at footprint radius, R, = 100 m and 141 m. C1 through C5 represent empirical curve-fitting coefficients, and N, S, E, and W correspond to cardinal directions (north, south east, and west).

All cases where 90% footprint exceeded 100 m occurred in the first two weeks after fertilization. This was due to higher wind speeds, common in Central Illinois during this time of year, and low surface roughness due to an undeveloped canopy. R = 100 m corresponds to the shortest distance from the measurement tower to the edge of the study plot; in this study R = 100 m was the distance from the measurement tower to the edge of the field in each of the four cardinal directions. R = 141 m is the longest footprint distance from the measurement tower to the edge of the study plot; in this study that is the distance to each corner of the square study plot.

The method described here to estimate flux contributions from an inhomogeneous study domain has not been previously reported in the literature. This estimation can be further used to scale measured fluxes based on the relative contribution in a study plot of interest. Using either a secondary set of measurements from the neighboring field or modeled emission estimates from the neighboring field, it is then possible to quantify the *relative* contribution from multiple

smaller study plots to a mean flux across a larger spatial area. This technique is used in Objective 3c to evaluate closure between measured NH_3 flux and DNDC modeled emission estimates.

4.3.3 Objective 3c: Closure Evaluation Between Modeled and Measured Fluxes

Comparison of modeled NH_3 fluxes under the four scenarios described in Section 4.2.2 with REA measurements is shown in Figure 4.4.

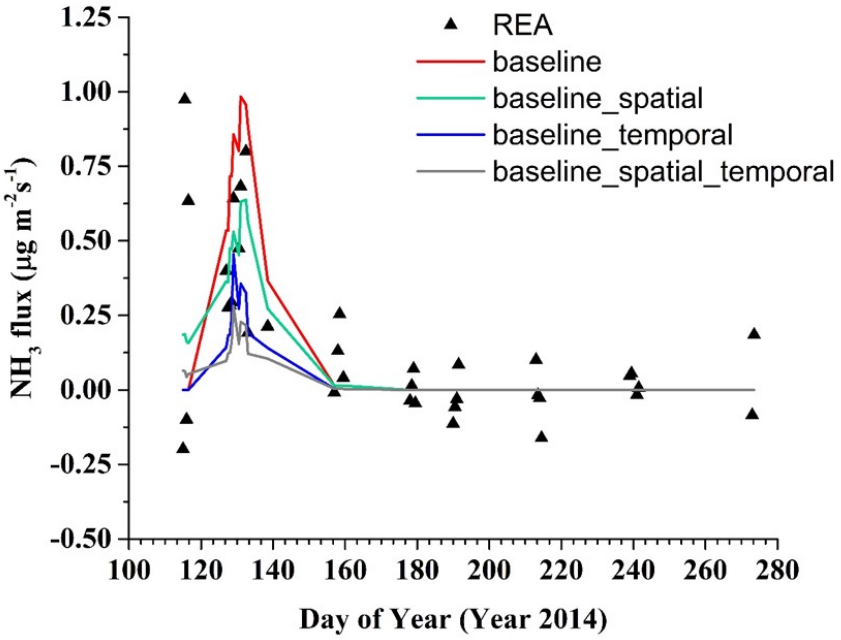

Figure 4.4: Comparison modeled and measured NH_3 fluxes. Four modeled scenarios are shown: 'baseline' = NH_3 fluxes from plot 1, 'baseline_spatial' = baseline adjusted with external flux contributions, 'baseline_temporal' = baseline adjusted with day to hour conversion profile, 'baseline_spatial_temporal' = baseline adjusted with both external flux contributions and day to hour temporal conversion. Data correspond to REA measurements over one corn-growing season (DOY 115-172). Fertilizer application occurred on DOY 126.

The baseline case represents direct outputs of DNDC for daily average fluxes across a homogenous study plot. The baseline_spatial case exhibited the highest fluxes prior to fertilization at the study plot (i.e., before DOY 128) because it incorporates contributions from the neighboring commercial corn field to the south of the study plot. Because the commercial

corn plot was fertilized on DOY 86 (compared to DOY 128 for the study plot), peak emissions from the commercial corn plot occurred earlier than the study plot, thereby increasing the modeled fluxes in the baseline_spatial case prior to study plot fertilization. The curve representing the baseline_temporal case is lower than both the baseline and baseline_spatial cases because it represents fluxes apportioned to REA sampling periods only. Due to the scale of the x-axis, and intermittent REA sampling periods, the baseline_temporal curve has a consistently lower magnitude than the baseline case. If baseline_temporal corrected fluxes were plotted on an hourly basis (rather than only those time periods corresponding to REA measurements), the curve would exhibit a sawtooth pattern, with peak fluxes typically exceeding the baseline case during afternoon periods. The baseline_spatial_temporal curve exhibits a lower maximum flux due to the influence of lower fluxes from the neighboring commercial corn plot, with higher fluxes prior to DOY 128 when compared with the baseline case due to contributions from the neighboring fields prior to fertilization of the study plot.

Overall, DNDC underestimated NH_3 fluxes compared to measurements, except for the baseline case (Table 4.4). Modeled fluxes after DOY 178 were zero for all cases. However, measurements indicated fluxes of smaller magnitudes (< 0.20 μg m^{-2} s^{-1}) in the same time period. No negative fluxes were captured by DNDC during the entire measurement period, indicating a limitation of the model in capturing depositional fluxes due to the uncertainty inherent in the DNDC model formulation (Balasubramanian et al., 2017).

Modeled NH_3 fluxes were evaluated for closure using coincidence and association statistics (Table 4.4) over two time frames: (1) for the entire time period for which REA measurements were available (DOY 115-272) and (2) a shorter time period characterized by

highest positive fluxes recorded by REA measurements in plot 1 (DOY 126-158, 14 samples), based on the sub-periods evaluated by Walker et al. (2013) and in Chapter 2 of this study.

Scenario		Coincidence statistics		Association statistics		
		DOY 115-272 (n=36)	DOY 126-159 (n=14)		DOY 115-272 (n=36)	DOY 126-159 (n=14)
baseline	**RMSE (%)**	168.8	114.6			
	t	0.86	1.04	$\mathbf{r_a^2}$	0.38	0.74
	p	{0.40}	{0.32}			
baseline_spatial	**RMSE (%)**	123.8	58.1			
	t	0.36	0.09	$\mathbf{r_a^2}$	0.47	0.74
	p	{0.72}	{0.93}			
baseline_temporal	**RMSE (%)**	145.7	76.6			
	t	2.56	1.33	$\mathbf{r_a^2}$	0.42	0.83
	p	{0.01}$^+$	{0.20}			
baseline_spatial_temporal	**RMSE (%)**	156.1	102.3			
	t	2.91	1.45	$\mathbf{r_a^2}$	0.52	0.83
	p	{0.01}$^+$	{0.17}			

$^+$ indicates significant difference at 0.95 confidence level

Table 4.4: Coincidence and association statistics for evaluating closure between modeled and measured NH_3 fluxes. Two time frames were considered for analysis: entire measurement period (DOY=115-272) and days characterized by high positive NH_3 fluxes following fertilizer application in plot 1 (DOY= 126-159).

RMSE for the baseline case was higher for the entire measurement period (169%) compared to DOY 126-159, characterized by higher measured positive fluxes (115%). RMSE also reduced from 169% to a minimum value of 124% for the entire measurement period and from 115% to a minimum value of 58.1% for DOY 126-159. Modeled and measured NH_3 fluxes were in agreement for DOY 126-159 using a two-tailed t-test. Two scenarios (baseline_temporal and baseline_spatial_temporal) resulted in significant differences when considering the entire measurement period. Association statistics (r_a^2 = 0.38 – 0.52) indicated poor correlation between measurements and modeled results for the entire growing season. However, r_a^2 values were considerably higher (0.74-0.83), for DOY 126-159, while r_a^2 values improved when external flux

contributions were accounted (baseline spatial) and when the day to hour conversion was applied (baseline_temporal and baseline_spatial_temporal). This result suggests that DNDC has better agreement with REA measurements when fluxes are larger and positive, indicating an under-prediction of negative NH_3 flux (deposition) using DNDC when compared to measurements.

RMSE for all four modeled cases and time frames was higher compared to RMSE reported by Cui et al. (2014) (77.4%) and Li (2000) (39%). This difference may be due to difference in duration between the present studies (157 days) and previously reported results (11 days). Improved RMSE for DOY 126-159 for all four modeled cases indicate that modeled NH_3 fluxes were more representative of the physico-chemical processes governing soil-atmosphere exchange of NH_3 as compared to the entire time period of DOY 115-272. Higher depositional fluxes after DOY 159 measured with REA (when compared with DNDC outputs) are indicative of possible limitations of the DNDC depositional algorithm for NH_3. Addition of flux contributions from adjacent fields when the REA footprint exceeded the 90% footprint limit, as well as adjustment to match the measurement and simulation time scales, resulted in improved model-measurement agreement for the time period when fluxes were to the atmosphere.

4.4 Summary and Conclusions

The DeNitrification DeComposition (DNDC) model is widely used to predict fluxes of greenhouse and trace gases to the atmosphere. While the model's performance for predicting greenhouse gas fluxes has been evaluated in many studies, assessment of NH_3 fluxes following chemical fertilizer application is reported only in two studies in China for periods of a few days (Li, 2000; Cui et al., 2014). In this study, DNDC's ability to model NH_3 fluxes following fertilizer application at a typical Midwest site over an entire corn growing season was evaluated. Modeled NH_3 fluxes were compared with measurements obtained using the REA method, at a

measurement site in Central Illinois in 2014. Practical issues in evaluating closure were also addressed.

In DNDC, a field site is conceptualized with uniform nutrient management and environmental parameters. While micrometeorological flux measurement methods rely on an assumption of spatial homogeneity in the measurement study domain, this is not always the case in practice due to natural variability of environmental conditions and differing farm management practices. To facilitate model-measurement inter-comparison, all REA measurements were considered (regardless of homogeneity of the measurement domain) and a method was devised to account for spatial inhomogeneity by apportioning fluxes to plots surrounding the measurement plot. An approach was also developed to scale down the daily DNDC predictions to the 4 h duration of REA measurements. Thus, to evaluate closure between modeled and measured fluxes, a four-scenario approach was developed, where different scenarios accounted for spatial inhomogeneity and temporal resolution differences. Overall, DNDC fluxes were generally less than measured fluxes for all scenarios and DNDC fluxes were in better agreement with REA measured fluxes during periods of high positive fluxes rather than periods of observed negative fluxes, indicating possible need for improvement of the NH_3 deposition algorithm of the model. Comparison of uni-directional to bi-directional parameterization of dry deposition have been found to account for up to 50% differences at the site scale (Dennis et al., 2013).

Accurate measurements of spatial and temporal variations in NH_3 emissions are needed as inputs to air quality models for accurate estimates of nitrogen loss in the environment and quantification of nitrogen deposition fluxes to sensitive and intensively managed ecosystems. This study is the first to evaluate the predictive capability of DNDC to model NH_3 fluxes over an entire growing season based on closure analysis with experimental field measurements. This

objective has important implications for two reasons: (1) it demonstrates that DNDC is able to capture timing of NH_3 emission peaks following chemical fertilizer application and (2) it highlights practical issues when examining closure between model predictions and measurements due to underlying assumptions of homogeneity in the study domain and differences in temporal resolution between model and measurements.

In a broader perspective, while measurements provide valuable site-level data, models are advantageously used to estimate trace gas fluxes at regional and global scales. Therefore, it is important that the most commonly used models are evaluated for the application used and their limitations are well understood. With this in mind, in the case of using DNDC for obtaining NH_3 fluxes following fertilizer application, these results point to the following areas for future improvements: a) improvement of the NH_3 deposition algorithm to include detailed parameterization describing the bi-directionality of the NH_3 fluxes (Nemitz et al., 2001); b) flux output at time scales relevant to air quality models (hourly); and c) further evaluation/closure studies at the site mode. A regional mode of DNDC is available and implemented widely (Neufeldt et al., 2006; Pathak et al., 2005). However, while multiple crops can be represented using the regional-scale version of DNDC, it does not allow for accounting detailed site-specific inputs, and modeled fluxes are obtained at the annual level for the sake of computational efficiency (Perlman et al., 2013). Therefore, large discrepancies between the use of site and regional modes have been highlighted by Perlman et al. (2013).

CHAPTER 5: SUMMARY, SIGNIFICANT CONTRIBUTIONS, AND FUTURE WORK

Improved understanding of the role of NH_3 in adverse environmental effects such as soil acidification, waterway eutrophication, and formation of secondary particulate matter pollution is important as the use of nitrogen-based fertilizers continues to increase globally (USEPA SAB, 2011). The goal of this research is to increase understanding of NH_3 flux from an intensively managed agricultural ecosystem in the Midwest United States (US). Application of nitrogen-based fertilizers in the area of this study is the majority contributor to anthropogenic atmospheric NH_3. This research is divided into three major thrust areas: (1) experimental quantification of NH_3 flux, (2) inter-comparison of NH_3 flux measurement methods with differing temporal resolution, and (3) evaluation of DeNitrification DeComposition (DNDC) model closure with experimental measurements from an inhomogeneous study domain. A summary of significant contributions from each of the primary study objectives follows.

5.1 Summary and Significant Contributions of this Research

5.1.1 Objective 1: Summary and Significant Contributions

Objective 1 quantified NH_3 flux above an intensively managed cornfield in the Midwest to improve understanding of NH_3 emissions and evaluations of new and existing emission models. A relaxed eddy accumulation (REA) system was designed, assembled, and calibrated at the Illinois State Water Survey prior to deployment above a corn canopy in Central Illinois (40° 3’ 46.209” N, 88° 11’ 46.0212” W) from May through September 2014 (day of year 115 – 273) to measure NH_3 fluxes due to chemical fertilizer application. NH_3 flux was measured in four-hour periods during mornings and afternoons. Mean atmospheric NH_3 concentration during the complete measurement period was 2.6 ± 2.0 μg m^{-3}. Larger upward fluxes of gaseous NH_3 were

measured during the first 30 days after fertilization, with variations observed throughout the field campaign. Measured NH_3 fluxes during the 2014 growing season ranged from -161 ng m^{-2} s^{-1} to 800 ng m^{-2} s^{-1} within two weeks of fertilization (where negative flux indicates deposition). Mean positive flux was 233 ± 203 ng m^{-2} s^{-1} in the morning and 260 ± 253 ng m^{-2} s^{-1} in the afternoon, while mean negative flux was -45.3 ± 38.6 ng m^{-2} s^{-1} in the morning and -78.4 ± 74.9 ng m^{-2} s^{-1} in the afternoon. NH_3 volatilization during the first 21 days after fertilization accounted for 79% of total nitrogen loss during the growing season.

Measurements reported in Objective 1 are necessary to improve understanding of agricultural NH_3 emissions in managed agricultural ecosystems dominated by rotations of highly fertilized corn and moderately to lightly fertilized soybeans, such as the plot studied herein. Specific significant contributions of this objective are:

1. The first reported NH_3 flux measurements over an intensively managed corn canopy in the Midwest for the duration of a corn-growing season.
2. The development of a new method to quantify under/over-estimation of NH_3 fluxes measured with an accumulating method due to spatial inhomogeneity of the study plot.
3. An inter-comparison of NH_3 flux measurements in the Midwest with measurements in North Carolina, identifying differences in magnitude and timing of maximum emission attributed to differences in field management practices and localized environmental conditions.

5.1.2 Objective 2: Summary and Significant Contributions

Studies of NH_3 flux over agricultural ecosystems in the US are limited by low temporal resolution (typically hours or days) and sparse spatial coverage, with no studies over corn in the Midwest. Objective 2 reports on NH_3 flux measurements over a corn canopy in Central Illinois

using the REA and flux-gradient (FG) methods, providing measurements at 4 h and 0.5 h intervals, respectively. The REA and FG systems were operated for the duration of the 2014 corn-growing season. Flux-footprint analysis was used to select data from both systems, resulting in 82 concurrent 4 h measurements. Mean NH_3 flux was 205 ± 300 ng m^{-2} s^{-1} from REA and 110 ± 256 ng m^{-2} s^{-1} from FG for all concurrent 4 h samples. Results from both methods were in agreement at a 0.95 confidence level for all coincident measurements. The FG method resolved NH_3 emission peaks at 0.5 h averaging time that were otherwise not observed with 4 h REA averaging. Two early-season emission periods were identified (DOY 130-132 and 140-143), where the timing and intensity of such emissions are attributed to a combination of urease inhibitor and localized soil temperature and precipitation.

NH_3 flux measurements with high temporal resolution (< 1 h), such as those from the FG method used in Objective 2, are important for evaluation of process-based models describing surface-atmosphere exchange of NH_3 and to better understand the impact of agricultural NH_3 emissions on air quality and the global Nitrogen Cycle. Objective 2 also investigated the effect of temporal resolution on the ability of measurement methods to capture variability in NH_3 fluxes. Specific significant contributions of objective 2 are:

1. The first reported use of the FG method with automated exchange mechanism to measure NH_3 flux in the US with 0.5 h averaging interval. This is the highest temporal resolution of NH_3 flux measurements over a corn canopy reported in the literature and represents a significant advancement in measurement of NH_3 flux.
2. An inter-comparison of 0.5 h and 4 h NH_3 flux measurements using FG and REA, respectively, demonstrating good agreement between methods for characterizing emission maxima and mean flux.

3. The first reported measurements of diurnal NH_3 flux over a corn canopy in the Midwest, where mean nighttime and daytime NH_3 flux were -0.23 ± 0.23 ng m^{-2} s^{-1} and 25.9 ± 93.5 ng m^{-2} s^{-1}, respectively, using the FG method. This measurement is important in the context of single-direction NH_3 emission models that do not characterize deposition, common of nighttime conditions.
4. Identification of two distinct periods of elevated NH_3 emission in the first 30 days following fertilization using both the REA and FG methods, attributed to a combination of environmental conditions (precipitation events and localized soil temperature) and the use of N-(n-butyl)-thiophosphoric triamide (nBTPT) urease inhibitor.

5.1.3 Objective 3: Summary and Significant Contributions

DeNitrification DeComposition (DNDC) model predictions of NH_3 flux following chemical fertilizer application were evaluated for closure with REA measurements in Central Illinois over the 2014 corn-growing season. Practical issues for evaluating closure were addressed by accounting for fluxes outside the measurement site and differences in temporal resolution. DNDC modeled NH_3 fluxes were in agreement with measurements ($p = 0.05$) and replicated trends satisfactorily ($r_a^2 > 0.74$) during the first 33 days after fertilizer application, when measured fluxes were to the atmosphere. DNDC did not replicate measured trends as closely during later time periods when depositional fluxes were measured ($r_a^2 < 0.52$). Results from Objective 3 represent the first study to evaluate the predictive capacity of DNDC to model NH_3 flux over an entire growing season using season-long NH_3 flux measurements above a corn canopy in the Midwest. These results can guide future improvements in DNDC for use in the development of NH_3 emission inventories with higher spatial and temporal resolution and in

upscaling emissions from the site (farm) to the regional scale using DNDC. Significant contributions from Objective 3 are:

1. Demonstration of the ability of DNDC to describe timing and NH_3 emission peaks following chemical fertilizer application.
2. Identification of practical issues when examining closure between model predictions and measurements due to underlying assumptions of homogeneity in the study domain and differences in temporal resolution between modeled and measured NH_3 flux.
3. Development of a new input data set of ancillary environmental parameters coupled with season-long NH_3 flux measurements at the same site that can be used for evaluation of NH_3 emission and flux models.

5.2 Recommendations for Future Research

Based on the results presented herein, several directions for future research are described in this section. Future research recommendations are broadly categorized in three themes: (1) method development for NH_3 flux quantification, (2) further NH_3 flux measurement needs, and (3) NH_3 flux model development and evaluation.

5.2.1 Method Development for NH_3 Flux Quantification

Objectives 2 & 3 of this research demonstrate the value of NH_3 flux measurements at timescales consistent with some process-based models of NH_3 flux from agricultural fields and air quality models describing subsequent transformation and fate (i.e., < 1 h). While DNDC outputs daily data as described in Objective 3, other process models such as Volt'Air-NH_3 and SURFATM-NH_3 model NH_3 flux at hourly timescales. Although the FG method as implemented in Objective 2 is capable of quantifying NH_3 flux at such timescales, the power requirements and complexity of the system limit the suitability of this approach for measurements at agricultural

field sites. The relatively high cost of equipment may also be a hindrance to widespread use across different ecosystems.

Recent advances in an open path quantum-cascade laser method to quantify NH_3 concentration is promising for potential future application in flux measurements (Miller et al., 2014). This instrument has been used to characterize NH_3 emissions from on-road mobile sources (Sun et al., 2014) and a beef cattle feedlot (Sun et al., 2015), reporting 0.5 h average NH_3 flux of 35 $\mu g\ m^{-2}\ s^{-1}$, three orders of magnitude greater than early-season fluxes measured in this study. This method does not yet provide sufficient limits of detection to quantify NH_3 flux from open agricultural fields, where concentration gradients are smaller and average NH_3 concentration is lower, but is a promising advancement in NH_3 concentration and flux measurements. As this method advances, its use for quantifying early-season NH_3 flux from open cropland should be considered.

Longer duration (> 1 week) accumulating measurements using passive NH_3 samplers such as the Radiello® device described in Section 2.2.2.7 may be suitable for use in a concentration-gradient method for flux quantification. While this approach would not provide high temporal resolution data such as that presented in Objective 2, it could be implemented more widely to characterize weekly NH_3 flux across a diverse range of ecosystems because of the low maintenance and instrumentation cost.

5.2.2 Further NH_3 Flux Measurements

Results from Objectives 1 and 2 of this research demonstrate that while there are similarities in NH_3 flux profiles across different geographic domains (i.e., Central Illinois and North Carolina) and differing field management practices, localized environmental and management practices affect the magnitude and temporal profile of NH_3 flux across different

ecosystems. Quantification of the relative impact of such factors requires further detailed studies designed to control for such conditions. Such uncertainty could be resolved with systematic measurement studies that involve carefully controlled inter-comparisons in similar environments and measurement-modeling studies for a broad range of environmental conditions and farm management practices. It is therefore important to collect additional measurements of NH_3 flux in agricultural systems using different management practices, with particular focus on those areas where fertilizer application is the dominant source of atmospheric NH_3, such as the Midwest. Measurements representative of different fertilizer types and application practices are important, including anhydrous NH_3, urea-ammonium nitrate (UAN), and urea, which are the most commonly used fertilizers in the Midwest as well as difference among fertilizer application methods (sprayed vs injected) and differing field management practices (till vs. no-till) and the use of urease inhibitors with urea-based fertilizer application Measurements across these varied conditions are needed to evaluate the performance of NH_3 emission models in different domains (Balasubramanian et al., 2015). Where possible, such measurements should be at < 1 h timescales for evaluation of process-based emission models at similar timescales such as Volt'Air-NH_3 (Garcia et al., 2012) and SURFATM-NH_3 (Personne et al., 2009). Measurements at this timescale could also be used to evaluate NH_3 emission models with longer timescales (e.g., DNDC) by averaging data. Results from Objectives 1 & 2 suggest that future measurement campaigns should be focused on the first 30 to 45 days after fertilizer application, corresponding to the time period when a majority of NH_3 emission occurs (>75% of total seasonal emission). This is also supported by Walker et al.'s 2017 results, where over 50% of NH_3 emission was observed within the first 21 days after fertilizer application. Given +/- 50% uncertainty in NH_3 emission inventories (Sutton et al., 2007), capturing these emissions in the period immediately

following fertilization (30 to 45 days) is important to bound current emission estimates and improve inputs to air quality models for subsequent modeling of transformation, transport, and impact associated with fertilization. Such measurements should focus on both spring and fall fertilization periods.

The size of study plots used in future field campaigns should be carefully considered in the context of flux footprint. When large (> 1 x 1 km^2) experimental plots are unavailable or not readily accesible for measurements it is important to couple measurements with a comprehensive analysis of the flux footprint, particularly for integrated measurement methods such as REA. In addition to measurement of NH_3 fluxes, future field studies should continue to include measurements of air temperature, precipitation, soil pH, soil moisture, soil temperature, soil organic carbon, and solar radiation to better understand the relative impact of underlying climactic and environmental conditions. Fertilizer type, application method, application depth (if tilled or injected), application date, and the use of urease inhibitor should also be reported for all future studies. Inclusion of both the type (i.e. specific brand and product formulation) and application rate of urease inhibitor is important to further develop an understanding of the impact of urease inhibitor on NH_3 emissions. Further, the use of satellite measurements, such as those described in Warner et al. (2017), to guide the location of future measurement campaigns should be considered to further investigate NH_3 fluxes in areas of higher relative concentrations.

Objective 2 identified two early-season periods of elevated NH_3 emission, consistent with results by Walker at al. (2013). Elevated emission periods were attributed to a combination of localized environmental conditions and the use of nBTPT urease inhibitor in both cases. However, the temporal allocation and relative intensity of elevated emissions were not consistent between these studies. Further, emission profiles reported here and by Walker et al. (2013) differ

from focused studies on the effect of urease inhibitor, as described in Section 3.2.1.2 (Rawluk et al., 2001; Engel et al., 2011). Due to the significant reduction of NH_3 emission attributed to nBTPT urease inhibitor (15 – 71% reduction, 44% mean reduction; Chadwick et al., 2005), it is important to more fully understand its effect on the temporal profile and magnitude of NH_3 emissions. Further field measurements with <1 h temporal resolution for the first 30 days after fertilization are needed. Previous studies have quantified the effect of urease inhibitor using chamber methods, which can limit or obfuscate the effect of local environmental conditions (Rawluk et al., 2001). Therefore, future research in this area should focus on the use of micrometeorological methods to elucidate the relative impact of local environmental conditions and urease inhibitor on NH_3 emissions.

While quantifying error in integrated flux measurements such as REA is challenging, evaluation of REA measurements with results from direct EC measurements of CO_2 and volatile organic compounds has shown strong correlation ($r^2 > 0.92$) between the measurement methods (Pattey et al., 1993; Bowling et al, 1998). Oncley et al., (1993) evaluated accuracy of the REA method for CO_2 quantification and observed errors of 20% when compared with direct eddy covariance measurement of CO_2. Further research is required to experimentally evaluate uncertainty in the REA system for NH_3 flux measurements, which could be accomplished through a field campaign with replicate REA systems operated with a single control system.

5.2.3 Improved NH_3 Flux Modeling and Evaluation

There is an opportunity to improve process-based biogeochemical models by further developing a parameterization for the effect of a urease inhibitor on NH_3 emission profiles. DNDC includes an input field to allow for the use of urease inhibitor where the user can input the efficiency and effective duration of the particular urease inhibitor. The present study and

work by others has demonstrated the combined effect of urease inhibitor and environmental conditions on NH_3 emissions (Engel et al., 2011; Walker et al., 2013). Because the efficiency and effective duration of urease inhibitor is a function of environmental conditions and application method and timing, it is necessary to more fully parameterize the effectiveness of such inhibitors in process-based models. While the current module in DNDC allows for some control of the effect of urease, a more complete parameterization based on DNDC input data may yield improved model results. Additional field experiments, described above, are required to support this parameterization with empirical inputs.

DNDC capabilities can be further improved by focusing on refinement of the NH_3 deposition algorithm to better account for bi-directionality of NH_3 flux (Nemitz et al., 2001). Additionally, development of DNDC flux outputs at timescales relevant to air quality models (i.e., hourly outputs) will further improve the relevance and value of the DNDC modeling approach.

CHAPTER 6: REFERENCES

Abendroth, L.J., Elmore, E.W., 2014. Corn Growth and Development. http://www.ipm.iastate.edu/ipm/files/03%20Corn%20Growth%20and%20Development.pdf Accessed 2/7/2015.

Alkezweeny, A.J., Laws, G.L., Jones, W., 1986. Aircraft and ground measurements of ammonia in Kentucky. Atmospheric Environment (1967) 20, 357–360. doi:10.1016/0004-6981(86)90038-7

Allen, R., Myles, L., Heuer, M.W., 2011. Ambient ammonia in terrestrial ecosystems: A comparative study in the Tennessee Valley, USA. Sci. Total Environ 409, 2768–2772. doi:10.1016/j.scitotenv.2011.04.017

Ammann, C., Meixner, F., 2002. Stability dependence of the relaxed eddy accumulation coefficient for various scalar quantities. J. Geophys. Res. 107. doi:10.1029/2001JD000649

Andreas, E.L., Hill, R.J., Gosz, J.R., Moore, D.I., Otto, W.D., Sarma, A.D., 1998. Stability Dependence of the Eddy-Accumulation Coefficients for Momentum and Scalars. Bound. Layer Meteorol. 86, 409–420. doi:10.1023/A:1000625502550

Aneja, V.P., Blunden, J., James, K., Schlesinger, W.H., Knighton, R., Gilliam, W., Jennings, G., Niyogi, D., Cole, S., 2008. Ammonia Assessment from Agriculture: U.S. Status and Needs. Journal of Environment Quality 37, 515–520. doi:10.2134/jeq2007.0002in

Aneja, V.P., Roelle, P.A., Murray, G.C., Southerland, J., Erisman, J.W., Fowler, D., Asman, W.A.H., Patni, N., 2001. Atmospheric nitrogen compounds II: emissions, transport, transformation, deposition and assessment. Atmos. Environ. 35, 1903–1911. doi:10.1016/S1352-2310(00)00543-4

Appel, K. W., Foley, K. M., Bash, J. O., Pinder, R. W., Dennis, R. L., Allen, D. J., and Pickering, K., 2011. A multi-resolution assessment of the community multiscale air quality (CMAQ) model v4.7 wet deposition estimates for 2002–2006. Geosci. Model Dev. 4, 357-371.

Ayers, R.U., Schlesinger, W.H., Socolow, R.H., 1994. “Human impacts on the carbon and nitrogen cycles” pp. 121-155 in Socolow, R.H., Andrews, C., Berkhourt, R. Thomas, V., eds. Industrial Ecology and Global Change. Cambridge University Press: Cambridge (MA).

Baker, J. M., Norman, J.M., and Bland, W.L., 1992. Field-scale application of flux measurement by conditional sampling. Agr. Forest Meteorol. 62, 31-52.

Balasubramanian, S., Koloutsou-Vakakis, S., McFarland, D. M., and Rood, M. J., 2015. Reconsidering emissions of ammonia from chemical fertilizer usage in Midwest USA. J. Geophys. Res. Atmos. 120, 6232-6246.

Balasubramanian, S., Koloutsou-Vakakis, S., Wang, M., Xiong, Y., Rood, M., 2014. Increasing spatial and temporal resolution of gaseous ammonia emissions from chemical fertilizer usage. National Atmospheric Deposition Program 2014 Scientific Symposium and Fall Meeting. Indianapolis, IN.

Balasubramanian, S., Nelson, A., Koloutsou-Vakakis, S., Lin, J., Rood, M. J., Myles, LT. and Bernacchi, C., 2017. Evaluation of DeNitrification DeComposition model for estimating ammonia fluxes from chemical fertilizer application. Agr. Forest Meteorol. 237-238, 123-134.

Baldocchi, D. D., Hincks, B. B., and Meyers, T. P. (1988). Measuring Biosphere-Atmosphere Exchanges of Biologically Related Gases with Micrometeorological Methods. Ecology 69, 1331-1340.

Bash, J. O., Walker, J.T., Katul, G.G., Jones, M.R., Nemitz, E., and W. P. Robarge, 2010. Estimation of in-canopy ammonia sources and sinks in a fertilized zea mays field. Environ. Sci. Technol. 44, 1683-1689.

Baumgardner, R.E., Lavery, T.F., Rogers, C.M., Isil, S.S., 2002. Estimates of the Atmospheric Deposition of Sulfur and Nitrogen Species: Clean Air Status and Trends Network, 1990−2000. Environ. Sci. Technol. 36, 2614–2629. doi:10.1021/es011146g

Behera, S.N., Sharma, M., Aneja, V.P., Balasubramanian, R., 2013. Ammonia in the atmosphere: a review on emission sources, atmospheric chemistry and deposition on terrestrial bodies. Environ Sci Pollut Res 20, 8092–8131. doi:10.1007/s11356-013-2051-9

Bennett, N.D., Croke, B.F.W., Guariso, G., Guillaume, J.H. a, Hamilton, S.H., Jakeman, A.J., Marsili-Libelli, S., Newham, L.T.H., Norton, J.P., Perrin, C., Pierce, S. a., Robson, B., Seppelt, R., Voinov, A. a., Fath, B.D., Andreassian, V., 2013. Characterising performance of environmental models. Environ. Model. Softw. 40, 1–20. doi:10.1016/j.envsoft.2012.09.011

Berger, B.W., Davis, K.J., Yi, C. Long-term carbon dioxide fluxes from a very tall tower in a northern forest: Flux measurement methodology, *J. Atmos. Ocean. Technol.* 2001.

Beusen, A.H.W., Bouwman, A.F., Heuberger, P.S.C., Van Drecht, G., Van Der Hoek, K.W., 2008. Bottom-up uncertainty estimates of global ammonia emissions from global agricultural production systems. Atmos. Environ. 42, 6067–6077. doi:10.1016/j.atmosenv.2008.03.044

Biermann, H.W., Tuazon, E.C., Winer, A.M., Wallington, T.J., Pitts, J.N., 1988. Simultaneous absolute measurements of gaseous nitrogen species in urban ambient air by long pathlength infrared and ultraviolet-visible spectroscopy. Atmos. Environ. 22, 1545–1554. doi:10.1016/0004-6981(88)90381-2

Biggs, W.W., Edison, A.R., Easton, J.D., Brown, K.W., Maranville, J.W., Clegg, M.D., 1971. Photosynthesis light sensor and meter. Ecology 52, 125-131.

Bouwman, A.F., Boumans, L.J.M., Batjes, N.H., 2002a. Estimation of global NH_3 volatilization loss from synthetic fertilizers and animal manure applied to arable lands and grasslands. Global Biogeochem. Cy. 16, 8–1–8–14. doi:10.1029/2000GB001389

Bouwman, A.F., Van Vuuren, D.P., Derwent, R.G., Posch, M., 2002b. A global analysis of acidification and eutrophication of terrestrial ecosystems. Water Air Soil Pollut 141, 349–382. doi:10.1023/A:1021398008726

Bowling, D.R., Delany, A.C., Turnipseed, A.A., Baldocchi, D.D., Monson, R.K., 1999. Modification of the relaxed eddy accumulation technique to maximize measured scalar mixing ratio differences in updrafts and downdrafts. J. Geophys. Res. 104, 9121–9133.

Bowling, D.R., Turnipseed, A.A., Delany, A.C., Baldocchi, D.D., Greenberg, J.P., Monson, R.K., 1998. The use of relaxed eddy accumulation to measure biosphere-atmosphere exchange of isoprene and other biological trace gases. Oecologia 116, 306–315. doi:10.1007/s004420050592

Bullard, R.L., Singh, A., Anderson, S.M., Lehmann, C.M.B., Stanier, C.O., 2017. 10-Month characterization of the aerosol number size distribution and related air quality and meteorology at the Bondville, IL Midwestern background site. Atmos. Environ. 1–14. doi:10.1016/j.atmosenv.2016.12.055

Burba, G., 2013. Eddy Covariance Method for Scientific, Industrial, Agricultural, and Regulatory Applications: A Field Book on Measuring Ecosystem Gas Exchange and Areal Emission Rates. LI-COR Biosciences, Lincoln, NE.

Businger, J., and Oncley, S.P., 1990. Flux measurement and conditional sampling. J. Atmos. Ocean Tech. 7, 349-352.

Businger, J.A., 1986. Evaluation of the Accuracy with Which Dry Deposition Can Be Measured with Current Micrometeorological Techniques. J. Clim. Appl. Meteorol. 25, 1100–1124. doi:10.1175/1520-0450(1986)025<1100:EOTAWW>2.0.CO;2

Carslaw, D.C. and Ropkins, K., 2012. openair — an R package for air quality data analysis. Environ. Modell. Soft. 27-28, 52–61.

Castro, M.S., Driscoll, C.T., Jordan, T.E., Reay, W.G., Boynton, W.R., 2003. Sources of nitrogen to estuaries in the United States. Estuaries 26, 803–814. doi:10.1007/BF02711991

Chadwick, D., Misselbrook, T., Gilhespy, S. Williams, J., Bhogal, A., Sagoo, L., Nicholson, F., Webb, J., Anthony, S., Chambers, B., 2005. WP1b Ammonia emissions and crop N use efficiency. Component report for Defra Project NT2605 (CSA 6579).

Christensen, C.S., Hummelshøj, P., Jensen, N.O., Larsen, B., Lohse, C., Pilegaard, K., Skov, H., 2000. Determination of the terpene flux from orange species and Norway spruce by relaxed eddy accumulation. Atmos. Environ. 34, 3057–3067. doi:10.1016/S1352-2310(99)00502-6

Conant, R. T., Berdanier, A. B., and Grace, P. R., 2013. Patterns and trends in nitrogen use and nitrogen recovery efficiency in world agriculture. Global Biogeochem. Cy. 27, 558-566.

Cooter, E. J., Bash, J.O., Walker, J.T., Jones, M.R., and Robarge, W., 2010. Estimation of NH3 bi-directional flux from managed agricultural soils. Atmos. Environ. 44, 2107-2115.

Cooter, E.J., Bash, J.O., Benson, V., Ran, L., 2012. Linking agricultural crop management and air quality models for regional to national-scale nitrogen assessments. Biogeosciences 9, 4023–4035. doi:10.5194/bg-9-4023-2012

Cuddington, K., Fortin, M.-J., Gerber, L.R., Hastings, A., Liebhold, A., O'Connor, M., Ray, C., 2013. Process-based models are required to manage ecological systems in a changing world. Ecosphere 4, 1–20. doi:10.1890/ES12-00178.1

Cui, F., Zheng, X., Liu, C., Wang, K., Zhou, Z., Deng, J., 2014. Assessing biogeochemical effects and best management practice for a wheat-maize cropping system using the DNDC model. Biogeosciences 11, 91–107. doi:10.5194/bg-11-91-2014

David, M.B., Del Grosso, S.J., Hu, X., Marshall, E.P., McIsaac, G.F., Parton, W.J., Tonitto, C., Youssef, M.A., 2009. Modeling denitrification in a tile-drained, corn and soybean agroecosystem of Illinois, USA. Biogeochemistry 93, 7–30. doi:10.1007/s10533-008-9273-9

Denmead, O.T., Simpson, J.R., Freney, J.R., 1977. A Direct Field Measurement of Ammonia Emission After Injection of Anhydrous Ammonia. Soil Sci. Soc. Am. J. 41, 1001–1004. doi:10.2136/sssaj1977.03615995004100050039x

Dennis, R.L., Schwede, D.B., Bash, J.O., Pleim, J.E., Walker, J.T., Foley, K.M., 2013. Sensitivity of continental United States atmospheric budgets of oxidized and reduced nitrogen to dry deposition parametrizations. Philos. Trans. R. Soc. B Biol. Sci. 368:201301.

Desjardins, R.L., 1972. A study of carbon-dioxide and sensible heat fluxes using the eddy correlation technique. *PhD dissertation* Cornell University, 189 pp.

Desjardins, R.L., 1977a. Description and evaluation of a sensible heat flux detector. Bound. Layer Meteorol. 11, 147–154. doi:10.1007/BF02166801

Desjardins, R.L., 1977b. Energy Budget by an Eddy Correlation Method. J. Appl. Meteor. 16, 248–250. doi:10.1175/1520-0450(1977)016<0248:EBBAEC>2.0.CO;2

Duyzer, J., 1994. Dry deposition of ammonia and ammonium aerosols over heathland. J. Geophys. Res. 99, 18757–7.

Edgerton, E.S., Saylor, R.D., Hartsell, B.E., Jansen, J.J., Alan Hansen, D., 2007. Ammonia and ammonium measurements from the southeastern United States. Atmos. Environ. 41, 3339–3351. doi:10.1016/j.atmosenv.2006.12.034

Engel, R., Jones, C., Wallander, R., 2011. Ammonia Volatilization from Urea and Mitigation by NBPT following Surface Application to Cold Soils. Soil Sci. Soc. Am. J. 75, 2348–10.

Erisman, J. W., Galloway, J. N., Seitzinger, S., Bleeker, A., Dise, N. B., Petrescu, A. M., Leach, A. M., and de Vries, W., 2013. Consequences of human modification of the global nitrogen cycle. Philos. T. R. Soc. B. 368, 20130116.

Erisman, J.W., Sutton, M.A., Galloway, J., Klimont, Z., Winiwarter, W., 2008. How a century of ammonia synthesis changed the world. Nat. Geosci. 1, 636–639. doi:10.1038/ngeo325

Erisman, J.W., Vermetten, A.W.M., Asman, W.A.H., Waijers-Ijpelaan, A., Slanina, J., 1988. Vertical distribution of gases and aerosols: The behaviour of ammonia and related components in the lower atmosphere. Atmos. Environ. 22, 1153–1160. doi:10.1016/0004-6981(88)90345-9

FAO, IFAD, WFP, 2014. The state of food insecurity in the world: Strengthening the enabling environment for food security and nutrition. FAO, Rome.

Farahbakhshazad, N., Dinnes, D.L., Li, C., Jaynes, D.B., Salas, W., 2008. Modeling biogeochemical impacts of alternative management practices for a row-crop field in Iowa. Agric. Ecosyst. Environ. 123, 30–48. doi:10.1016/j.agee.2007.04.004

Fenn, L.B., Hossner, L.R., 1985. Ammonia Volatilization from Ammonium or Ammonium-Forming Nitrogen Fertilizers, in: Stewart, B.A. (Ed.), Advances in Soil Science. Springer New York, pp. 123–169.

Ferm, M., 1998. Atmospheric ammonia and ammonium transport in Europe and critical loads: a review. Nutr. Cycl. Agroecosys. 51, 5–17. doi:10.1023/A:1009780030477

Ferrara, R.M., Loubet, B., Decuq, C., Palumbo, A.D., Di Tommasi, P., Magliulo, V., Masson, S., Personne, E., Cellier, P., Rana, G., 2014. Ammonia volatilisation following urea fertilisation in an irrigated sorghum crop in Italy. Agr. Forest Meteorol. 195-196, 179–191.

Flechard, C.R., Massad, R.S., Loubet, B., Personne, E., Simpson, D., Bash, J.O., Cooter, E.J., Nemitz, E., Sutton, M.A., 2013. Advances in understanding, models and parameterizations of biosphere-atmosphere ammonia exchange. Biogeosciences 10, 5183–5225.

Fotiadi, A. K., Lohou, F., Druilhet, A., Serça, D., Said, F., Laville, P., and Brut, A., 2005. Methodological development of the conditional sampling method. Part II: quality control criteria of relaxed eddy accumulation flux measurements. Bound-Lay. Meteorol. 117, 577-603.

Fumoto, T., Kobayashi, K., Li, C., Yagi, K., Hasegawa, T., 2008. Revising a process-based biogeochemistry model (DNDC) to simulate methane emission from rice paddy fields under various residue management and fertilizer regimes. Glob. Chang. Biol. 14, 382–402. doi:10.1111/j.1365-2486.2007.01475.x

Gallagher, M.W., Clayborough, R., Beswick, K.M., Hewitt, C.N., Owen, S., Moncrieff, J., Pilegaard, K., 2000. Assessment of a relaxed eddy accumulation for measurements of fluxes of biogenic volatile organic compounds: study over arable crops and a mature beech forest. Atmos. Environ. 34, 2887–2899. doi:10.1016/S1352-2310(00)00066-2

Galloway, J.N., 1998. The global nitrogen cycle: changes and consequences, Presented at the First International Nitrogen Conference, Elsevier Ltd, pp. 15–24. doi:10.1016/B978-0-08-043201-4.50008-3

Galloway, J.N., Aber, J.D., Erisman, J.W., Seitzinger, S.P., Howarth, R.W., Cowling, E.B., Cosby, B.J., 2003. The nitrogen cascade. Bioscience 53, 341–356. doi:10.1641/0006-3568(2003)053%5B0341:TNC%5D2.0.CO;2

Galloway, J.N., Townsend, A.R., Erisman, J.W., Bekunda, M., Cai, Z., Freney, J.R., Martinelli, L.A., Seitzinger, S.P., Sutton, M.A., 2008. Transformation of the nitrogen cycle: recent trends, questions, and potential solutions. Science 320, 888–892. doi:10.1126/science.1136674

Gao, W., 1995. The vertical change of coefficient b, used in the relaxed eddy accumulation method for flux measurement above and within a forest canopy. Atmos. Environ. 29, 2339–2347. doi:10.1016/1352-2310(95)00147-Q

Garcia, L., Génermont, S., Bedos, C., Simon, N.N., Garnier, P., Loubet, B., Cellier, P., 2012. Accounting for surface cattle slurry in ammonia volatilization models: the case of Volt'Air. Soil Sci. Soc. Am. J. 76, 2184-2194.

Gay, L. W., Fritschen, L. J., 1979. An exchange system for precise measurements of temperature and humidity gradients in the air near the ground. Hydrology and Water Resources in Arizona and the Southwest, 2986, 37-42.

Génermont, S., Cellier, P., 1997. A mechanistic model for estimating ammonia volatilization from slurry applied to bare soil. Agr. Forest Meteorol. 88, 145-167.

Gilhespy, S.L., Anthony, S., Cardenas, L., Chadwick, D., del Prado, A., Li, C., Misselbrook, T., Rees, R.M., Salas, W., Sanz-Cobena, A., Smith, P., Tilston, E.L., Topp, C.F.E., Vetter, S., Yeluripati, J.B., 2014. First 20 years of DNDC (DeNitrification DeComposition): Model evolution. Ecological Modelling 292, 51–62. doi:10.1016/j.ecolmodel.2014.09.004

Gilliland, A.B., Appel, K., Pinder, R.W., and Dennis, R.L., 2006. Seasonal NH3 emissions for the continental united states: Inverse model estimation and evaluation. Atmos. Environ. 40, 4986–4998.

Goebes, M.D., Strader, R., Davidson, C., 2003. An ammonia emission inventory for fertilizer application in the United States. Atmos. Environ. 37, 2539–2550. doi:10.1016/S1352-2310(03)00129-8

Google Maps. 2016. 40.0628, -88.1961. https://www.google.com/maps/place/40%C2%B003'46.1%22N+88%C2%B011'46.0%22W/@40.0628,88.1977286,530m/data=!3m2!1e3!4b1!4m5!3m4!1s0x0:0x0!8m2!3d40.0628!4d-88.1961?hl=en. Retrieved 5/21/2016.

Gopalakrishnan, G., Cristina Negri, M., Salas, W., 2012. Modeling biogeochemical impacts of bioenergy buffers with perennial grasses for a row-crop field in Illinois. GCB Bioenergy 4, 739–750. doi:10.1111/j.1757-1707.2011.01145.x

Graus, M., Hansel, A., Wisthaler, A., Lindinger, C., Forkel, R., Hauff, K., Klauer, M., Pfichner, A., Rappenglück, B., Steigner, D., Steinbrecher, R., 2006. A relaxed-eddy-accumulation method for the measurement of isoprenoid canopy-fluxes using an online gas-chromatographic technique and PTR-MS simultaneously. Atmos. Environ. 40, 43–54. doi:10.1016/j.atmosenv.2005.09.094

Green M. C., Chen L. W., DuBois D. W., and Molenar J. V., 2012, Fine particulate matter and visibility in the Lake Tahoe Basin: chemical characterization, trends, and source apportionment, J. Air Waste Manage., 62, 953-65.

Grönholm, T., Haapanala, S., Launiainen, S., Rinne, J., Vesala, T., Rannik, Ü., 2008. The dependence of the β coefficient of REA system with dynamic deadband on atmospheric conditions. Environ. Pollut. 152, 597–603.

Gruber, N., Galloway, J.N., 2008. An Earth-system perspective of the global nitrogen cycle. Nature 451, 293–296. doi:10.1038/nature06592

Gyldenkærne, S., Skjøth, C.A., Hertel, O., Ellermann, T., 2005. A dynamical ammonia emission parameterization for use in air pollution models. J. Geophys. Res. Atmos. 110, 1–14. doi:10.1029/2004JD005459

Hand, J.L., Schichtel, B.A., Pitchford, M., Malm, W.C., Frank, N.H., 2012. Seasonal composition of remote and urban fine particulate matter in the United States. J. Geophys. Res. 117, n/a–n/a. doi:10.1029/2011JD017122

Harper, L.A., Sharpe, R.R., 1995. Nitrogen Dynamics in Irrigated Corn: Soil-Plant Nitrogen and Atmospheric Ammonia Transport. Agron. J. 87, 669–675.

He, Z., Wright, L.P., Zhang, L., 2013. Model-Measurement Comparison of Ammonia Bi-Directional Air-Surface Exchange Fluxes over Agricultural Fields. Atmos. Climate Sci. 2013, 465–474.

Heaton, E.A., Dohleman, F.G., Long, S.P., 2008. Meeting US biofuel goals with less land: The potential of Miscanthus. Glob. Chang. Biol. 14, 1–15. doi:10.1111/j.1365-2486.2008.01662.x

Hensen, A., Nemitz, E., Flynn, M. J. , Blatter, A. , Jones, S. K., Sørensen, L. L. , Hensen, B., Pryor,S. C. , Jensen, B., Otjes, R. P., Cobussen, J. , Loubet, B. , Erisman,J. W., Gallagher, M.W., Neftel, A., and Sutton, M. A., 2009. Inter-comparison of ammonia fluxes obtained using the Relaxed Eddy Accumulation technique. Biogeosciences 6, 2575-2588.

Hicks, B.B., M.L. Wesely. 1978. An examination of some micrometeorological methods for measuring dry deposition. EPA Publ. EPA-600/7-78-116. USEPA, Research Triangle Park, NC.

Hicks, B.B., McMillen, R.T., 1984. A simulation of the eddy accumulation method for measuring pollutant fluxes. J. Clim. Appl. Meteorol. 23, 637–643. doi:10.1175/1520-0450(1984)023<0637:ASOTEA>2.0.CO;2

Hollinger, S.E., 1995. Midwestern climate center soils atlas and database, Circular 179. Champaign, Illinois.

Hsieh, C.-I., Katul, G., Chi, T.-W., 2000. An approximate analytical model for footprint estimation of scalar fluxes in thermally stratified atmospheric flows. Adv. Water Resour. 23, 765–772. doi:10.1016/S0309-1708(99)00042-1

ISWS, 2016. Prairie Research Institute, July 2014 Weather Observations for Champaign-Urbana, Illinois. http://www.isws.illinois.edu/atmos/statecli/urbana/urbana-monthly-2014.htm Accessed 5/20/2016.

ISWS, 2017. Water and Atmospheric Resources Monitoring Program (WARM). http://www.isws.illinois.edu/warm/datatype.asp Accessed 10/1/2017.

Jacob, D., 1999. Introduction to Atmospheric Chemistry. Princeton University Press, Princeton NJ.

Jantalia, C.P., Halvorson, A.D., Follett, R.F., Alves, B.J.R., Polidoro, J.C., Urquiaga, S., 2012. Nitrogen Source Effects on Ammonia Volatilization as Measured with Semi-Static Chambers. Agron. J. 104, 1595–1603. doi:10.2134/agronj2012.0210

Kaimal, J.C., JJ.. Finnigan, 1994. Atmospheric Boundary Layer Flows: Their Structure and Measurement. Oxford University Press, UK, pp. 289.

Kaimal, J.C., Wyngaard, J.C., Izumi, Y., Coté, O.R., 1972. Spectral characteristics of surface-layer turbulence. Q.J.R. Meteorol. Soc. 98, 563–589. doi:10.1002/qj.49709841707

Katul, G.G., 1994. A model for sensible heat flux probability density function for near-neutral and slightly-stable atmospheric flows. Bound. Layer Meteorol. 71, 1–20.

Katul, G.G., Finkelstein, P.L., Clarke, J.F., Ellestad, T.G., 1996. An Investigation of the Conditional Sampling Method Used to Estimate Fluxes of Active, Reactive, and Passive Scalars. J. Appl. Meteor. 35, 1835–1845. doi:10.1175/1520-0450(1996)035<1835:AIOTCS>2.0.CO;2

Kim, Y.J., Spak, S.N., Carmichael, G.R., Riemer, N., Stanier, C.O., 2014. Modeled aerosol nitrate formation pathways during wintertime in the Great Lakes region of North America 1–26. doi:10.1002/(ISSN)2169-8996

Kljun, N., P. Calanca, M. W. Rotach, and H. P. Schmid., 2004. A simple parameterisation for flux footprint predictions. Bound-Lay. Meteorol. 112, 503-523.

Kormann R., Meixner F. X., 2001. An analytical footprint model for non-neutral stratification, Bound-Lay. Meteorol. 99, 207–224.

Krupa, S.V., 2003. Effects of atmospheric ammonia (NH3) on terrestrial vegetation: a review. Environ. Pollut. 124, 179–221. doi:10.1016/S0269-7491(02)00434-7

Lawrence, M.G., 2005. The Relationship between Relative Humidity and the Dewpoint Temperature in Moist Air: A Simple Conversion and Applications. Bull. Amer. Meteor. Soc 86, 225–233. doi:10.1175/BAMS-86-2-225

Leclerc, M.Y., Thurtell, G.W., 1990. Footprint prediction of scalar fluxes using a Markovian analysis. Bound. Layer Meteorol. 52, 247–258. doi:10.1007/BF00122089

Legge, A.H., Nosal, M., Peake, E., Strosher, M., Hansen, M., Lefohn, A.S., 1990b. “Air quality of an area proximal to anthropogenic emissions” A.H Legge, S.V Krupa, Eds., Acidic Deposition: Sulphur and Nitrogen Oxides, Lewis Publishers, Chelsea, MI, pp. 249–346

Legge, A.H., Peake, E., Strosher, M., Nosal, M., McVehil, G.E., Hansen, M., 1990a. “Characteristics of the background air quality” A.H Legge, S.V Krupa, Eds., Acidic Deposition: Sulphur and Nitrogen Oxides, Lewis Publishers, Chelsea, MI, pp. 129–248

Lenhard, U., Gravenhorst, G., 1980. Evaluation of ammonia fluxes into the free atmosphere over Western Germany. Tellus 32, 48–55. doi:10.1111/j.2153-3490.1980.tb01721.x

Leuning, R., 2000. Estimation of Scalar Source/Sink Distributions in Plant Canopies Using LaGrangian Dispersion Analysis: Corrections for Atmospheric Stability and Comparison with a Multilayer Canopy Model. Bound. Layer Meteorol. 96, 293–314. doi:10.1023/A:1002449700617

Lewin, E.E., De Pena, R.G., Shimshock, J.P., 1986. Atmospheric gas and particle measurements at a rural northeastern U.S. site. Atmos. Environ. 20, 59–70. doi:10.1016/0004-6981(86)90207-6

Li, C., Frolking, S., Frolking, T.A., 1992. A model of nitrous oxide evolution from soil driven by rainfall events: 1. Model structure and sensitivity. J. Geophys. Res.-Atmos. 97, 9759–9776. doi:10.1029/92JD00509

Li, C.S., 2000. Modeling trace gas emissions from agricultural ecosystems. Nutr. Cycl. Agroecosys. 58, 259–276. doi:10.1023/A:1009859006242

Li, Y., Schichtel, B.A., Walker, J.T., Schwede, D.B., Chen, X., Lehmann, C.M.B., Puchalski, M.A., Gay, D.A., Collett, J.L., Jr., 2016. Increasing importance of deposition of reduced nitrogen in the United States. Proc Natl Acad Sci USA 113, 5874–5879.

Loubet, B., Decuq, C., Personne, E**.,** Massad, R.S., Flechard, C., Fanucci, O., Mascher, N., Gueudet, J.C., Masson, S., Durand, B., Genermont, S., Fauvel, Y., Cellier, P., 2012. Investigating the stomatal, cuticular and soil ammonia fluxes over a growing tritical crop under high acidic loads. Biogeosciences, 9, 1537-1552.

Madigan, M.T., Martinko, J.M., Dunlap, P.V., Clark, D.P. 2009. Brock biology of microorganisms, 12th ed. Pearson, London UK.

Mathur, R., Dennis, R.L., 2003. Seasonal and annual modeling of reduced nitrogen compounds over the eastern United States: Emissions, ambient levels, and deposition amounts. J. Geophys. Res.-Atmos. (1984–2012) 108, 4481. doi:10.1029/2002JD002794

Mattsson, M., Herrmann, B., David, M., Loubet, B., Riedo, M., Theobald, M.R., Sutton, M.A., Bruhn, D., Neftel, A., and Schjoerring, J.K., 2008. Temporal variability in bioassays of ammonia exchange potential in relation to plant and soil nitrogen parameters in intensively managed grassland. Biogeosciences 6, 171-179.

McCarthy J. 1973. A method for correcting airborne temperature data for sensor response time. J. Appl. Meteorol. 12: 211–214.

Meyers, T. P., Hall, M. E., Lindberg, S. E., Kim, K., 1996. Use of the modified Bowen-ratio technique to measure fluxes of trace gases. Atmos. Environ., 30, 3321 – 3329.

Meyers, T.P., Luke, W.T., Meisinger, J.J., 2006. Fluxes of ammonia and sulfate over maize using relaxed eddy accumulation. Agr. Forest Meteorol. 203–213.

Milford, C., Theobald, M. R., Nemitz, E., Hargreaves, K. J., Horvath, L., Raso, J., Dämmgen, U., Neftel, A., Jones, S. K., Hensen, A., Loubet, B., Cellier, P., and Sutton, M. A., 2009. Ammonia fluxes in relation to cutting and fertilization of an intensively managed grassland derived from an inter-comparison of gradient measurements, Biogeosciences, 6, 819-834.

Miller, D.J., Sun, K., Tao, L., Khan, M.A., Zondlo, M.A., 2014. Open-path, quantum cascade-laser-based sensor for high-resolution atmospheric ammonia measurements. Atmos. Meas. Tech. 7, 81–93.

Milne, R., Beverland, I.J., Hargreaves, K., Moncrieff, J., 1999. Variation of the β coefficient in the relaxed eddy accumulation method. Bound. Layer Meteorol. 93, 211–225. doi:10.1023/A:1002061514948

Monin, A.S., Obukhov, A.M., 1954. Basic turbulent mixing laws in the atmospheric surface layer. *Tr. Geofix. Inst. Akad. Nauk SSSR.* 24, 163-187.

Moosmüller, H., Varma, R., Arnott, W. P., 2005. Cavity ring-down and cavity-enhanced detection techniques for the measurement of aerosol extinction. Aerosol Science and Technology, 39, 30-39.

Myhre, G., Shindell, D., Bréon, F.M., Collins, W., Fuglestvedt, J., Huang, J., Koch, D., Lamarque, J.-F., Lee, D., Mendoza, B., Nakajima, T., Robock, A., Stephens, G., Takemura, T. and Zhang, H., 2013. Anthropogenic and natural radiative forcing. In: Climate Change 2013: The Physical Science Basis. Contribution of Working Group I to the Fifth Assessment Report of the Intergovernmental Panel on Climate Change [Stocker, T.F., D. Qin, G.-K. Plattner, M. Tignor, S.K. Allen, J. Boschung, A. Nauels, Y. Xia, V. Bex and P.M. Midgley (eds.)]. Cambridge University Press, Cambridge, United Kingdom and New York, NY, USA.

Myles, L., Kochendorfer, J., Heuer, M. W., and Meyers, T. P., 2011. Measurement of trace gas fluxes over an unfertilized agricultural field using the flux-gradient technique. J. Environ. Qual. 40, 1359-65.

Myles, L., Meyers, T.P., Robinson, L., 2007. Relaxed eddy accumulation measurements of ammonia, nitric acid, sulfur dioxide and particulate sulfate dry deposition near Tampa, FL, USA. Environ. Res. Lett. 2, 034004.

NADP, 2008. Standard Operating Procedure for the Determination of Passive Ammonia (Phenolate) by Flow Injection Analysis, SOP Number: AN-0022, Revision 0.0.

NADP, 2012. Standard Operating Procedure for Preparation and Extraction of URG Denuders. SOP Number PR-4074, Revision 1.1.

NADP, 2013. Standard Operating Procedure for Ambient Ammonia Using Radiello-Type Passive Samplers. SOP Number SS-4070, Revision 5.1.

NADP, 2014. Standard Operating Procedure for the Determination of Passive Ammonia (Phenolate) by Flow Injection Analysis. SOP Number: AN-4022.1.

NADP, 2017a. Ambient Ammonia Monitoring Network Fact Sheet. http://nadp.sws.uiuc.edu/amon/AMoNFactSheet.pdf Accessed 12/23/2017.

NADP, 2017b. Ammonia Monitoring Network (AMoN). URL http://nadp.sws.uiuc.edu/amon/ Accessed 12/28/2017.

NADP, 2018. National Trends Network (NTN). NRPS-3. URL http://nadp.sws.uiuc.edu/NTN/ Accessed 1/4/2018.

NADP, 2018b. Quality Assurance Report, National Atmospheric Deposition Program, 2014. URL http://nadp.slh.wisc.edu/lib/qa/cal_qar_2014.pdf Accessed 3/27/2018.

Nafziger, E., 2014. Corn. *in* Illinois Agronomy Handbook. http://extension.cropsci.illinois.edu/handbook/pdfs/chapter02.pdf Accessed 3/23/2014.

Neirynck, J. and Ceulemans, R., 2008. Bidirectional ammonia exchange above a mixed coniferous forest. Environ. Pollut. 154, 424-438.

Nelson, A.J., Koloutsou-Vakakis, S., Rood, M.J., Myles, L., Lehmann, C., Balasubramanian, S., Joo, E. Heuer, M., Vieira-Filho, M., Lin, J. 2017. Season-long ammonia flux measurements above fertilized corn in central Illinois, USA, using relaxed eddy accumulation. Agr. Forest Meteorol., 239, 202-212.

Nemitz, E., Milford, C., and Sutton, M.A., 2001. A two-layer canopy compensation point model for describing bi-directional biosphere-atmosphere exchange of ammonia, Q. J. R. Meteorol. Soc. 127, 815-833.

Nemitz, E., Sutton, M.A., Schjoerring, J.K., Husted, S., Paul Wyers, G., 2000a. Resistance modelling of ammonia exchange over oilseed rape. Agr. Forest Meteorol. 105, 405–425. doi:10.1016/S0168-1923(00)00206-9

Neufeldt, H., Scha, M., Angenendt, E., Li, C., Kaltschmitt, M., Zeddies, J., 2006. Disaggregated greenhouse gas emission inventories from agriculture via a coupled economic-ecosystem model. Agric. Ecosyst. Environ. 112, 233–240. doi:10.1016/j.agee.2005.08.024

Norman, M., Spirig, C., Wolff, V., Trebs, I., Flechard, C., Wisthaler, A., Schnitzhofer, R., Hansel, A., and Neftel, A., 2009. Intercomparison of ammonia measurement techniques at an intensively managed grassland site (Oensingen, Switzerland). Atmos. Chem. Phys. 9, 2635-2645.

Oncley, S.P., Delany, A.C., Horst, T.W., Tans, P.P., 1993. Verification of flux measurement using relaxed eddy accumulation. Atmos. Environ. 27, 2417–2426. doi:10.1016/0960-1686(93)90409-R

Paerl, H.W., 1997. Coastal eutrophication and harmful algal blooms: Importance of atmospheric deposition and groundwater as“ new” nitrogen and other nutrient sources. Limnol. Oceanogr. 42, 1154–1165. doi:10.4319/lo.1997.42.5_part_2.1154

Park, C., Schade, G.W., Boedeker, I., 2010. Flux measurements of volatile organic compounds by the relaxed eddy accumulation method combined with a GC-FID system in urban Houston, Texas. Atmos. Environ. 44, 2605–2614. doi:10.1016/j.atmosenv.2010.04.016

Pathak, H., Li, C., Wassmann, R., 2005. Greenhouse gas emissions from Indian rice fields: calibration and upscaling using the DNDC model. Biogeosciences Discuss. 2, 77–102. doi:10.5194/bgd-2-77-2005

Pattey, E., Desjardins, R.L., Rochette, P., 1993. Accuracy of the relaxed eddy-accumulation technique, evaluated using CO2 flux measurements. Bound. Layer Meteorol. 66, 341–355. doi:10.1007/BF00712728

Paulot, F., Jacob, D. J., Pinder, R. W., Bash, J. O., Travis, K., and Henze, D. K., 2014. Ammonia emissions in the United States, European Union, and China derived by high-resolution inversion of ammonium wet deposition data: Interpretation with a new agricultural emissions inventory (MASAGE_NH3). J. Geophys. Res.-Atmos. 119, 4343-4364.

Pearson, K., 1909. On a new method of determining correlation between a measured character A, and a character B, of which only the percentage of cases wherein B exceeds (or falls short -of) a given intensity is recorded for each grade of A. Biometrika 7, 96–105. doi:10.1093/biomet/7.1-2.96

Perlman, J., Hijmans, R.J., Horwath, W.R., 2013. Modelling agricultural nitrous oxide emissions for large regions. Environ. Model. Softw. 48, 183–192. doi:10.1016/j.envsoft.2013.07.002

Personne, E., Loubet, B., Herrmann, B., Mattsson, M., Schjoerring, J.K., Nemitz, E., Sutton, M.A., Cellier, P. 2009. SURFATM-NH3: a model combining the surface energy balance and bi-directional exchanges of ammonia applied at the field scale. Biogeosciences, 6:1371–1388.

Personne, E., Tardy, F., Génermont, S., Decuq, C., Gueudet, J.-C., Mascher, N., Durand, B., Masson, S., Lauransot, M., Fléchard, C., Burkhardt, J., Loubet, B., 2015. Investigating sources and sinks for ammonia exchanges between the atmosphere and a wheat canopy following slurry application with trailing hose. Agric. For. Meteorol., 207, 11-23.

Phillips, S.B., Arya, S.P., and Aneja, V.P., 2004. Ammonia flux and dry deposition velocity from near-surface concentration gradient measurements over a grass surface in North Carolina. Atmos. Environ. 38, 3469-3480.

Pinder, R.W., Adams, P.J., Pandis, S.N., 2007. Ammonia Emission Controls as a Cost-Effective Strategy for Reducing Atmospheric Particulate Matter in the Eastern United States. Environ. Sci. Technol. 41, 380–386.

Pinder, R.W., Appel, K.W., Dennis, R.L., 2011. Trends in atmospheric reactive nitrogen for the Easter United States. Environ. Pollut. 159, 3138–3141. doi:10.1016/j.envpol.2011.04.042

Pleim, J.E., Bash, J.O., Walker, J.T., Cooter, E.J., 2013. Development and evaluation of an ammonia bidirectional flux parameterization for air quality models. J. Geophys. Res. Atmos. 118, 3794–3806. doi:10.1002/jgrd.50262

R Core Team (2013). R: A language and environment for statistical computing. R Foundation for Statistical Computing, Vienna, Austria. http://www.R-project.org/.

Rattray, G., Sievering, H., 2001. Dry deposition of ammonia, nitric acid, ammonium, and nitrate to alpine tundra at Niwot Ridge, Colorado. Atmos. Environ. 35, 1105–1109. doi:10.1016/S1352-2310(00)00276-4

Raupach, M.R., 1994. Simplified expressions for vegetation roughness length and zero-plane displacement as functions of canopy height and area index. Bound-Lay. Meteorol. 71, 211–216.

Rawluk, C.D.L., Grant, C.A., Racz, G.J., 2001. Ammonia volatilization from soils fertilized with urea and varying rates of urease inhibitor NBPT. Can. J. Soil. Sci. 81, 239–246.

Reis, S., Pinder, R.W., Zhang, M., Lijie, G., Sutton, M.A., 2009. Reactive nitrogen in atmospheric emission inventories. Atmos. Chem. Phys. 9, 7657–7677. doi:10.5194/acp-9-7657-2009

RStudio Team (2018). RStudio: Integrated Development for R. RStudio, Inc., Boston, MA URL http://www.rstudio.com/ Accessed 2/1/2018.

Sakabe, A., Ueyama, M., Kosugi, Y., Hamotani, K., Hirano, T., Hirata, R., 2014. Is the empirical coefficient b for the relaxed eddy accumulation method constant? Journal of Atmospheric Chemistry 71, 79–94. doi:10.1007/s10874-014-9282-0

Scherer, J. J., Paul, J.B., O'Keefe, A., Saykally, R.J., 1997. Cavity ringdown laser absorption spectroscopy: History, development, and application to pulsed molecular beams. Chem. Rev. 97, 25-51.

Seinfeld, J.H., Panids, S.N., 2006. Atmospheric Chemistry and Physics: From Air Pollution to Climate Change, 2nd Ed. Wiley, Hoboken NJ.

Sharpe, R.R., Harper, L.A., 1995. Soil, plant and atmospheric conditions as they relate to ammonia volatilization. Fertil. Res. 42, 149–158. doi:10.1007/BF00750509

Simmons, F.W., Nafziger, E.D., 2014. Soil Management and Tillage, in: Illinois Agronomy Handbook. University of Illinois at Urbana-Champaign, College of Agriculture, Cooperative Extension Service, Champaign, Illinois, pp. 133–142.

Sintermann, J., Spirig, C., Jordan, A., Kuhn, U., Ammann, C., Neftel, A., 2011. Eddy covariance flux measurements of ammonia by high temperature chemical ionisation mass spectrometry. Atmos. Meas. Tech., 4, 599-616.

Smith, B., Richards, R.L., Newton. W.E., 2004. Catalysts for nitrogen fixation: Nitrogenases, relevant chemical models and commercial processes. Kluwer Academic Publishers, Boston MA.

Smith, J., Smith, P.W., 2007. How to evaluate a model, in: Introduction to Environmental Modeling. Oxford University Press, New York, USA, pp. 69–118.

Sommar, J., Zhu, W., Shang, L., Feng, X., and Lin, C.-J., 2013. A whole-air relaxed eddy accumulation measurement system for sampling vertical vapour exchange of elemental mercury. Tellus B 65, 19940.

Sommer, S. G., Jensen, C., 1994. Ammonia volatilization from urea and ammoniacal fertilizers surface-applied to winter wheat and grassland. Fert. Res. 37, 85–92.

Sommer, S.G., Schjoerring J.K., Denmead, O.T., 2004. Ammonia emission from mineral fertilizers and fertilized crops. Adv. Agron., 82, 557-622.

Spindler, G., Teichmann, U. and Sutton, M.A., 2001. Ammonia dry deposition over grassland-micrometeorological flux-gradient measurements and bidirectional flux calculations using an inferential model. Quarterly Journal of the Royal Meteorological Society, 127, 795-814.

Stull, R.B., 1988. An Introduction to Boundary Layer Meteorology. Kluwer Academic Publishers, London.

Sun, K. Tao, L., Miller, D.J., Zondlo, M.A., Shonkwiler, K.B., Nash, C., Ham, J.M., 2015. Open-path eddy covariance measurements of ammonia fluxes from a beef cattle feedlot. Agr. Forest Meteorol. 213, 193–202.

Sun, K., Tao, L., Miller, D.J., Khan, M.A., Zondlo, M.A., 2014. On-Road Ammonia Emissions Characterized by Mobile, Open-Path Measurements. Environ. Sci. Technol. 48, 3943–3950. doi:10.1021/es4047704

Sutton, M. A., Milford, C., Nemitz, E., Theobald, M. R., Hill, P. W., Fowler, D., Schjoerring, J. K., Mattsson, M. E., Nielsen, K. H., Husted, S., Erisman, J. W., Otjes, R., Hensen, A., Mosquera, J., Cellier, P., Loubet, B., David, M., Genermont, S., Neftel, A., Blatter, A., Herrmann, B., Jones, S. K., Horvath, L., F¨uhrer, E., Mantzanas, K., Koukoura, Z., Gallagher, M.,Williams, P., Flynn, M., and Riedo, M., 2011. Biosphere-atmosphere interactions of ammonia with grasslands: experimental strategy and results from a new European initiative, Plant Soil, 228, 131–145.

Sutton, M. A., Nemitz, E., Erisman, J. W., Beier, C., Bahl, K. B., Cellier, P., de Vries, W., Cotrufo, F., Skiba, U., Di Marco, C., Jones, S., Laville, P., Soussana, J. F., Loubet, B., Twigg, M., Famulari, D., Whitehead, J., Gallagher, M. W., Neftel, A., Flechard, C. R., Herrmann, B., Calanca, P. L., Schjoerring, J. K., Daemmgen, U., Horvath, L., Tang, Y. S., Emmett, B. A., Tietema, A., Penuelas, J., Kesik, M., Brueggemann, N., Pilegaard, K., Vesala, T., Campbell, C. L., Olesen, J. E., Dragosits, U., Theobald, M. R., Levy, P., Mobbs, D. C., Milne, R., Viovy, N., Vuichard, N., Smith, J. U., Smith, P., Bergamaschi, P., Fowler, D., and Reis, S., 2007. Challenges in quantifying biosphere-atmosphere exchange of nitrogen species. Environ. Pollut. 150, 125-39.

Sutton, M.A., Fowler, D., Burkhardt, J.K., Milford, C., 1995. Vegetation atmosphere exchange of ammonia: Canopy cycling and the impacts of elevated nitrogen inputs. Water Air Soil Pollut. 85, 2057–2063.

Taylor, G.I., 1922. Diffusion by Continuous Movements. Proc. London Math. Soc. s2-20, 196–212. doi:10.1112/plms/s2-20.1.196

Treloar, A.E., 1942. Correlation Analysis. Burgess, Minneapolis MN.

Tsai, J.-L., Tsuang, B.-J., Kuo, P.-H., Tu, C.-Y., Chen, C.-L., Hsueh, M.-T., Lee, C.-S., Yao, M.-H., Hsueh, M.-L., 2012. Evaluation of the relaxed eddy accumulation coefficient at various wetland ecosystems. Atmos. Environ. 60, 336–347.

UI, 2009. Illinois Agronomy Handbook, 24th edition. University of Illinois Extension.

USDA, 2010. Field Crops Usual Planting and Harvesting Dates. Agric. Handb. Number 628. URL http://usda.mannlib.cornell.edu/usda/current/planting/planting-10-29-2010.pdf Accessed 5/20/2016.

USDA, 2015a. Web Soil Survey. Soil Surv. Staff. Nat. Resour. Conserv. Serv. URL http://websoilsurvey.nrcs.usda.gov/ Accessed 1/1/2015.

USDA, 2015b. Chemical Distribution Rate. Quick Stats 2.0. URL http://www.nass.usda.gov/Quick_Stats/ Accessed 5/1/2016.

USDA, 2017, Illinois Corn County Estimates, Available from: https://www.nass.usda.gov/Statistics_by_State/Illinois/Publications/County_Estimates/2014/IL_Corn_Production_by_County.pdf. Accessed 9/1/2017.

USDOC-NOAA, 2013 Regional Climate Trends and Scenarios for the U.S. National Climate Assessment Part 3. Climate of the Midwest U.S., NOAA Technical Report NESDIS 142-3,, Washington, D.C., January 2013

USEPA (2000), Atmospheric ammonia: Sources and fate. A review of ongoing Federal research and future needs. http://www.esrl.noaa.gov/csd/AQRS/reports/ammonia.pdf Accessed 1/30/2014

USEPA (2004), Estimating ammonia emissions from anthropogenic nonagricultural sources, Draft final report. http://www.epa.gov/ttnchie1/eiip/techreport/volume03/eiip_areasourcesnh3.pdf Accessed 2/15/2015.

USEPA (2017), The 2011 National Emissions Inventory, Available from: http://www.epa.gov/ttnchie1/net/2011inventory.html Accessed 9/1/2017.

USEPA SAB (2011), Reactive nitrogen in the United States: An analysis of inputs, flows, consequences, and management options. A report of the EPA Science Advisory Board. http://yosemite.epa.gov/sab/sabproduct.nsf/WebBOARD/INCSupplemental?OpenDocument Accessed 2/15/2015.

Vaittinen, O., Metsälä, M., Persijn, S., Vainio, M. and Halonen, L., 2014. Adsorption of ammonia on treated stainless steel and polymer surfaces. App. Phys. B, 115, 185-196.

Vitousek, P.M., Aber, J.D., Howarth, R.W., Likens, G.E., Matson, P.A., Schindler, D.W., Schlesinger, W.H., Tilman, D.G., 1997. Human Alteration of the Global Nitrogen Cycle: Sources and Consequences. Ecol. Appl. 7, 737–750. doi:10.1890/1051-0761(1997)007[0737:HAOTGN]2.0.CO;2

Von Bobrutzki, K., Braban, C.F., Famulari, D., Jones, S.K., Blackall, T., Smith, T.E.L., Blom, M., Coe, H., Gallagher, M., Ghalaieny, M., McGillen, M.R., Percival, C.J., Whitehead, J.D., Ellis, R., Murphy, J., Mohacsi, A., Pogany, A., Junninen, H., Rantanen, S., Sutton, M.A., Nemitz, E., 2010. Field inter-comparison of eleven atmospheric ammonia measurement techniques. Atmos. Meas. Tech. 3, 91–112. doi:10.5194/amt-3-91-2010

Walker, J.T., Jones, M.R., Bash, J.O., Myles, L., Meyers, T., Schwede, D., Herrick, J., Nemitz, E., Robarge, W., 2013. Processes of ammonia air–surface exchange in a fertilized *Zea mays* canopy. Biogeosciences 10, 981–998.

Walker, J.T., Robarge, W.P., Wu, Y., Meyers, T.P., 2006. Measurement of bi-directional ammonia fluxes over soybean using the modified Bowen-ratio technique. Agr. Forest Meteorol. 138, 54–68.

Wang, S., Nan, J., Shi, C., Fu, Q., Gao, S., Wang, D., Cui, H., Saiz-Lopez, A., Bin Zhou, 2015. Atmospheric ammonia and its impacts on regional air quality over the megacity of Shanghai, China. Nature Publishing Group 1–13. doi:10.1038/srep15842

Watson, C.J., Miller, H., Poland, P., Kilpatrick, D.J., Allen, M.D.B., Garrett, M.K., Christianson, C.B., 1994. Soil Properties and the Ability of the Urease Inhibitor N-(n-BUTYL) Thoiphosphoric Triamide (nBTPT) to Reduce Ammonia Volatilization from Surface-Applied Urea. Soil Biologoy and Biochemistry 26, 1165–1171.

Warner, J.X., Dickerson, R.R., Wei, Z., Strow, L.L., Wang, Y., Liang, Q., 2017. Increased atmospheric ammonia over the world's major agricultural areas detected from space. Geophysical Research Letters 44, 2875–2884. doi:10.1002/2016GL072305

Wesely, M.L., Hart, R.L., 1985. Variability of short term eddy-correlation estimates of mass exchange. *In* Forest-atmosphere interactions. B.A. Hutchinson, B.B. Hicks, eds. D. Reidel, Dordrecht, The Netherlands; pp. 591-612.

Wu, Y., Walker, J., Schwede, D., Peters-Lidard, C., Dennis, R.L., Robarge, W.P., 2009. A new model of bi-directional ammonia exchange between the atmosphere and biosphere: Ammonia stomatal compensation point. Agr. Forest Meteorol. 149, 263–280. doi:10.1016/j.agrformet.2008.08.012

Wyngaard, J.C., Coté, O.R., 1972. Cospectral similarity in the atmospheric surface layer. Q.J.R. Meteorol. Soc. 98, 590–603.

Zemmelink, H.J., Gieskes, W.W.C., Klaassen, W., de Groot, H.W., de Baar, H.J.W., Dacey, J.W.H., Hintsa, E.J., McGillis, W.R., 2002. Simultaneous use of relaxed eddy accumulation and gradient flux techniques for the measurement of sea-to-air exchange of dimethyl sulphide. Atmos. Environ. 36, 5709–5717.

Zeri, M., Anderson-Teixeira, K., Hickman, G., Masters, M., DeLucia, E., Bernacchi, C.J., 2011. Carbon exchange by establishing biofuel crops in Central Illinois. Agr. Ecosyst. Environ. 144, 319–329.

Zhu, T., Pattey, E., Desjardins, R.L., 2000. Relaxed Eddy-Accumulation Technique for Measuring Ammonia Volatilization. Environ. Sci. Technol. 34, 199–203.

Zhu, L., D. K. Henze, J. O. Bash, K. E. Cady-Pereira, M. W. Shephard, M. Luo, S. L. Capps, Sources and impacts of atmospheric NH3: Current understanding and frontiers for modeling, measurements, and remote sensing, *Current Pollution Reports,* 1 (2), 95–116, 2015.